PNNL-10996
UC-810
Project Technical Information

Minor Component Study for Simulated High-Level Nuclear Waste Glasses (DRAFT)

H. Li
M.H. Langowski
P.R. Hrma
M.J. Schweiger
J.D. Vienna
D.E. Smith

February 1996

Prepared for the U.S. Department of Energy
under Contract DE-AC06-76RLO 1830

Pacific Northwest National Laboratory
Operated for the U.S. Department of Energy
by Battelle Memorial Institute

Battelle

PNNL-10996
UC-810
Project Technical Information

Minor Component Study for Simulated High-Level Nuclear Waste Glasses (Draft)

H. Li
M. H. Langowski
P. R. Hrma
M. J. Schweiger
J. D. Vienna
D. E. Smith

February 1996

Prepared for
the U.S. Department of Energy
under Contract DE-AC06-76RLO 1830

Pacific Northwest National Laboratory
Richland, Washington 99352

DISCLAIMER

PACIFIC NORTHWEST NATIONAL LABORATORY
operated by
BATTELLE
for the
UNITED STATES DEPARTMENT OF ENERGY
under Contract DE-AC06-76RLO 1830

Printed in the United States of America

Available to DOE and DOE contractors from the
Office of Scientific and Technical Information, P.O. Box 62, Oak Ridge, TN 37831;
prices available from (615) 576-8401.

Available to the public from the National Technical Information Service,
U.S. Department of Commerce, 5285 Port Royal Rd., Springfield, VA 22161


The document was printed on recycled paper.

SUMMARY

During the waste vitrification process, troublesome minor components in high-level radioactive waste streams (HLW) could adversely affect either waste vitrification rate or melter life-time. Knowing the solubility limits for these minor components and their effects on properties associated with waste vitrification operation and product durability are important in many aspects, such as a determination of pretreatment options for waste streams, and glass formulation to prevent potential problems during the waste vitrification as well as to improve glass durability.

This letter report provides the research results obtained mainly from the Pacific Northwest Laboratory (FY94 and FY95) and some preliminary results obtained from a subcontractor, Nuclear Research Institute Řež (Czech Republic). During this period, under the HLW minor component project, seven borosilicate based HLW glass systems were investigated, which covered four types of Hanford wastes: complexant concentrate waste (CCW), plutonium finishing plant waste (PFP), double shell tank/single shell tank blend waste (DST/SST), and complexant concentrate for tank waste SY103 (CC103-SY92SW). In addition, a West Valley HLW glass was studied. A summary of this study follows for these six areas: molten salt phase segregation during batch melting, solubility of sulfate as a function of glass composition, chromate formation during batch reaction, crystallinity as a function of glass composition and minor component concentration, effects of phosphate, chromium, and titanium on glass melt viscosity, and effects of these minor components of interest on glass durability.

Molten Salt Phase Segregation

Molten sulfate segregation during HLW waste vitrification is a kinetic process, which initiates at an early state of the batch melting. Segregated sulfate tends to flow toward the surface of the molten glass and accumulates at the top of the melt where it evaporates. Glass composition was found to have a significant influence on phase segregation. Alumina in glass enhances sulfate segregation, while batches containing high boric acid and low sodium can completely suppress it; this suppression is associated with melt foaming. Molten sulfate segregation has been found to promote phase segregation of phosphate-rich phases, including alkali-/alkaline- and rare earth- phosphates. An increase in alumina content in glass enhances an overall segregation of both sulfate and phosphate phases.

Composition Dependence of Sulfate in Glass

Sulfate solubility in glass varies significantly with glass composition (0.5 - 1.4 wt% SO_3), especially with phosphate present. Effects of various components on sulfate solubility were investigated in terms of glass basicity, alumina content, and phosphate content. With the exception of high phosphate glasses, sulfate solubility was successfully modeled using a semi-empirical approach based on glass structure. According to the current understanding, sulfate solubility in borosilciate waste glass is affected by the concentrations of non-bridging and bridging oxygen, increasing with nonbridging oxygen concentration. Phosphate addition increases the sulfate solubility (up to 1.4 wt% SO_3),compared to 0.9 wt% SO_3 for a glass with an identical ratio of nonbridging over bridging oxygen.

Chromate Formation during Batch Reaction

Chromate formation in an early stage of waste vitrification is inevitable; it peaks approximately 650°C, depending on the glass composition. Chromate formation, mostly Na_2CrO_4, is transient, depending on batch reaction time at a given temperature. Reaction of chromate occurs above the peak temperature also. At the glass processing temperature, however, the fraction of chromate, Cr^{6+}, is negligibly small; the most stable form is Cr^{3+} for waste glasses vitrified in ambient air. For waste initially containing chromium oxide, no chromate phase segregation was observed. Although the current results suggest no significant impact of high chromic oxide content in the waste on HLW vitrification process, further investigation is necessary to examine the impact of high chromate contents in HLW wastes on HLW glass melting process.

Effects of Minor Components on Crystallization

Crystallization of certain phases containing minor components of interest in HLW glasses is a complex process which not only depends on the temperature, thermal history of glass, and amount of minor component in glass, but also is significantly affected by other glass components. Results from this study show that the limiting factors of phosphate solubility in glass are the concentrations of Na, Li, La, Nd, and Al. At relatively high concentrations of alkalis, rare earth oxides, and alumina, crystallization of a variety of phosphate-bearing phases were found, including Na_3PO_4, Li_3PO_4, $Na_3RE(PO_4)_2$, and $AlPO_4$. In glasses with high concentration of Cr_2O_3 (> 1.0 wt%), eskolait (Cr_2O_3) precipitated from the melt. No settling

of fine Cr_2O_3 crystals (~10 μm) was observed. In HTB651 glasses containing relatively high concentrations of both Cr and other transition metals (Mn, Ni, and Fe), a small amount of spinel crystals formed, which were found at the interface between the melt and crucible wall. No spinel settlement was found. Solubility of TiO_2 in borosilciate based HLW glasses was found to be much greater than 1.0 wt% previously considered. A high melting temperature glass dissolved as much as 5.0 wt% TiO_2 without precipitating any titanium bearing crystalline phases for melting time as long as 24 hr at 1250 and 1350°C. However, at higher TiO_2 concentration (8.0 wt%), TiO_2 crystals precipitated from the melt at a lower temperature (1185°C). In this case, no crystal settlement was observed. In addition, no effects of Al_2O_3 and ZrO_2 on the solubility limit of TiO_2 were observed in HTB651 glasses.

Effects of Minor Components on Glass Melt Viscosity

Effects of minor components on glass melt viscosity depends on glass composition. An addition of 1 wt% P_2O_5 increases the glass melting temperature at 5 Pa.s approximately 6°C in CVS3 glasses, but only 3°C in HTB651 glass, and 2°C in PFP2 glass. The effect of Cr_2O_3 on glass viscosity is negligibly small. Formation of Cr_2O_3 crystals does not change the normal Arrhenius behavior of glass viscous flow at high temperature. An addition of 1.0 wt% TiO_2 decreases glass melting temperature by about 10°C.

Effects of Minor Components on Glass Durability

Impact of sulfate on glass durability appears to be strongly glass composition dependent. For CCW glasses, two distinct types of glass dissolution were observed, one by network dissolution, and another by preferential leaching of Na-O-S-O and Li-O-S-O groups. The preferential leaching, however, is not associated with crystals of Na_2SO_4 and Li_2SO_4 in glass, suggesting that clusters of Na-O-S-O and Li-O-S-O exist in glass. Micro-channels of these clusters are suspected to cause high leaching rates of these species from the glass matrix. Chemical durability of HLW glasses is affected by phosphate in two aspects, which are associated with crystal formation in glass through the change of residual glass composition. For a glass with a small fraction of phosphate crystals, Na_3PO_4 or Li_3PO_4 or both, glass durability was either unchanged or improved slightly. This can be explained by the removal of alkali oxides from the glass matrix, which in turn strengthens the residual glass network. However, crystallization decreases glass durability when large amounts of alkali-phosphate crystals

precipitate in the glass. For glass containing high P_2O_5, crystallization of $AlPO_4$ and $NaAlSiO_4$ occurs in slowly cooled glass samples (using the canister centerline cooling treatment). The crystallization is detrimental to glass durability, resulting in a sharp increase (up to a factor of 10) in sodium release tested using the 7-day PCT procedure. The deterioration of glass durability in this case can be attributed to weakening of the glass network by removal of Al or Si from the glass matrix through crystallization. In HLW glasses spiked with Cr_2O_3 (up to 0.8 wt%) and TiO_2 (up to 5 wt%), no impact on glass durability was found.

ACKNOWLEDGEMENTS

The authors wish to acknowledge and thank Nuclear Research Institute Řež (Czech Republic) for the research contributions in this project for high-level nuclear waste glass. Laboratory assistance, especially from Greg Sullivan, Suzanne Palmer, Karl Pool, Ron Sanders, Jim Coleman, Dave McCready, and Meilin Gong are greatly appreciated. Discussions with Don-Song Kim, Xiangdong Feng, John Darab, and Peter Smith are acknowledged. Donald Larson is acknowledged for this leadership and beneficial inputs in the HLW program and reviewing the manuscript of this letter report.

CONTENTS

TABLES

FIGURES

1. INTRODUCTION

Hanford Site single-shell tank (SST) and double-shell tank (DST) wastes are planned to be separated into low activity (or low-level waste, LLW) and high activity (or high-level waste, HLW) fractions, and to be vitrified for disposal. Formulation of HLW glass must comply with glass processibility and durability requirements, including constraints on melt viscosity, electrical conductivity, liquidus temperature, tendency for phase segregation on the molten glass surface, and chemical durability of the final waste form. A wide variety of HLW compositions are expected to be vitrified. In addition these wastes will likely vary in composition from current estimates. High concentrations of certain troublesome components, such as sulfate, phosphate, and chrome, raise concerns about their potential hinderance to the waste vitrification process. For example, phosphate segregation in the cold cap (the layer of feed on top of the glass melt) in a Joule-heated melter may inhibit the melting process (Bunnell, 1988). This has been reported during a pilot-scale ceramic melter run, PSCM-19, (Perez, 1985). Molten salt segregation of either sulfate or chromate is also hazardous to the waste vitrification process. Excessive (Cr, Fe, Mn, Ni) spinel crystal formation in molten glass can also be detrimental to melter operation.

Titanium has aroused recent interest due to the possible use of silicotitanate as an ion-exchanger to remove radioactive Cs and Sr from the tank waste (Bunker, 1994 and Balmer and Bunker, 1995). This would increase the amount of TiO_2 in HLW glass through the addition of the loaded (or used) silicotitanate to the HLW stream. The solubility of TiO_2 in silicate glass can be as high as 10.0 wt% (Labarbe, et al., 1988). However, the current adopted TiO_2 solubility limit is about 1.0 wt% in HLW borosilicate waste glass (Bickford, et al., 1990). The exact range of solubility limits of TiO_2 as a function of glass composition for the waste glass is unknown. Excessive TiO_2 would increase the liquidus temperature of glass and hence would be expected to adversely affect the melting process.

To better understand the roles of these components in HLW glass and their effects on vitrification and chemical durability, two consecutive studies were proposed (Langowski, et al., 1994, and Langowski and Hrma, 1995). These studies have been carried out according to milestone number PVTD-C94-03.01E Rev. 1 and PVTD-C95-02.01S, respectively. The effects of SO_3, P_2O_5, Cr_2O_3, and TiO_2 on the vitrification and durability of a variety of HLW types have

been studied. This report summarizes the experimental results and a current understanding of how these components affect the vitrification process and glass durability, and its completion satisfies milestone PVTD-T3C-95-125.

2. TEST MATRIX DESIGN

Both low-melting (1150°C) and high-melting (≥1300°C) HLW glasses were formulated with a variety of simulated Hanford HLW streams (West Valley glass, WV182, was also tested). These wastes include complexant concentrate waste (CCW) pretreated by sludge dissolution and transuranic extraction (May and Watrous, 1992), plutonium finishing plant waste (PFP) pretreated by sludge washing (May and Watrous, 1992), DST/SST all blend waste (Lambert and Kim, 1994, and Kim and Hrma, 1994), and West Valley waste (Perez, 1985) from which WV 182 glass was made. The following sections describe formulation of HLW glasses using the five wastes listed above.

2.1 CCW Glass

CCW glasses were formulated (using the CCW composition found in Appendix A) to examine molten salt phase segregation during glass melting and glass durability while encompassing the following parameters: waste loading (from 28.0 to 79.0 wt% of waste oxides in glass), glass basicity (from 27.5 to 42.8 kcal/avogadro bond), Al_2O_3 (from 0.0 to 15.0 wt%), and P_2O_5 (from 4.5 to 12.0 wt%). All glasses were formulated using a first-order mixture Arrhenius viscosity model (Hrma, et al., 1994). The formulation targeted a vitrification temperature of 1150°C, at which the estimated melt viscosity of about 5.0 Pa·s (only CCW4-4 had the estimated glass viscosity of 2.9 Pa·s). Appendix B1 summarizes nominal compositions of the seventeen CCW glasses. Except for the waste loading series (CCW1), the glasses were formulated with 67.0 wt% waste loading.

For CCW glasses, the glass basicity number, *BN*, was estimated according to Krämer (1991):

$$BN = 119.0 - \sum(x_i \cdot bn_i) \qquad \text{(kcal/avogadro bond)} \qquad (1)$$

where 119.0 is the basicity number of pure B_2O_3, and x_i and bn_i are the mole fraction of i-th oxide and its corresponding basicity number, respectively. Appendix B1 also summarizes the

glass basicity numbers.

2.2 PFP Waste Glass

Molten salt phase segregation was also studied using glasses formulated with 40.0 wt% loading of PFP1 waste described in Appendix A, which contains high concentrations of sulfate, phosphate, and chrome. The PFP1 glasses fit into two categories: low B_2O_3 - high Na_2O (PFP1-1 to PFP1-3) and high B_2O_3 - low Na_2O (PFP1-4 to PFP1-7). In addition, Li_2O content varied in all glasses to examine its role in phase segregation. The glass formulation targeted a vitrification temperature of 1150°C, at which the glass melt viscosity was about 7.5 Pa·s as estimated from the first-order mixture viscosity model (Hrma, et al., 1994). Appendix B2 summarizes nominal compositions of the seven PFP1 glasses tested.

The effects of phosphate on glass melt viscosity and chemical durability were separately studied using PFP2 waste, a variation of the PFP waste with lower NiO and SeO_2 than PFP1 (Appendix A). The PFP2 glasses were formulated with 28.0 wt% waste loading and targeted to melt at 1150°C, at which the estimated melt viscosities were about 6 Pa·s. Appendix B3 tabulates the nominal compositions of the five PFP2 glasses tested.

2.3 WV Waste Glass

A West Valley simulated radioactive waste glass (WV-182) was chosen as a base-line glass to study phosphate segregation observed during a pilot scale ceramic melter run, PSCM-19 (Perez, 1985). Appendix B4 tabulates the compositions of WV-182 glass and its modified forms in which SO_3 was increased (using Na_2SO_4) to 1.0, 1.5, and 2.0 wt%. The glass melt viscosities at 1150°C were about 4.5 Pa· s. In addition, two more modifications were tested with increased Al_2O_3 of 6.0 and 10.0 wt% at the expense of SiO_2 on an equal mass basis. Each of these modified glasses were tested with the varied SO_3 levels. The estimated viscosities of the higher alumina glasses at 1150°C varied from 4.7 to 6.1 Pa·s (using the first-order viscosity model).

2.4 All Blend Waste Glass

All blend (DST/SST) waste composition was used to formulate CVS3 glasses (Langowski, et al., 1994), in which CVS3-1 was a baseline glass. These glasses had 50.0 wt% waste loading and the estimated melt viscosity of 4.0 Pa·s at a vitrification temperature of 1350°C. Four CVS3 glasses (nominally, 37 to 40) based on CVS3-1 with increased P_2O_5 from 3.0 to 9.0 wt% were tested to study the effects of P_2O_5 on glass melt viscosity, crystallinity, and chemical durability

(Langowski et al, 1994). Appendix B5 summaries the nominal compositions of the CVS3 glasses.

2.5 HTB651 Glass

Using the same all blend (DST/SST) waste (cf. Appendix A), HTB651 (high-temperature blend) glasses were formulated based on 65.0 wt% waste loading with modifications to these glasses of P_2O_5 (5.0, 7.0, and 9.0 wt%), Cr_2O_3 (0.6 and 0.8 wt%), and TiO_2 (1.0, 3.0, 5.0, and 8.0 wt%). Additionally, two HTB651 glasses with 5.0 wt% TiO_2 but higher Al_2O_3 (12.0 wt%) or ZrO_2 (8.0 wt%) were formulated. The base-line glass was HTB651, a modification of HTB650 (Kim and Hrma, 1994), in which several minute species were removed from HTB650, including B_2O_3, MgO, CdO, K_2O, MoO_3, PbO, RuO_2, and WO_3. Appendix B6 summarizes the nominal compositions of twelve HTB561 glasses tested. Based on 5.0 Pa·s melt viscosity, all glasses had a vitrification temperature of 1350°C as estimated from the first-order mixture viscosity model.

2.6 CC103 Glass

Using high Cr_2O_3 waste, CC103-SY95SW, glasses were formulated with the waste loading from 30.0 to 55.0 wt%. Since CC103-SY95SW waste contained high concentration of Al_2O_3 (54.0 wt%), the glass melting temperature varied from 1150 to 1450°C based on each particular waste loading used in the formulation. The estimated melt viscosity at each specified melting temperature varied from 1.7 to 9.9 Pa·s. Appendix B7 summarizes the nominal compositions of the five CC103 glasses tested.

3. EXPERIMENTAL

3.1 Sample Preparation

Chemical reagents (oxides, boric acid, carbonates, and salts, cf. Appendix A) were used to prepare each glass batch which was blended in an agate disc mill for 4 min. In the study of phase segregation, batch size varied from 40.0 to 130.0 g as well as glass melting duration from 1 to 2 hr. Melting occurred in Pt-10%Rh crucibles except for WV182 glasses, for which alumina crucibles were used. To prepare glasses for viscosity and durability measurements, 500.0 g of glass was prepared. Glass was melted in a Pt-10%Rh crucible. To achieve composition homogeneity, molten glasses were quenched on a stainless steel plate after the first hour melting, and ground in a tungsten carbide disk mill for 5 min, and remelted for the second hour. The

crucibles were covered through the entire vitrification process.

For PFP1 glass melting, especially within the first hour, the crucible was periodically taken out of the furnace to visually examine the melt for phase segregation. Crystallinity of HTB651 based glasses were studied using isothermal 24 hr-heat treatments at and 100°C below the glass processing temperature (corresponding to viscosity of 5 Pa·s). PFP2 and CVS3 glasses were heat-treated using different center-line canister cooling (CCC) schedules as shown in Appendix C.

3.2 Characterization

Glass compositions were selectively analyzed using XRF/EDS (x-ray fluorescence with energy dispersive spectroscopy), and ICP/AES (inductively coupled plasma with atomic emission spectroscopy). An optical microscope, LECO® PGM-3, was used to characterize segregated a phase on the glass surface and crystals in the bulk. Segregated salt(s) and other crystalline phases were further analyzed using x-ray diffraction (XRD) and scanning electron microscopy with energy dispersive spectroscopy (SEM/EDS).

3.3 Melt Viscosity

Glass melt viscosities were measured using the standard test procedures, GDL-VIS Rev.0., in a temperature range ±150°C of the glass melting temperature. Using a Brookfield® DV-II viscometer, the viscosity measurements were performed in a Deltech® DT-31 furnace. The apparatus was calibrated using NBS 711 standard glass.

3.4 Chemical Durability

Duplicate samples were evaluated using 7-day product consistency test (PCT) (Jantzen and Bibler, 1990) in 90°C deionized water. Upon the completion of the PCT, the solution was filtered through a 0.45 μm membrane, and concentrations of cations (Si, Al, B, Na, Ca, P, S, and Cr) were analyzed using ICP/AES, from which normalized elemental mass losses, $(NL)_i$, were calculated according to :

$$(NL)_i = C_i / [\, f_i \cdot (S/V) \,] \qquad (2)$$

where C_i is the i-th element concentration (g/m^3) in the solution and f_i is the i-th element mass fraction in the glass.

Certain types of crystals in the CCC-treated or quenched glass samples may dissolve in water during sample prewashing for the PCT at room temperature. This may affect the final PCT

data. To examine the prewashing effect, rinse water was collected for each PCT sample of the CCC-treated PFP2 and CVS3 glasses, and concentrations of elements in rinse water were analyzed using ICP.

4. RESULTS AND DISCUSSION

This study covered a variety of waste streams and glass property measurements. For clarity, experimental results and discussion are going to be grouped in terms of properties instead of each individual type of waste and related glasses.

4.1 Molten Salt(s) Phase Segregation

Phase segregation of sulfate and phosphate was investigated in CCW, PFP1, and WV glasses at 1150°C. The primary segregated phase was Na_2SO_4 as identified by XRD. Glass composition effects on phase segregation is going to be addressed in terms of waste loading, glass basicity, alumina content, and phosphate content. And then the composition effect on sulfate solubility in glass is evaluated. The relationship between boric acid-induced melt foaming and phase segregation will also be addressed. The mechanisms of phase segregation are explored in connection with the study of PFP1 and WV glasses.

4.1.1 Composition Effect on Molten Salt(s) Phase Segregation

Segregated molten sulfate on the melt surface was observed in CCW1-(3-5) glasses with SO_3 content greater than 1.3 wt% (in batch). These higher sulfate glasses exhibited significant volatility at 1150°C. As a result, yellowish sulfate beads precipitated inside as well as outside the crucible on its walls. Results clearly showed that at 1150°C the phase segregation and volatility of sulfate increased with the increase of waste loading.

For the remaining CCW glasses with a fixed amount of sulfate (1.6 wt% in batch), the molten salt phase segregation was observed except in CCW2-1, the composition of which was on an immiscibility boundary established for high-level CVS glasses (Peeler and Hrma, 1994). A correlation between glass amorphous phase separation and molten sulfate segregation is not well understood at present. High boric acid and low sodium in CCW2-1 glass (cf. Appendix B1) suggested an effect of melt foaming on suppression of sulfate phase segregation (Li, et al., 1995a), which is going to be addressed in detail in section 4.1.3.

Water rinsing on the melt surface dissolved sulfate layer easily, and by doing so, another segregated phase, Li_3PO_4, was revealed on the melt surface (identified by XRD). The result suggested that both sulfate and phosphate segregated from the melt at the glass melting temperature.

4.1.2 Composition Effect on Sulfate Solubility in Glass

Sulfate content in each CCW glass was determined by XRF/EDS using a quenched glass sample without the segregated phase and is tabulated in Table 1. Each measured sulfate concentration can be approximately treated as a solubility limit for that particular glass based on the observations that an excessive amount of sulfate was separated out of the bulk of glass and no sulfate crystalline phase in glass was detectable under XRD. However, it should be noted that molten sulfate segregation started at an early stage of glass batch melting (see section 4.1.3), which might result in sulfate slightly under-saturated in glass.

Figure 1 shows that except for glasses in the waste loading series, correlations of sulfate solubility limit exist with glass basicity, alumina content, and phosphate content. The solubility of sulfate increases with an increase in either glass basicity (CCW2 glasses) or phosphate concentration (CCW4 glasses), but decreases with an increase in alumina content (CCW3 glasses).

Solubility of sulfate in simple silicate melts has been theoretically analyzed by Papadouplos (1973) and Krämer (1991). Under a given sulfate partial pressure, the solubility of sulfate was shown to be affected by the concentration of nonbridging oxygen, $Si\text{-}O^-$, in the glass network (Papadouplos, 1973). However, this model has shown to be applicable to sodium rich silicates, but not calcium rich silicates. Correlating the sulfate solubility with free oxygen concentration (O^{2-}) in the melt, or glass basicity, Krämer (1991) proposed that logarithmic sulfate solubility is linearly proportional to the glass basicity with a slope of one. Under a given sulfate partial pressure and melting temperature, the slope was experimentally found to be much greater, and yet the linearity was preserved (Krämer, 1991). In this study, a linearity is evident in CCW glasses as shown in Figure 1. The slope, however, varies according to the experimental series, and is even less than zero in case of the alumina content variation. Furthermore, no straightforward correlation exists between the basicity value and sulfate solubility in glasses with different waste loadings. Hence, the basicity model fails in complicated waste glass systems.

Currently, a better semi-empirical model is under development (Li, et al., 1995b) for borosilicate based waste glasses. It correlates the glass structure with the solubility of sulfate by considering influences from a variety of glass constituents (in terms of oxide), i.e., an overall glass structural effect on sulfate solubility. Preliminary results show that for CCW glasses, as well as low-level waste glasses (Li, 1995 and Feng, et al., 1995), the sulfate solubility correlates well with a glass structure factor, C_{NBO}^2/C_{BO}, (where C_{NBO} and C_{BO} are nonbridging and bridging oxygen concentration, respectively). Figure 2 represents that correlation, in which only two CCW glasses with high concentrations of phosphate do not fit. Investigation on structural interaction between phosphate and sulfate in borosilicate waste glasses is underway (Li, et al., 1995c).

4.1.3 Possible Mechanisms for Phase Segregation

Considering Na_2SO_4 is the primary segregated phase, it seems logical to relate the sulfate segregation to its solubility in glass. In the earlier study of CCW glasses discussed above, microscopic and visual inspections were made for each quenched glass after 60 min melting. To better understand the phase segregation process, it is desirable to examine the entire melting process. Hence, in the later study of PFP1 glasses, the crucible was periodically taken out of the furnace for visual inspection. Several melts were selectively chosen for microscopic examination as well.

Figure 3(a-c) illustrates the melting process of PFP1-7 glass spiked with 1.0 wt% SO_3. No phase segregation is evident during the entire glass melting process, indicating that sulfate was completely soluble in the melt. Similar results have been observed in low-level waste glass having high sulfate solubility limit (Feng, et al., 1995 and Li, et al., 1995c).

Figure 4(a-f) illustrates PFP1-1 glass batch melting and phase segregation process. At the beginning, batch melting occurred on the surface of batch pile only (including the contacting interface with the crucible wall, cf. Figure 4a). After 2 min (Figure 4b), droplets of yellowish sulfate could be seen. After 7 min, batch reaction appeared to be completed, and a significant amount of yellowish sulfate phase accumulated on the melt surface (Figure 4c). The sulfate accumulation proceeded further during the next 15 min (Figure 4d). Upon further melting, no detectable increase in the sulfate accumulation was found (Figures 4e and 4f). The sulfate retained in the melt was 0.86 ± 0.08 wt%.

A sample of the segregated layer was collected for phase analysis. Figure 5 illustrates

XRD patterns, identifying the two segregated phases as Na_2SO_4 and Na_3PO_4. This is further evidence that segregation of sulfate and phosphate occurred simultaneously as observed in CCW glasses (see section 4.1.1).

Sulfate solubility in PFP1-1 glass is expected to be higher than in PFP1-7, based on the proposed effect of nonbridging oxygen concentration (see section 4.1.2), since the former has relatively lower concentrations of sodium but higher concentrations of boron. Hence, the sulfate phase segregation in PFP1-1 melt is not expected under an assumption that sulfate solubility is a limiting factor. Figure 4(a-f) clearly demonstrates that phase segregation is a kinetic process occurring in an early stage of batch melting before a homogeneous melt occurs. Accordingly, the sulfate segregation can be affected by factors which influence the early stages of batch melting. Once sulfate is segregated out of the melt, it is difficult to be redissolved back into the melt. Hence, sulfate phase segregation is not governed by the sulfate solubility in glass.

Figures 6(a,b) illustrates optical micrographs of the surface and the bulk of the melts of PFP1-5 glasses, demonstrating an occurrence of melt foaming both on the surface and in the bulk during the glass melting. Various degrees of melt foaming were also observed in PFP1-4, -6, and -7 glasses. Although the extent of melt foaming varies among these glasses, a common feature was apparent, that the foaming was persistent during the entire melting process. All of these glasses showed no sulfate segregation from the beginning of the glass melting. In contrast, PFP1-1, -2, and -3 showed significant sulfate segregation, started from an early stage of glass melting, while no foam was observed. An example is shown in Figure 6(c,d) for PFP1-1 glass. A mild sulfate content in silicate glass was reported to suppress the melt foaming (Kim and Hrma, 1990, 1991 and 1992). The results from this study suggest that the melt foaming, on the other hand, can suppress sulfate segregation.

Although persistent melt foaming appears to be beneficial in suppressing sulfate segregation, foaming itself can be hazardous to the melter operation. Whether the melt foaming exists appears to be related to a ratio of B_2O_3 to Na_2O in PFP1 glasses. The ratio is high in PFP1-4 to -7 glasses, but significantly lower in PFP1-1 to -3 glasses. Furthermore, for glasses having the high ratio of B_2O_3/Na_2O, the extent of the melt foam was significantly reduced by deceasing the B_2O_3/Li_2O ratio in glass without changing Na_2O. An example is shown in Figure 7, demonstrating that PFP1-7 glass with a lower B_2O_3/Li_2O ratio had less foam than PFP1-4 with

a higher B_2O_3/Li_2O ratio.

Results discussed so far do not tell whether the two phases, sulfate and phosphate, were segregated independently or they were influenced by one another. In laboratory crucible testing, WV182 glasses with $SO_3 \leq 1.0$ wt% exhibited neither sulfate nor phosphate segregation at any level of alumina content. At the same phosphate level (2.6 wt% P_2O_5), but higher sulfate contents, 1.5 or 2.0 wt% SO_3, a yellowish molten sulfate phase segregated out of the melt. An example is shown in Figure 8 for WV182-4, -8, and -12 melted at 1150°C for 60 min. The melt surface area, covered by the segregated layer, appears to increase with alumina content (Figure 8). SEM/EDS analyses showed that EDS signals of Na, S, Ca, La, and P were significantly higher in the segregated phases as shown in Figure 9 (EDS signals of Cr, Fe, and Ni in Figure 9c resulted from spinel crystals trapped in the molten salt layer). The results not only reveal the simultaneous phase segregation of sulfate and phosphate, but also demonstrate that phosphate segregation was induced by the segregated sulfate. Furthermore, high Al_2O_3 increased the extent of phase segregation in WV glasses. The presence of Al_2O_3 is known to slow down the batch melting process (Takahashi, 1962). Since the phase segregation initiated at an early stage of batch melting, higher alumina content in batch delays the generation of a glass-forming melt, allowing more sulfate and phosphate to segregate from the melt.

4.2 Effects of Glass Composition and Temperature on Chromate Formation

In addition to segregation of sulfate and phosphate phases, chromate phase segregation, such as molten salt Na_2CrO_4, was also investigated using high chrome CC103 glasses. The investigation was primarily conducted by Nuclear Research Institute Řež (Czech Republic, cf. Vojtěch, et al., 1995) under a subcontract.

Choosing $Cr_2O_3.nH_2O$ hydroxide as a chemical source for Cr^{3+} in the batch, the conversion of Cr^{3+} to Cr^{6+} during batch melting was investigated using CC103-2 and CC103-3 glass compositions (cf. Appendix B7). Figure 10 illustrates chromate formed in the reacted batch versus batch reaction temperature for various experiment durations, which is expressed as CrO_3 in wt% related to the weight of the initial batch. Apparently, chromate formation is sensitive to temperature, time, and batch composition. Although the reaction of Cr^{3+}-Cr^{6+} was not in equilibrium at those temperatures studied, the formation of Cr^{6+} peaked at 600°C for CC103-2, and at 700°C for CC103-3, the positions of which seemed to be not affected by the reaction

equilibrium.

Below the peak temperature, an increase in Cr^{6+}, in a form of Na_2CrO_4, can be interpreted as a reaction of Cr_2O_3 with Na_2O under atmospheric oxygen. The rate of reaction increases as temperature increases. Above the peak temperature, a decrease in the Cr^{6+} fraction results from a shift of the redox equilibrium.

According to the trend depicted in Figure 10, the amount of Cr^{6+} in a molten glass should be negligibly small at temperatures greater than 1000°C. In fact, no chromate molten salt segregation was observed in the two glasses during vitrification at 1150 or 1450°C. According to these observations, it can be concluded that for a waste containing a high concentration of Cr_2O_3, chromate formation is unavoidable, but its related molten salt phase segregation is unlikely. However, it is still not certain whether chromate molten salt phase segregation occur in the large-scale vitrification of HLW waste containing high concentration of chromic anions, CrO_4^{2-}. Based on the current understanding (Darab, et al., 1995), chromium in borosilicate waste glass exists mostly in the form of Cr^{3+}, each of which associates with 6 oxygens. Combining the above results (Vojtěch, et al., 1995) with a pervious chromium spectroscopic study in borosilicate based waste glasses (Darab, et al., 1995), it can be further concluded that under a normal glass melting condition (ambient air), Cr^{3+} is the most stable form in HLW glasses regardless the oxidation state of the chromium in the batch. However, it is necessary to conduct further tests to examine whether chromate segregates from the melt in the large-scale vitrification of HLW waste containing a high concentration of chromate (instead of Cr_2O_3).

4.3 Crystallinity

Table 2 summaries results of the crystallinity study. Discussion will be divided into two subsections, crystallinity in quenched and 24-hr isothermal or the CCC-treated glasses.

4.3.1 Quenched Glass

In the bulk of CCW1-(4&5) glasses, Li_2SiO_3 and Li_3PO_4 were identified by XRD, with a greater proportion of Li_3PO_4. There were no crystals detectable by XRD in the bulk of CCW1-(1-3) glasses. The primary crystalline phase of Li_3PO_4 was also identified by XRD in the rest of CCW glasses. In CCW4-(1-3) glasses, two minor phases, $Ca_5(PO_4)_2SiO_4$ and $Ca_2P_2O_7$, were detected by XRD as well.

Crystallization of Li_3PO_4 in CCW1 glasses initiated when phosphate content was greater

than 1.0 wt% P_2O_5. However, the same phase formed at 0.5 wt% P_2O_5 in CCW4-1 glass. Comparison of compositions between CCW1-3 and CCW4-1 (Appendix B1) suggests that higher alumina, 7.64 wt%, in CCW4-1 might reduce phosphate solubility, resulting in formation of phosphate crystals at a lower P_2O_5 level. The adverse effect of Al_2O_3 on phosphate solubility in borosilicate based waste glass, such as CCW glasses, is not well understood. Based on previously published experimental results (Tomozawa, 1979), an incorporation of Al_2O_3 into silicate glass with phosphate (on an equal molar basis) was beneficial for the stability of phosphate in the glass network. Further investigation is needed to clarify this discrepancy for the role of alumina in silicate and in borosilicate glasses.

Crystallization of Li_3PO_4 was also found in PFP2 glasses with P_2O_5 ranging from 3.3 to 7.3 wt%. The amount of crystals increased with the increase of P_2O_5 content in glass (cf. Table 2). Also, Cr_2O_3 precipitated from all PFP2 melts, simply because its concentration was well above the solubility limit of Cr_2O_3 in borosilicate waste glasses, typically ≤ 1.0 wt% Cr_2O_3 (Li, et al. 1995b).

Concentrations of Li_2O and Al_2O_3 in CVS3 glasses were much lower compared with those in CCW and PFP2 glasses. However, CVS3 glasses had much higher concentrations of rare earths, RE (= La, Nd, Ce), which promoted crystallization of $Na_3RE(PO_4)_2$ as identified by XRD. The primary phase was $Na_3Nd(PO_4)_2$, and it increased, up to 7 vol%, with the increase of phosphate content (cf. Table 2). CVS3-40 glass with 9.0 wt% P_2O_5 also exhibited amorphous phase separation as shown in Figure 11.

$Na_3Nd(PO_4)_2$ was also found by XRD in HTB651 glasses spiked with P_2O_5. The amount of crystals increased from 10.0 to 25.0 vol%, while P_2O_5 increased from 5.0 to 9.0 wt%. In addition, HTB651-4 glass with 9.0 wt% P_2O_5 also exhibited amorphous phase separation as shown in Figure 12.

Eskolaite (Cr_2O_3) appeared to be soluble up to 0.8 wt% in HTB561 glass melted at 1350°C for as long as 24 hr. However, glass with 0.8 wt% Cr_2O_3 exhibited spinel crystals when heat-treated at a lower temperature, 1245°C (cf. 4.2.2). Crystallization of eskolaite (Cr_2O_3) were observed in CC103 glasses at all levels of Cr_2O_3 (≥ 4.1 wt%). An example is shown in Figure 13. Although Cr_2O_3 forms agglomerates, crystal settling was not observed. In CC103 glasses with waste loading at 45.0 wt% or higher, nepheline ($NaAlSiO_4$) was detected by XRD. Crystalline

phases of nepheline ($NaAlSiO_4$) and beta-eucryptite (β-$Li_2Al_2Si_2O_8$) were found in CC103-4 glass by XRD.

No crystals were detectable under both SEM and optical microscope in quenched HTB651 glasses with 1.0 - 8.0 wt% TiO_2, suggesting that 8 wt% TiO_2 in glass was soluble at the glass processing temperature.

4.3.2 Heat-Treated Glass

PFP2 glasses with various amounts of phosphate were treated using the canister-centerline-cooling schedule (CCC). Crystalline phases of $AlPO_4$, Li_3PO_4, and Cr_2O_3, were detected by XRD (cf Table 2). The total volume of the crystals in each CCC-treated glass sample was greater than that of the quenched sample with the same composition.

A primary crystalline phase of $Na_3Nd(PO_4)_2$ and two minor phases of $LiPO_3$ and $NdPO_4$ were found in CCC-treated CVS3 glasses. The total crystallinity increased with the increased phosphate content (cf. Table 2). Figures 14-17 illustrate SEM micrographs and EDS patterns of the treated CVS3 glass samples. Figure 14 shows spinel crystals, enriched in Cr, Mn, Fe, and Ni, in CVS3-37. An unidentified phase can be also seen, which is assumed to be similar to the phase found in the CCC-treated CVS3-38 glass (Figure 15). In CVS3-38 glass with higher phosphate content (5.0 wt% P_2O_5 compared to 3.0 wt% P_2O_5 in CVS3-37 glass), the same heat-treatment resulted in a larger spherical phase enriched in P, Ca, Nd, and Fe (Figure 15c). A similar spherical phase became even bigger in size in CVS3-39 glass with higher phosphate (7.0 wt% P_2O_5) after the same heat-treatment (Figure 16a). Overall, the spherical phase is enriched in P, Ca, Ce, and Nd (Figure 16b). It is also evident that elongated phosphate crystals precipitated in this glass (Figure 16a), which are enriched in P, Ce, and Nd. In CVS3-40 glass with the highest phosphate content (9.0 wt% P_2O_5), the CCC-treatment resulted in the formation of a large spherical phase as compared with that in the quenched glass (Figure 11). These spheres had similar compositions, both enriched in P, Ca, Nd, Fe, and Ni (Figures 17b and 17c).

Based on the morphology of these spherical phases and their compositions according to EDS analyses, it is likely that they separated from the melt at the processing temperature, and subsequently crystallized during melt cooling. In all of the CCC-treated CVS3 glasses, spinel phase was found by SEM/EDS and also detected by XRD in CVS3-39 and CVS3-40 with higher phosphate concentrations.

HTB651 glasses with P_2O_5 (5.0, 7.0, and 9.0 wt%), Cr_2O_3 (0.6 and 0.8 wt%), and TiO_2 (1.0, 3.0, and 5.0 wt%) were separately heat-treated at and 100°C below the melting temperature for 24 hr. For phosphate-spiked samples, no crystals were detectable under optical microscope using both treatments. However, XRD revealed the presence of $Na_3Nd(PO_4)_2$ as discussed previously for the quenched samples which were melted at 1350°C for 2 hr. The discrepancy may be related to different melt cooling rate. The rate of melt quenching for the 2 hr-melt was believed to be much lower than that of the 24 hr-melt because of the size of the former being 200 times larger than that of the latter.

For HTB651-6 glass with 0.8 wt% Cr_2O_3, the heat-treatment at 1245°C for 24 hr (100°C below the glass melting temperature) resulted in formation of spinel crystals as shown in Figure 18a. A majority of the crystals was at the bottom of the melt surrounding the surface of bubbles. EDS analysis (Figure 18c) suggested that the crystals belong to spinel crystal type, AB_2O_4, where A can be Mn and Ni, and B can be Cr and Fe (Evans, 1978). The crystals appeared to nucleate at the interface between the melt and the crucible wall, rather than settled from the melt. The connection between the crystals and bubbles suggests that the formation of spinel crystals released oxygen due to the reduction of the associated transition metal species, M (most likely Fe), according to the reaction (Schreiber, et al., 1986):

$$4M^{m+}_{(melt)} + 2n\ O^{2-}_{(melt)} = 4M^{(m-n)+}_{(melt)} + nO_{2\ (g)}\ . \qquad (3)$$

In CC103-2 glass with 4.1 wt% Cr_2O_3, both eskolaite (Cr_2O_3) crystals and a solid solution of Cr_2O_3-Fe_2O_3 were found after the heat-treatment at 1050°C for 24 hr (100°C below the glass melting temperature). The solid solution had the same crystal structure as eskolaite (Vojtěch, et al., 1995). In the CCC-treated CC103-2 glass, Cr_2O_3 and Cr_2O_3-Fe_2O_3 solid solution were also found (Figure 19a). In CC103-3 glass with 6.2 wt% Cr_2O_3, the heat-treatment at 1350°C for 24 hr (100°C below glass melting temperature) also resulted in crystallization of Cr_2O_3 and Cr_2O_3-Fe_2O_3 solid solution (Vojtěch, et al., 1995). However, the CCC-treatment almost devitrified the glass sample completely, in which beta-eucryptite (β-$LiAlSiO_4$) and nepheline ($NaAlSiO_4$) also formed (Figure 19b) in addition to Cr_2O_3 and Cr_2O_3-Fe_2O_3 solid solution.

For HTB651 glasses spiked with TiO_2 up to 5.0 wt%, no Ti-containing crystals were found using 24 hr-isothermal and CCC treatments. However, an isothermal treated sample with 8.0 wt% TiO_2 at a lower temperature, 1185°C, showed uniformly distributed TiO_2 crystals

precipitated from the melt as shown in Figure 20. The above results suggest that HTB651 glass with 5.0 wt% TiO_2 can be safely vitrified without a potential processing problem associated with crystallization of TiO_2. In addition, other types of non-titanium-bearing crystals were observed in HTB651 glasses spiked with TiO_2. HTB651-7 glass with 1 wt% TiO_2, after the isothermal treatment at 1339°C for 24 hr, had a small amount of isolated Ca-S bearing crystals (Figure 21). There was no evidence suggesting the connection between these crystals and TiO_2 in glass. In HTB651-9 glass with 5 wt% TiO_2, after the treatment at 1203°C for 24 hr, a cluster of ZrO_2 particles was found near the bottom of the melt (Figure 22). HTB651-12 glass samples with 5.0 wt% TiO_2 and 8.0 wt% ZrO_2 also showed ZrO_2 crystals after heat-treatments at 1328°C and 1228°C for 24 hr, respectively. Figure 23 shows the heat-treated HTB651-12 glass at 1328°C, demonstrating the settlement of ZrO_2 particles at the bottom of the melt. In all cases, it is likely that these ZrO_2 particles were undissolved batch material. No crystals were found in HTB651-11 glass samples with 5.0 wt% TiO_2 and 12.0 wt% Al_2O_3, which were treated at 1354°C and 1254°C for 24 hr, respectively.

4.4 Glass Melt Viscosity

4.4.1 Phosphate Effect

The Effect of P_2O_5 on glass melt viscosity was experimentally determined using PFP2, HTB651, CVS3, and CC103 glasses. Figures 24-26 illustrate the melt viscosities as a function of temperature for the three types of glasses with various amounts of phosphate. In all cases, incorporation of P_2O_5 into glass increases the melt viscosity. The phosphate effect can also be evaluated in terms of glass melting temperature at a given viscosity, such as at 5 Pa·s, which are also shown in these figures.

Glass melt viscosity increase with increased phosphate may be related to the reaction phosphorous with sodium. Phosphorous competing with silicon for sodium has been found by nuclear magnetic resonance (NMR) study of Na_2O-CaO-P_2O_5-SiO_2 glasses (Lockyer, et al., 1995), showing that phosphorous is preferentially bonded with alkali or alkaline earth cations in the network. Hence, the glass network is expected to be strengthened with reduced number of Na reacting with bridging oxygen, Si-O-Si.

4.4.2 Chrome and Titania Effect

Incorporation of Cr_2O_3 into HTB651 glass slightly decreased the viscosity of the baseline glass as shown in Figure 27. The role of Cr_2O_3 in borosilciate glass is either that of a glass former or a glass modifier, depending on glass composition (Li, et al., 1995d). Figure 28 illustrates the melt viscosity of CC103-2 and CC103-3 glasses. As shown by the results of CC103-2 glass, crystallization of Cr_2O_3 or Cr_2O_3-Fe_2O_3 did not alter viscous flow. However, this anomaly was observed in the lower temperature viscosity data of the CC103-3 melt, which can be attributed to crystallization of beta-eucryptite in the melt. In this case, the melt viscosity appeared to be reduced with the increase of beta-eucryptite crystals.

Titania has a negative effect on HTB651 glass melt viscosity as shown in Figure 29. Analogous to Cr_2O_3, TiO_2 in silicate glass plays a dual role, depending on glass composition. For a small fraction of TiO_2 (<1.0 wt%), more Ti^{4+} ions enter into the network forming positions than into the modifying positions, while the opposite is true at higher TiO_2 concentration (Morsi and El-Shennawi, 1984). The experimental data obtained here suggest that TiO_2 acts as a glass modifier in HTB651 glasses.

4.4.3 Prediction of Melt Viscosity using First-Order Mixture Model

Using the first-order mixture model for Arrhenius viscosity (Hrma, et al., 1994), the viscosity of a particular glass at the glass melting temperature was estimated, for which P_2O_5, TiO_2, and Cr_2O_3 were treated as components of Others. Figure 30 compares the predicted values with the experimentally determined. Overall, the predictions appears to underestimate glass melt viscosity, which increases with increasing concentration of phosphate in glass. A better predictability by the revised viscosity model considering the phosphate effect can be found in a separate report on HLW glasses (Vienna, 1995).

For glasses spiked with TiO_2, the predictions appears to be better at higher TiO_2 concentration. Since HTB651 glass contains no B_2O_3, which exceeded the model constraint for B_2O_3 (5.0 - 20.0 wt%), the effect is fortuitous.

The predictions for CC103-2 and -3 glasses with very high Cr_2O_3 concentrations are affected by the significant amount of Cr_2O_3 crystals in the melt. Furthermore, in CC103-3 glass (melted at 1450°C), the residual glass composition was changing with temperature due to the crystal growth of beta-eucryptite. Therefore, the viscosity can not be properly predicted by the

model.

4.5 Chemical Durability

The effect of composition on glass durability as treated by statistically designed experiments can be defined in two ways: an averaged compositional effect due to changes of several glass constituents and a single component effect due to a change of one component of interest in glass. The experimental design of CCW and CC103 glasses fits into the former, which is going to be addressed first. Then, the single component effect is to be examined using PFP2, CVS3, and HTB561 glasses, which cover the effects of phosphate, chrome, and titania.

4.5.1 Glass Composition Effect

Figure 31 illustrates 7-day PCT releases of Na, Li, B, S, and Cr for CCW1-(1-5) glasses as a function of waste loading. The releases increase with waste loading. CCW1 glasses had lower normalized Na releases than the EA glass, 6.67 g/m^2, when the waste loading was kept at or below 54.0 wt%. A significant deterioration in glass durability at higher waste loadings is apparent. At and below 54 wt% waste loading, glasses were free from crystals. Crystals of Li_2SiO_3 and Li_3PO_4 were found at higher waste loadings. Crystallization affects the residual glass composition, and in turn, results in either increasing glass durability by taking alkalis away from the network or decreasing glass durability by taking glass formers away from the network (Kim, Peeler and Hrma, 1995). In high waste loading CCW1 glasses with less than 2.0 vol% crystals, both Li and Si were extracted from the network via crystallization through which more Li was removed than Si. Furthermore, in terms of an individual effect of Li and Si on 7-day PCT glass durability, a removal of Li has a greater influence (Hrma, et al., 1994). Therefore, the observed durability deterioration can not be associated with the residual glass composition after crystallization of these two phases.

Figure 32 illustrates 7-day PCT data for CCW2-(1-4) glasses which had a wide range of glass basicities. A baseline glass, CCW1-4, is also included for comparison. In this case, sodium release has a similar trend as the release of sulfur. All CCW2 glasses had the same waste loading (67.0 wt%); glass durability appears to be improved by either a decrease or increase in glass basicity. A maximum release of Na was seen at a basicity of 36.2 kcal/avogadro bond.

Figure 33 shows a plot of 7-day PCT data versus alumina content for CCW3-(1-4) glasses. Contrary to expectation, glass durability is improved by reducing alumina content in the

baseline glass, and deteriorated as the alumina content increased. Once again, for all CCW3 glasses, sodium and sulfur releases have similar trends.

Figure 34 illustrates a comparison between the release of sodium and that of sulfur for CCW4-(1-3) glasses along with those of the baseline glass. Results show the durability of CCW1-4 glass being substantially improved by an addition of 8.0 wt% P_2O_5.

In CCW glasses formulated at 67.0 wt% waste loading, preferential dissolution of Na, Li, and S are apparent. Figure 35 plots concentrations of alkali ions in solution versus concentration of either sulfur or a sum of sulfur and phosphorous in solution after 7-day PCT. Because concentrations of sulfur and sodium in leachates are significantly higher in most cases, it was first assumed that the two species, Na and S, are released into water congruently, i.e., in a ratio of 2:1 between Na and S (based on analogy of dissolution of crystalline Na_2SO_4 in water). The slope, K_1, determined from a linear regression analysis (Figure 35a) suggests that the previous assumption should be further corrected by taking lithium (in solution) into account in order to balance sulfur in solution. The revised approach resulted in a higher ratio, K_2, between the total alkali in solution and sulfur released indicating alkali ion in excess. Alkalis in excess in leachates are not unexpected, which were not associated with sulfur in glass and could leach into water via ion-exchange with hydronium, H_3O^+, (Schnatter et al., 1988, Feng, 1991, and Li and Tomozawa, 1995). Furthermore, from XRD analysis, crystalline phase of Li_3PO_4 was detected in high phosphate glasses, and hence a small portion of lithium could leach into water from dissolution of Li_3PO_4 crystals.

To verify the contribution of Li_3PO_4 dissolution, Figure 35b shows concentration of (2S+3P) in leachate versus that of (Na+Li) in leachate. In this case, a ratio of lithium to phosphorous was assumed to be 3 : 1 based on Li_3PO_4 precipitated in these glasses. The identical slope, K_3, was obtained as compared with the K_2-value. Although there exists no difference statistically between the two treatments in data analyses (K_2 versus K_3), the third treatment was considered more appropriate based on XRD data. According to the result shown in Figure 35b, it can be concluded that the preferential dissolution of Na, Li, and S is mainly associated with R-O-S-O groups in the glass network, and the contribution of Li_3PO_4 crystals to lithium release is negligibly small.

Interestingly, PCT results show a correlation in dissolution of alkali species with that of

sulfur (SO_4^{2-}). The preferential dissolution of Na-O-S-O and Li-O-S-O can be further demonstrated in terms of the percentage of the elemental release into solution over its original concentration in glass. Figure 36 illustrates the percentage of releases of sulfur, sodium, and lithium against that of boron release (a representative of the glass network) for CCW glasses. The results are consistent with the previous conclusion that alkali-sulfate groups dissolved faster than the network, and also indicate that the concentration of Na-O-S-O in glass is greater than that of Li-O-S-O.

The observed parallel trends between sodium and sulfur releases in CCW glasses suggest that Na-O-S-O groups formed in glass are highly soluble in water, and there exists some degree of clustering for these Na-O-S-O groups, and yet the clusters have not become crystalline Na_2SO_4 based on the XRD results. Formation of Na-O-S-O groups has been recently confirmed in borosilicate waste glasses (Darab, et cl., 1995). Another possibility is that fracture surfaces created by glass crushing pass through the Na-O-S-O enriched areas. However, preferential sulfur leaching did not occur in other types of borosilcate waste glasses with a comparable level of sulfate (Li, et al, 1995e). Hence, the role of glass composition on the behavior of sulfur-bearing species is still not well understood.

The effect of waste loading was also studied in CC103 glasses. Figure 37 illustrates 7-day PCT releases of Si, B, Na, and Li as a function of waste loading. Apparently, glass durability deteriorates sharply once the waste loading is above 45.0 wt%. Solution pH also jumped to a corresponding higher level. Crystals of Cr_2O_3 were found in all glasses, which appeared not to affect glass durability according to the PCT data at lower waste loading. At the waste loading of 50.0 wt%, nepheline ($NaAlSiO_4$) crystallized in quenched CC103 glasses (cf. Table 2), which in turn reduce Al and Si in the residual glass matrix and is the main factor causing a great reduction in glass durability (Kim, Peeler and Hrma, 1995, and Bailey and Hrma, 1995). This was confirmed in CC103-4 glass with 55.0 wt% waste loading, which had the greatest amount of nepheline crystals, and the glass durability further decreased by about 100% as compared with that of CC103-3. The detrimental effect of nepheline formation on durability of borosilciate HLW glasses was studied in detail by Kim, Peeler and Hrma (1995), and Baily and Hrma (1995).

Summarizing the effect of composition on glass durability, the above results clearly show that by manipulating glass composition, glass durability can be improved significantly.

Additionally, nepheline formation should be avoided because of its detrimental effect on glass durability.

4.5.2 Single Component Effect

4.5.2a Phosphate

Three types of HLW glasses were used to evaluate the effect of phosphate on chemical durability assessed by 7-day PCT, including PFP2, CVS3, and HTB651 glasses. Depending on glass composition, the phosphate effect varies, which is discussed in detail in the following.

Figure 38 illustrates dissolution of Si, B, Li, and P of PFP2-(1-3, and 5) glasses both as quenched and CCC-treated, along with pH values of solutions after the test. For the quenched samples, phosphate in glass did not affect glass durability. The primary crystalline phases in these glasses are Li_3PO_4 and Cr_2O_3, both of which have a very limited solubility in water. Concentrations of PO_4^{3-} anions in the solution increased with phosphate content in glass, and in turn decreased solution pH as shown in Figure 38(A2). However, in CCC-treated samples, phosphate adversely affected glass durability as shown in Figure 38(B1). In the CCC-treated samples, in addition to Li_3PO_4 and Cr_2O_3, AlJ_3PO_4 crystals also formed, taking aluminum from the glass matrix. Previous study (Kim, Peeler, and Hrma, 1995) showed that a crystalline phase has a detrimental effect on glass durability if it removes glass former oxides from the glass matrix, and leaves the residual glass matrix rich in alkali species. No direct correlation of glass dissolution with solution pH was observed for quenched and treated samples,.

Figure 39 represents the effect of phosphate on CVS3 glasses both quenched and CCC-treated. For the quenched glasses, the results suggested that crystallization of $Na_3RE(PO_4)_2$ was beneficial, which strengthened residual glass network by taking Na from glass. However, for the CCC-treated samples, lithium and phosphorous releases were significantly higher for samples with higher phosphate contents.

Figure 40 illustrates a ternary phase diagram of a submixture of $(Na+Li_{(equivalent)})$-SiO_2-B_2O_3 established for similar HLW glasses according to Peeler and Hrma (1994). Based on information of semi-quantitative XRD data on crystallinity in the CCC-treated samples (cf. Table 2), the submixture of the residual glass compositions was determined (cf. Figure 40), in which the position of CCC-treated CVS3 glasses moves towards the glass immiscibility boundary with increased phosphate content and hence increased phosphate-bearing crystals in glass, suggesting

that the treated glasses were prone to amorphous phase separation, which were confirmed by SEM results shown in Figures 14-17. Accordingly, preferential dissolution of Li and P can be attributed to the amorphous phase separation. Similar to the previous case of PFP2 glasses, there appeared to be no correlation between solution pH and glass dissolution.

Figure 41 illustrates normalized releases of Si, Al, and Na, and solution pH values versus phosphate content in HTB651 glasses. In contrast to the previous glasses, phosphate in HTB651 glasses appears to be beneficial, i.e., sodium release decreased with the increase of the phosphate content. Since all glasses contained $Na_3Nd(PO_4)_2$ crystals, which increased with the increase of the phosphate content, it is expected that the residual glass matrix should have a less sodium and hence, the network is strengthened. On the other hand, crystalline $Na_3Nd(PO_4)_2$ appears to be at least as durable as residual glass matrix. HTB651-5 glass with 9.0 wt% P_2O_5 exhibited amorphous phase separation as shown in Figure 12. Similar to the case of CCC-treated CVS3-37 (cf. Figure 37[B1]), amorphous phase separation did not lower glass durability. No correlation of solution pH and glass dissolution was found in this case.

To summarize the effect of phosphate on glass durability, two important conclusion can be drawn from this investigation. First, below phosphate solubility limit, phosphate in glass had a negligible effect on glass durability. Secondly, crystallization of phosphate-bearing species in glass with phosphate in excess of its solubility limit ultimately changed the residual glass composition in such a way that can either improve or deteriorate glass durability, depending on the crystalline phases and their concentrations in the glass. Crystalline $Na_3Nd(PO_4)_2$ was shown at least as durable as strengthened residual glass matrix, while Li_3PO_4 was more soluble in hot water compared to its surrounding residual glass matrix.

4.5.2b Chrome and Titania

Although the amount of soluble Cr_2O_3 and TiO_2 in glass affected glass melt viscosity as shown previously, their influence on glass durability was negligibly small, as illustrated in Figures 42 and 43. The presence of either Cr_2O_3 or TiO_2 in glass was previously reported to affect glass durability to some extent, depending on the glass composition (Li, et al., 1995e, and Rao, 1963). Based on the current results, it appears that Cr_2O_3 and TiO_2 in borosilicate based HLW glass do not deteriorate glass durability significantly.

4.5.3 Prediction of Glass Dissolution using First-Order Mixture 7-Day PCT Model

Using the first-order mixture model of 7-day PCT sodium and boron releases (Hrma, et al., 1994), dissolution of glasses investigated in this study was predicted based on nine major oxide components and Others. Figure 44(a,b) illustrates the predicted versus the measured sodium releases for HTB651 and CVS3 glasses. Considering the composition range, some of which exceeded the constraints of the model applicability, the predictability was reasonably good, within about a factor of two. However, for same CCW, CC103, and PFP2 glasses, predictions were not so close to the measurements as shown in Figure 44(c-e). For CCW glasses, the prediction on boron release appears to be higher, while much lower on sodium release. In these predictions, neither crystallization nor liquid phase separation were taken into consideration. Hence, the predictability can be significantly affected by these two phenomena. However, in the worst cases, the prediction of sodium release was about a factor of ± 10. By considering the effect of crystallization on the residual glass composition, the model predictability can be significantly improved according to a previous study on HLW glasses (Bailey and Hrma, 1995).

4.5.4 Examination of the Impact of Sample Washing on 7-day PCT Results

The CCC-treated glass samples had crystals which may dissolve in rinse water during the sample preparation for PCT. If so, the PCT results obtained from washed particles of glass would not give a complete description of the effect of crystallization on glass durability. Appendix F summarizes the normalized releases of B, Li, Na, P, and Si in solution collected from rinse water of CCC-treated PFP2 and CVS3 glasses. For the CCC-treated PFP2 and CVS3 glasses, the normalized lithium loss from particle washing was at the most 10% (release of lithium from the PCT test was the highest in most cases). Additionally, quenched HTB651 glasses were also examined (cf. Appendix F), in which the normalized sodium loss from powder washing is less than 10%. Based these results, it was concluded that alkali losses from particle washing does not affect the outcome of 7-day PCT results in this study. However, the obtained results should not be over-generalized. In cases where glass contains much higher concentrations of soluble crystals, it is recommended to modify the PCT procedures by washing the sample in acetone rather than water and ethanol in order to obtain more accurate durability test results.

5. CONCLUSIONS

In FY94 and FY95, under the HLW minor component project, seven borosilicate based HLW glass systems were investigated, which covered several Hanford wastes: complexant concentrate waste (CCW and CC103-SY92SW), plutonium finishing plant waste (PFP), and double shell tank/single shell tank blended waste (DST/SST). In addition, a West Valley HLW glass was studied. Several conclusions can be drawn from the research results as follows:

5.1. Molten Salt Phase Segregation

Sulfate segregation during HLW waste vitrification is a kinetic process, which initiates at an early stage of the batch melting. Accumulation of segregated sulfate tends to flow toward molten glass surface, especially at the top of the melt, and is followed by sulfate evaporation. The overall segregation extent depends on glass composition. However, its composition dependency significantly differs from the composition dependency of sulfate solubility in glass. Alumina in glass enhances the sulfate segregation, while batches containing high boric acid and low sodium can suppress the segregation, which appears to be associated with the melt foaming. Glass formulation can be optimized to control melt foaming and suppress the sulfate segregation. Molten sulfate segregation has been found to promote segregation of phosphate-rich phases, including alkali-/alkaline- and rare earth- phosphates. An increase in alumina content in glass enhances the overall segregation of both sulfate and phosphate phases.

5.2 Composition Dependency of Sulfate in Glass

Sulfate solubility in glass varies significantly with glass composition (0.5 - 1.4 wt% SO_3), especially with phosphate content (up to 1.4 wt% SO_3). Various component effects on sulfate solubility were investigated in terms of glass basicity, alumina concentration, and phosphate concentration. With the exception of high phosphate glasses, sulfate solubility can be predicted (correlated with glass composition) using a semi-empirical model based on glass structure. Based on the current understanding, sulfate solubility in borosilciate waste glass is affected by the concentrations of non-bridging and bridging oxygen. Sulfate solubility in glass increases with the increase of nonbridging oxygen in glass. Increasing phosphate content in glass appears to increase sulfate solubility (~1.4 wt% SO_3); without phosphate, the solubility would be much lower (0.9 wt% SO_3) in a glass of identical ratio of nonbridging over bridging oxygen.

5.3 Chromate Formation during Batch Reaction

Chromate formation in early stages of vitrification is inevitable. The fraction of chromate (Na_2CrO_4) peaks at a temperature about 650°C, depending on the glass composition. A process of chromate formation (from Cr_2O_3) was transient, decreasing with further increase of temperature. At the glass processing temperature, the fraction of chromate is negligibly small; the most stable form in ambient air is Cr^{3+}. For CC103 glasses initially containing high concentrations of Cr_2O_3, no chromate phase segregation was observed. However, an additional study is necessary to evaluate a tendency of chromate molten salt segregation in waste streams containing high concentrations of CrO_4^{2-} anion.

5.4 Effects of Minor Components on Crystallization

Crystallization of certain phases containing minor components in HLW glasses is a complex process which depends on the temperature, thermal history of glass, the concentration of minor components in glass, and concentrations of other glass components. Results from this study show that the limiting factors to phosphate solubility in glass are the concentrations of Na, Li, La, Nd, and Al. Further, Cr_2O_3 generally precipitates from the melt during cooling, yet settling of fine Cr_2O_3 crystals (~10 μm) was not observed. However, in glass with higher concentrations of Mn, Ni, and Fe, spinel crystals are found mostly at the bottom of the melt after 24 hr of melting. These crystals appeared to be nucleated at the interface between the molten glass and the crucible wall. Finally, solubility of TiO_2 in borosilciate based HLW glasses was found to be much greater than 1.0 wt% previously considered. In this study, high melting temperature glass dissolved as much as 5.0 wt% TiO_2 without precipitating any titanium associated crystalline phases during melting times as long as 24 hr at 1250 and 1350°C.

5.5 Effects of Minor Components on Glass Melt Viscosity

The effect of minor components on glass melt viscosity depends on glass composition. The glass melting temperature at 5 Pa.s increased approximately 6°C per wt% P_2O_5 addition in CVS3 glass, by 3°C in HTB651 glass, and by 2°C in PFP2 glass. The effect of Cr_2O_3 was negligibly small. Formation of Cr_2O_3 crystals did not change the normal Arrhenius behavior of glass viscous flow at high temperature. A negative effect of TiO_2 on glass viscosity was established for HTB651 glass, approximately 10°C decrease per wt% TiO_2 within the measured temperature range.

5.6 Effects of Minor Components on Glass Durability

The impact of sulfate on glass durability appears to be strongly glass composition dependent. For CCW glasses, two distinct dissolution mechanisms were observed, one by network dissolution, the other by preferential leaching of Na-O-S-O and Li-O-S-O. The preferential leaching, however, is not associated with crystals of Na_2SO_4 and Li_2SO_4 in glass, suggesting that clusters of Na-O-S-O and Li-O-S-O may exist in glass. Micro-channels of these clusters, which permit a high leaching rate of these species from the glass matrix, are suspected. Chemical durability of HLW glasses is affected by phosphate. For a glass with a small amount of phosphate crystals, Na_3PO_4 and/or Li_3PO_4, glass durability is either unchanged or improves slightly, which can be explained by the removal of alkali oxides from glass matrix resulting in a stronger residual glass network. However, for a glass with a large amount of these crystals, glass durability deteriorated. In addition, for glass containing high P_2O_5, crystallization of either $AlPO_4$ or $NaAlSiO_4$ occurs in slow cooled glass samples (using the canister centerline cooling treatment). In both cases, crystallization is detrimental to glass durability, resulting in a sharp increase (up to a factor of 10) in normalized boron release from the 7-day PCT. The deterioration of glass durability in the latter case can be also related to weakening of the glass network as a result of the removal of Al or Si from the glass matrix by crystallization. In HLW glasses spiked with Cr_2O_3 (up to 0.8 wt%) and TiO_2 (up to 5 wt%), no impact on glass durability was found.

6. REFERENCES

Bailey, A.W. and P. Hrma (1995). "Waste Loading Maximization for Vitrified Hanford HLW Blend" Proceedings in *International Symposium on the Environmental Issues and Waste Management Technologies in Ceramic and Nuclear Industry*, American Ceramic Society, Columbus, OH (in press).

Balmer, M.L. and B.C. Bunker (1995) Inorganic Ion Exchange Evaluation and Design - Silicotitanate Ion Exchange Waste Conversion, Prepared for the U.S. Department of Energy under Contract DE-AC06-76RLO 1830, a milestone number TWTSPP-94-118, January.

Bunker, B.C. (1994). Evaluation of Inorganic Ion Exchanger for Removal of Cesium From Tank Wastes, Prepared for the U.S. Department of Energy under Contract DE-AC06-76RLO 1830, a milestone number TWRSSP-94-085, Pacific Northwest Laboratory, Richland, WA, September.

Bunnell, L.R. (1988) Laboratory Work in Support of West Valley Glass Development Prepared for the U.S. Department of Energy under Contract DE-AC06-76RLO 1830, PNL-6539, UC-510., Pacific Northwest Laboratory, Richland, WA.
Bickford, D.F., A. A. Applewhite, C.M. Jantzen and K.G. Brown. 1990. "Control of Radioactive Waste Glass Melters: I, Preliminary General Limits at Savannah River," J. Am. Ceram. Soc., 73(10) : 2896-2902.

Darab, J.G., H. Li, D.W. Matson, P.A. Smith and R.K. MacCrone (1995). "Chemical and Structural Elucidation of Minor Components in Simulated Hanford Low-Level Waste Glasses" (invited presentation), Proceedings in *Application of Synchrotron Radiation in Chemistry and Related Fields*, 201th American Chemical Society Annual Meeting, Chicago, IL (in press).

Evans, R.C. (1964) An Introduction to Crystal Chemistry 2nd Edition, Cambridge University Press, London, p.171-174.

Feng, X. (1991) "Effects of pH on the Leaching Mechanism of Nuclear Waste Glasses." in *Ceramic Transactions, Nuclear Waste Management IV*, Vol. 23, ed. by G.G. Wicks, D.F. Bickford, and L.R. Bunnell, Am. Ceram. Soc. Columbus, OH. p. 95-104.

Feng, X., P.R. Hrma, M.J. Schweiger, D.K. Peeler, S.E. Palmer, B.P. McGrail, D.E. Smith, D.S. Kim, Y. Peng, and H. Li (1995). Evaluation of Phase II Glass Formulations for Vitrification of Hanford Site Low-Level Waste, Prepared for the U.S. Department of Energy under Contract DE-AC06-76RLO 1830, a milestone number PVTD-T3B-95-206, Pacific Northwest Laboratory, Richland, WA, August.

Lockyer, M.W.G., D. Holland, and R. Dupree (1995) "NMR Investigation of the Structure of Some Bioactive and Related Glasses" J. Non-Crystal. Solids, 188 : 207-219.

Hrma, P.R., G.F. Piepel, M.J. Schweiger, D.E. Smith, D.S. Kim, P.E. Redgate, J.D. Vienna, C.A. LoPresti, D.B. Simpson, D.K. Peeler and M.H. Langowski. (1994) Property/Composition Relationships for Hanford High-Level Waste Glasses Melting at 1150°C Vol. 2, PNL-10359, Pacific Northwest Laboratory, Richland, WA, December.

Jantzen, C.M., and N.E. Bibler (1990) Nuclear Waste Glass Product Consistency Test (PCT) Method, Version 3.0(U)." WSRC-TR-90-539 Rev. 1, Savannah River Laboratory, Alkene, South Carolina.

Kim, D.S. and Hrma, P. (1991), "Foaming in Glass Melts Produced by Sodium Sulfate Decomposition under Isothermal Conditions," J. Am. Ceram. Soc., Vol. 74, 551-555.

Kim, D.S. and P. Hrma (1992) "Foaming in Glass Melts Produced by Sodium Sulfate Decomposition under Ramp Heating Conditions" J. Am. Ceram. Soc., 75: 2959-2963.

Kim, D.S. and P. Hrma, (1990). "Volume Changes During Batch to Glass Conversion," Ceramic Bulletin, 69[6]: 1039-1043.

Kim, D.S. and P. Hrma (1994). PNL Vitrification Technical Development Project (PVTD) High-Waste Loaded High-Level Waste Glasses for High-Temperature Melter. Prepared for the U.S. Department of Energy under Contract DE-AC06-76RLO 1830, a milestone number PVTD C94-03.01Y, Pacific Northwest Laboratory, Richland, WA, July.

Kim, D.S., D.K. Peeler, and P. Hrma. (1995) "Effect of Crystallization on the Chemical Durability of Simulated Nuclear Waste Glasses." *International Symposium on the Environmental Issues and Waste Management Technologies in Ceramic and Nuclear Industry*, American Ceramic Society, Columbus, OH (in press).

Krämer, F.W. (1991) "Contribution to Basicity of Technical Glass Melts in Relation to Redox Equilibria and Gas Solubility" Glastech. Ber., 64 : 71-80.

Labarbe, P.D., J.S. Lin, and A.F. Wright (1988). "Small Angle Neutron Scattering Study of Phase Separation in the Binary Glass System TiO_2-SiO_2." Phys. Chem. Glasses., 29 : 91-99.

Lambert, S.L. and D.S. Kim (1994). Tank Waste Remediation System High-Level Waste Feed Processability Assessment Report, WHC-SP-1143, Westinghouse Hanford Company, Richland, WA, December.

Langowski, M.H., J.D. Vienna, P.R. Hrma, G.F. Piepel, and E.V. Morrey (1994) PNL Vitrification Technical Development Project (PVTD) - The Glass Composition Envelope Definition (GCED) Fiscal Year 1994 (FY 94) Test Plan, Prepared for the U.S. Department of Energy under Contract DE-AC06-76RLO 1830, a milestone number PVTD C94-03.01E Rev. 1, Pacific Northwest Laboratory, Richland, WA, April.

Li, H. (1995) Letter Report - Minor Component Study for Low-Level Radioactive Waste Glasses, Prepared for the U.S. Department of Energy under Contract DE-AC06-76RLO 1830, a milestone number PVTD C95-02.01B, Pacific Northwest Laboratory, Richland, Washington, December.

Li, H., M.H. Langowski and P.R. Hrma (1995a). "Segregation of Sulfate and Phosphate in the Vitrification of High-Level Wastes" Proceedings in *International Symposium on the Environmental Issues and Waste Management Technologies in Ceramic and Nuclear Industry*, American Ceramic Society, Columbus, OH (in press).

Li, H., M.H. Langowski, P.R. Hrma, and X. Feng (1995b). "Sulfate in Simulated Nuclear Waste Glasses, I. Composition Effect on Solubility of Sulfate." (manuscript in preparation and to be submitted to J. Am. Ceram. Soc.)

Li, H., J.G. Darab, D.W. Matson, S.K. Sharma, P.A. Smith, P.R. Hrma, Y.L. Chen and J. Liu (1995c) "Phosphate-Sulfate Interaction in Low-Level Simulated Nuclear Waste Glasses" Proceedings in *Scientific Basis for Nuclear Waste Management XIX*, Materials Research Society Fall Meeting, Boston, MA (manuscript in preparation).

Li, H., J.G. Darab, P.A. Smith, M.J. Schweiger, D.E. Smith, and P.I. Hrma. (1995d) "Effect of Minor Components on Vitrification of Low-Level Simulated Nuclear Waste Glasses" Proceedings in *36th Annual Meeting of Institute of Nuclear Materials Management*, Palm Desert, CA (in press).

Li, H., J.G. Darab, P.A. Smith, X. Feng, and D.K. Peeler. (1995e) "Chemical Durability of Low-Level Simulated Nuclear Waste Glasses with High Concentrations of Minor Components" Proceedings in *36th Annual Meeting of Institute of Nuclear Materials Management*, Palm Desert, CA (in press).

Li, H. and M. Tomozawa (1995). "Chemical Durability of Simulated Nuclear Waste Glasses Containing Water." Proceedings in *International Symposium on the Environmental Issues and Waste Management Technologies in Ceramic and Nuclear Industry*, American Ceramic Society, Columbus, OH (in press).

Morsi, M.M., and A.W.A. El-Shennawi (1984) "Some Physical Properties of Silicate Glasses Containing TiO_2 in Relation to Their Structure" Phys. Chem. Glasses, 25[3] : 64-68.

May, T.H. and R.A. Watrous (1992) Hanford Waste Vitrification Plant Feed Processability Assessment, WHC-SP-0705, Westinghouse Hanford Company, Richland, WA, July.

Papadopoulos, K. (1973) "The Solubility of SO_3 in Soda-Lime-Silica Melts" Phys. Chem. Glasses, Vol. 14, 60-65.

Peeler, D.K. and P.R. Hrma (1994) "Predicting Liquid Immiscibility in Multicomponent Nuclear Waste Glasses." in *Environmental and Waste Management Issues in the Ceramic Industry II*, Ceramic Transactions, Vol. 45, ed. by D. Bickford, S. Bates, V. Jain and G. Smith, Am. Ceram. Soc., Westerville, OH, p. 219-229.

Perez, J.M., Jr., (1985). "West Valley Pilot-Scale Melter Experiment PSCM-19/19E Run Summary" Report, 7H35-85-2, January, PNL, Richland, WA.

Rao, B.V.J. (1963) "The Dual Role of Titanium in the System K_2O-SiO_2-TiO_2." Phys. Chem. Glasses, 4(1): 22-34.

Schreiber, H.D., S.J. Kozak, R.C. Merkel, G.B. Balazs and P.W. Johns, Jr., (1986) "Redox Equilibrium and Kinetics of Iron in a Borosilicate Glass-Forming Melt." J. Non-Cryst. Solids 84 : 186-195.

Schnatter, K.H., R.H. Doremus and W.A. Lanford (1988) "Hydrogen Analysis of Soda-Lime Silicate Glass." J. Non-cryst. Solids., 102 : 11-18.

K. Takahashi, K. (1962) "Binary Phosphate, Silicophosphate, Borophosphate, and Aluminophosphate Glasses, Their Properties and Structure," *Advances in Glass Technology*, Am. Ceram. Soc., Columbus, OH, p. 366-376.

Tomozawa, M. (1972) "Effects of Oxide Nucleation Agents on Phase Separation of Simple Glass Systems" *Advances in Nucleation and Crystallization in Glasses*, L.L. Hench and S.W. Freiman, eds., Am. Ceram. Soc., Columbus, Ohio, pp. 41-50.

Vienna, J.D., P.R. Hrma, M.J. Schweiger, M.H. Langowski, C.Y. Chang, D.S. Kim, P.E. Redgate, G.F. Piepel, D.E. Smith, and H. Li, (1995) Effect of Composition and Temperature on the Properties of High-Level Waste (HLW) Glasses Melting above 1200°C Prepared for the U.S. Department of Energy under Contract DE-AC06-76RLO 1830, a milestone number PVTD C95-02.01E, Pacific Northwest Laboratory, Richland, WA, September.

Vojtěch, O, J. Süssmilch, Z. Urbanec, and P. Novy (1995) The Effect of Chromium Oxide on the Properties of Simulated Nuclear Waste Glasses, Final Report Prepared for Battelle Memorial Institute, Pacific Northwest Laboratory, under Contract No. 209344-A-F1, Nuclear Research Institute, Řež, Czech Republic, July.

Table 1 SO3 Content (wt%) in CCW Glasses

Glass ID	SO3 (nominal)	SO3 (measured)
CCW1-1	0.67	0.66
CCW1-2	1.00	0.94
CCW1-3	1.30	1.17
CCW1-4(1)	1.60	1.09
CCW1-4(2)	1.60	1.06
CCW1-4(3)	1.60	0.96
CCW1-4(4)	1.60	1.03
CCW1-5	1.90	1.06
CCW2-1	1.60	0.64
CCW2-2	1.60	0.85
CCW2-3	1.60	1.13
CCW2-4	1.60	1.34
CCW3-1	1.60	1.13
CCW3-2	1.60	1.02
CCW3-3	1.60	1.01
CCW3-4	1.60	0.89
CCW4-1	1.60	1.04
CCW4-2	1.60	1.15
CCW4-3	1.60	1.36

(Experimental error within 10 %)

Table 2 XRD Results of Crystalline Phases in Selected HLW Glasses

Glass ID	PFP2-2		PFP2-3		PFP2-4		PFP2-5	
P2O5 (wt%)	3.3	3.3	5.3	5.3	5.5	5.5	7.3	7.3
Treatement	Quenched	CCC-treated	Quenched	CCC-treated	Quenched	CCC-treated	Quenched	CCC-treated
Major Crystalline Phases (wt%)		80Cr2O3 20unknown	75Cr2O3 25Li3PO4	30Cr2O3 20Li3PO4 50AlPO4	65Cr2O3 35Li3PO4	40Cr2O3 40Li3PO4 20AlPO4	55Cr2O3 45Li3PO4	20Cr2O3 50Li3PO4 30AlPO4
Total Vol (%)	0.0	7.0	6.9	17.0	7.7	14.0	9.4	16.0

Glass	CVS3-37		CVS3-38		CVS3-39		CVS3-40	
P2O5 (wt%)	3.0	3.0	5.0	5.0	7.0	7.0	9.0	9.0
Treatement	Quenched	CCC-treated	Quenched	CCC-treated	Quenched	CCC-treated	Quenched	CCC-treated
Major Crystalline Phases (wt%)		43Na3Nd(PO4)2 43Li3PO4 14NdPO4	100Na3RE(PO4)2	54Na3Nd(PO4)2 25Li3PO4 21NdPO4	100Na3RE(PO4)2	52Na3Nd(PO4)2 17Li3PO4 23NdPO4 8spinel	100Na3RE(PO4)	61Na3Nd(PO4)2 17Li3PO4 10NdPO4 12spinel
Total Vol (%)	0.0	2.0	1.0	7.0	3.0	17.0	7.0	22.0

Glass	CC103-2		CC103-3		CC103-4	CC103-5
Al2O3 (wt%)	16.2	16.2	4.8	4.8	6.2	7.6
Cr2O3 (wt%)	4.1	4.1	6.2	6.2	6.9	7.6
Na2O (wt%)	6.3	6.3	11.2	11.2	11.2	11.2
Treatement	Quenched	CCC	Quenched	CCC	Quenched	Quenched
Major Crystalline Phases (wt%)	100Cr2O3	100Cr2O3	100Cr2O3	Cr2O3 beta-LiAlSiO4 Li2Al2Si2O8 NaAlSiO4	90Cr2O3 10NaAlSiO4	35Cr2O3 45NaAlSiO4 20Li2Al2Si2O8
Total Vol (%)	<10		10.0	> 10.0	20.0	80.0

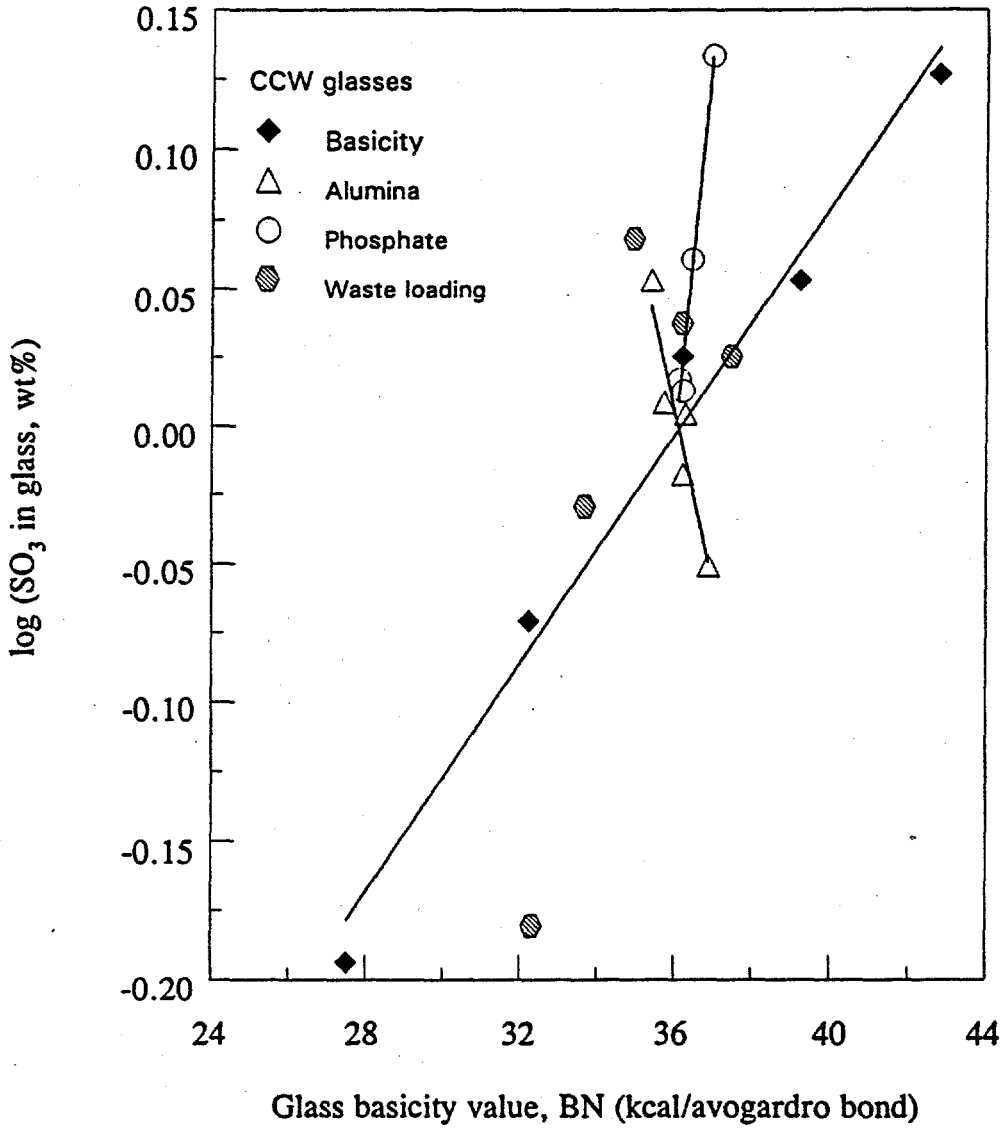

Figure 1. Sulfate solubility limits in CCW glasses as a function of glass basicity.

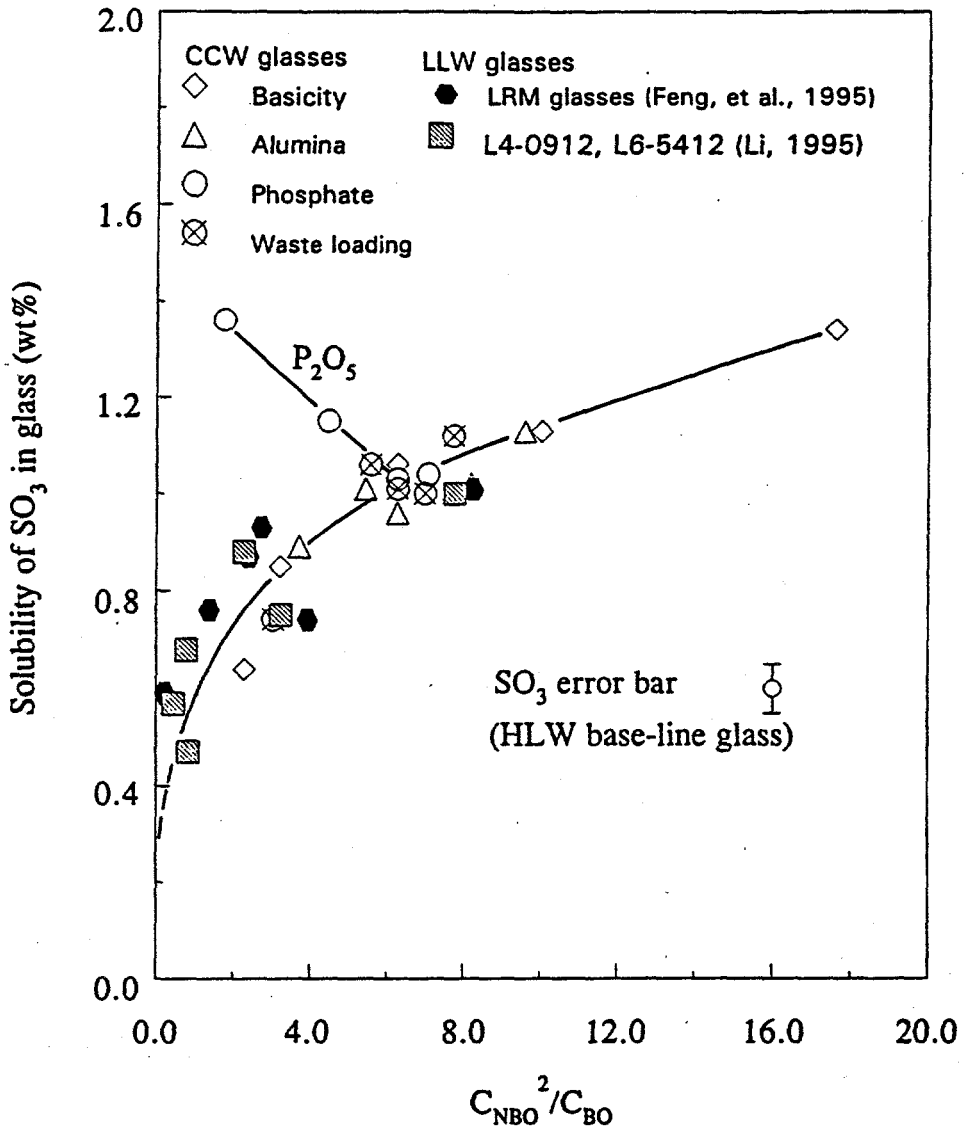

Figure 2. Sulfate solubility limits in CCW glasses as a function of C_{NBO}^2/C_{BO} (where C_{BNO} and C_{BO} are the concentrations of nonbridging and bridging oxygen in glass).

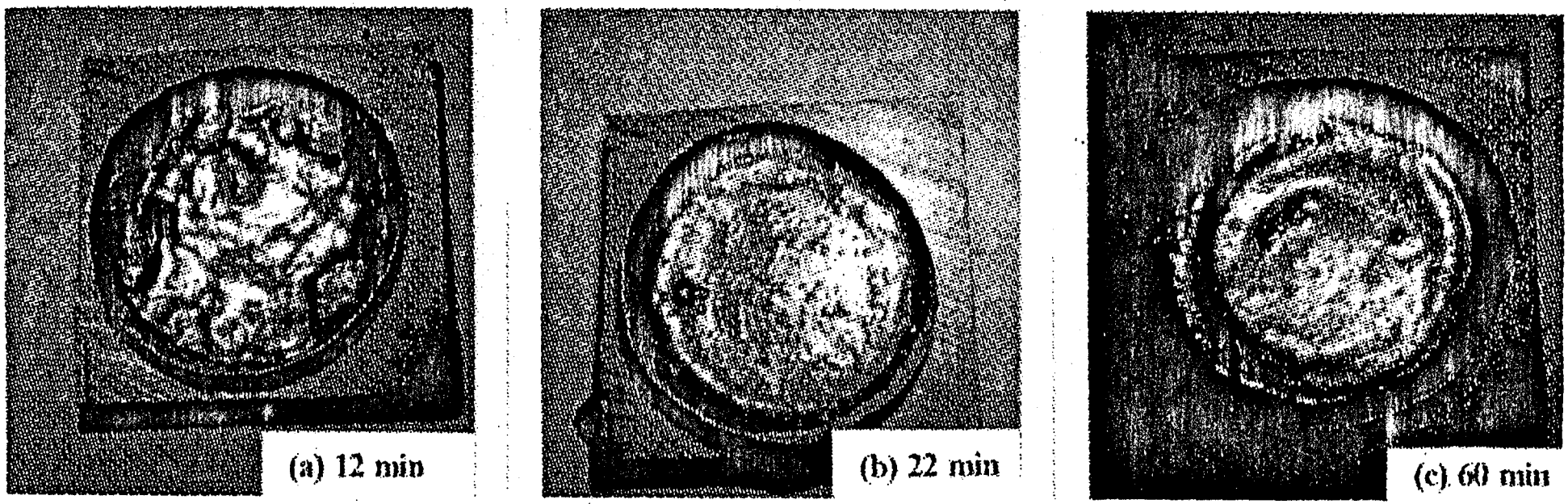

Figure 3. Vitrification process observed under a laboratory crucible melting (PFP1-7 glass at 1150 °C) after 12 min (a), 22 min (b), and 60 min (c) (Photos were taken after the crucible was cooled to room temperature)

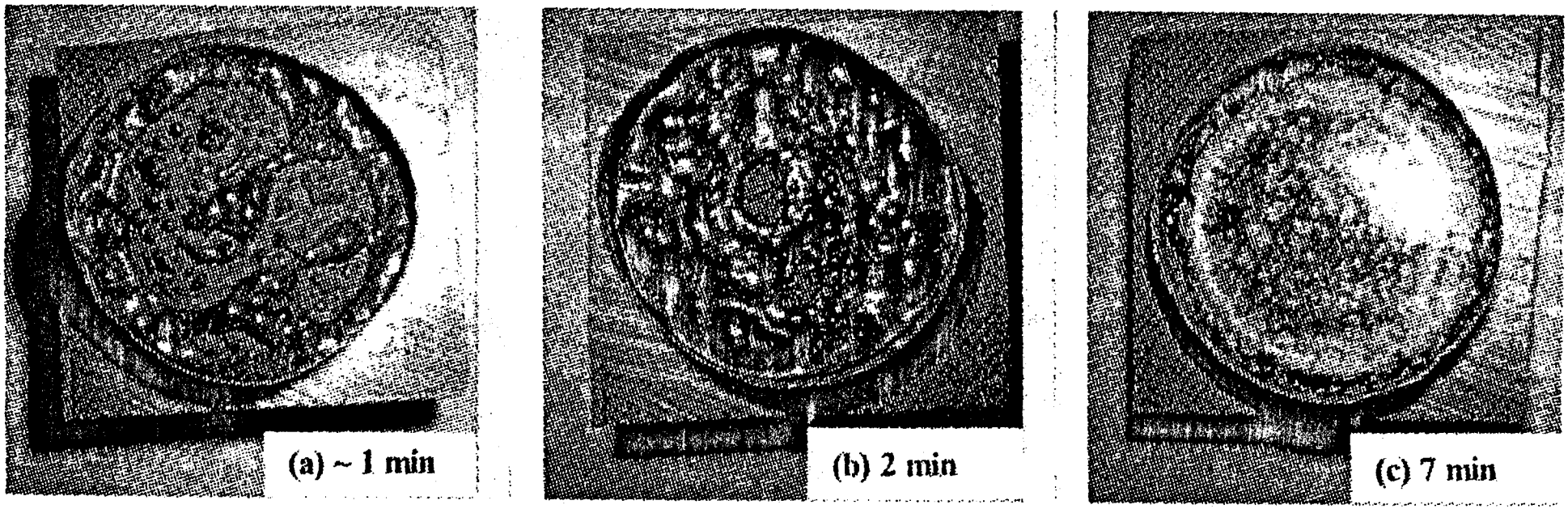

Figure 4. Vitrification process observed under a laboratory crucible melting (PFP1-1 glass at 1150 °C) after 1 min (a), 2 min (b), and 7 min (c), 22 min (d), 60 min (d), and 120 min (Photos were taken after the crucible was cooled to room temperature).

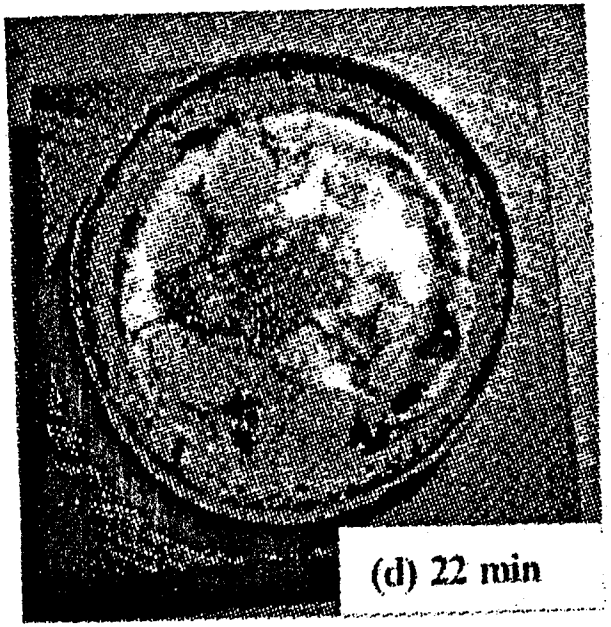

(d) 22 min

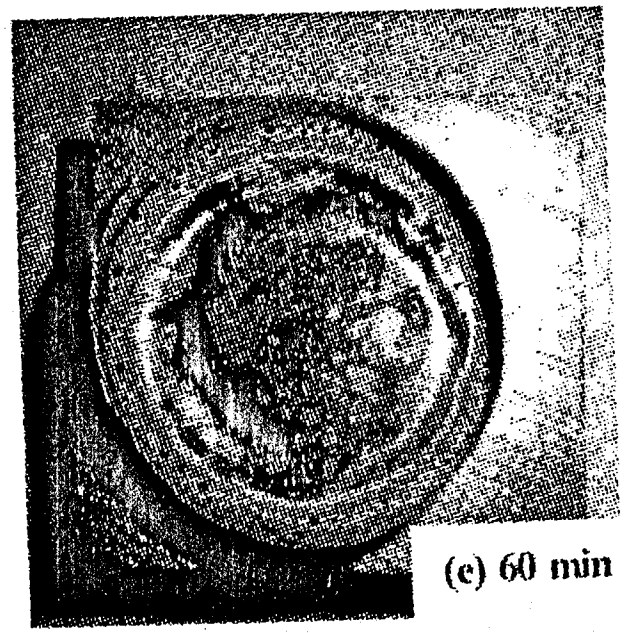

(e) 60 min

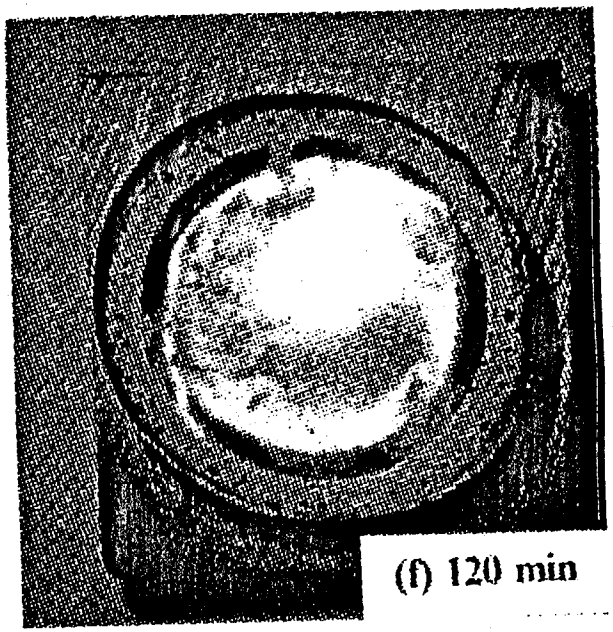

(f) 120 min

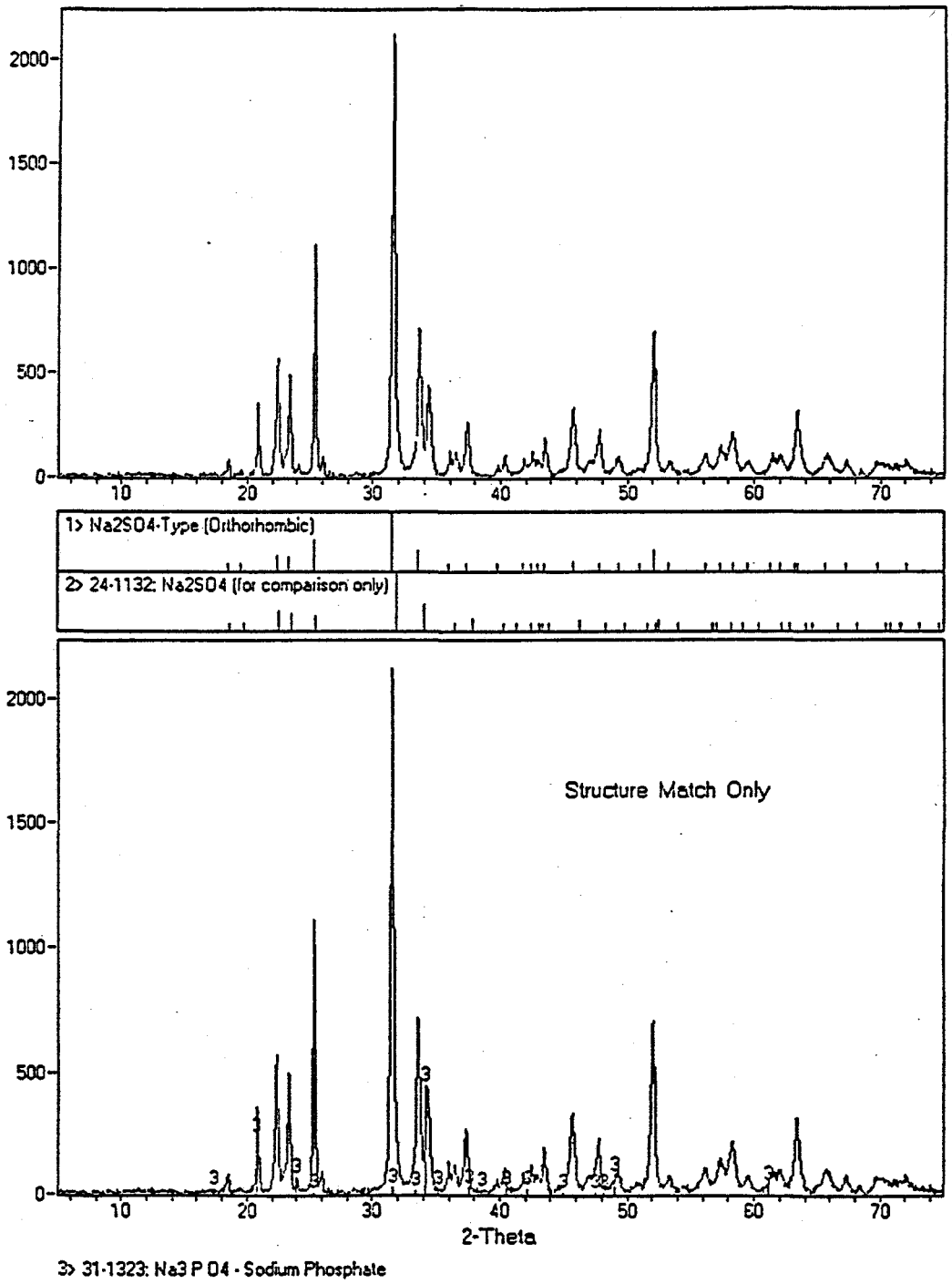

Figure 5. XRD analysis for a sample taken from the yelowish phase segregated area (cf. Figure 4c) of PFP1-1 glass, identifying the segregated phases as Na_2SO_4 and Na_3PO_4.

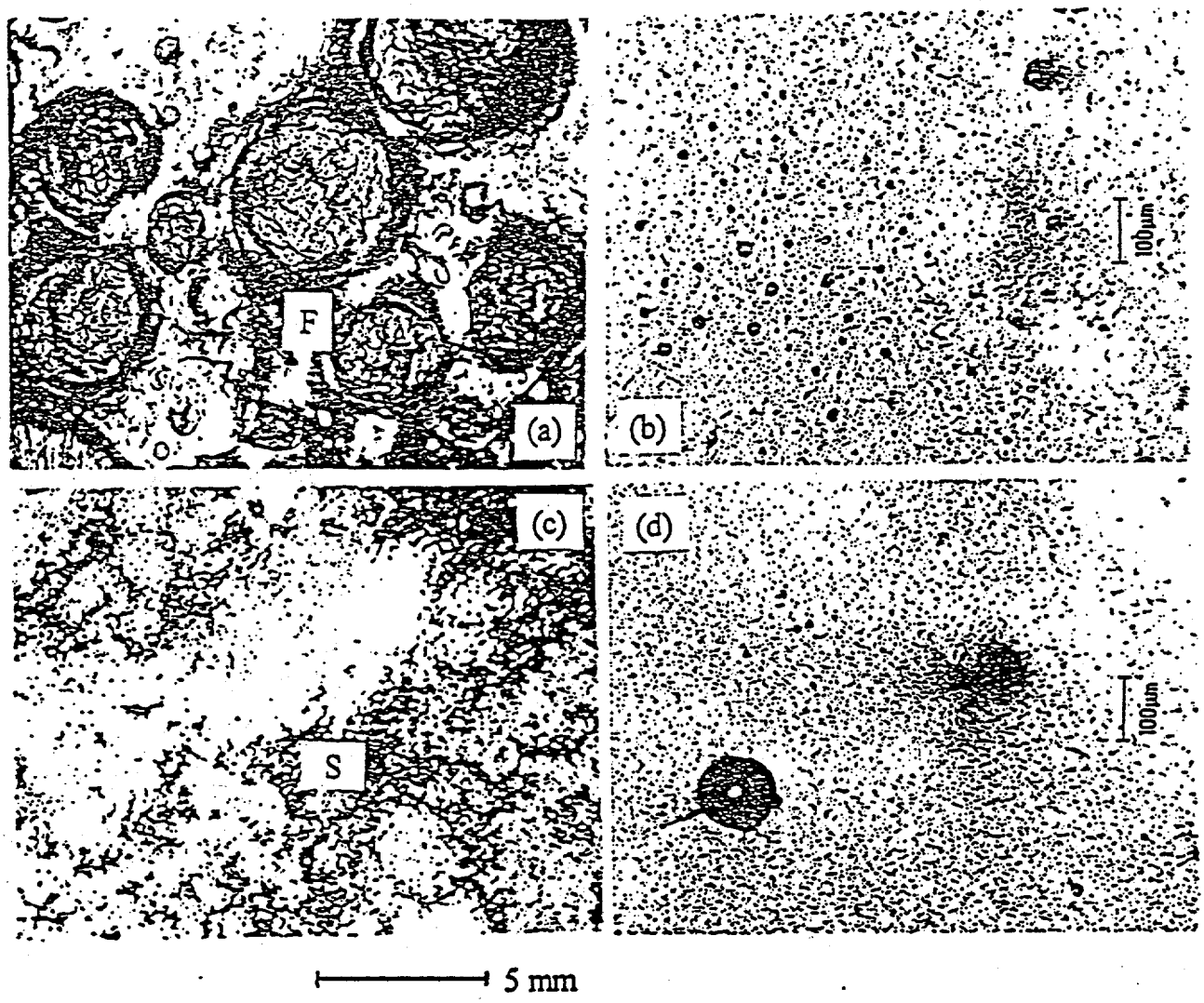

Figure 6. Optical micrographs showing the absence of phase segregation associated with melt foaming in PFP1-5 glass (a,b), and phase segregation when no melt foaming occurred in PFP1-1 glass (c,d) (Both glasses were melted at 1150°C for 60 min. F and S stand for melt foaming and segregated phase, respectively).

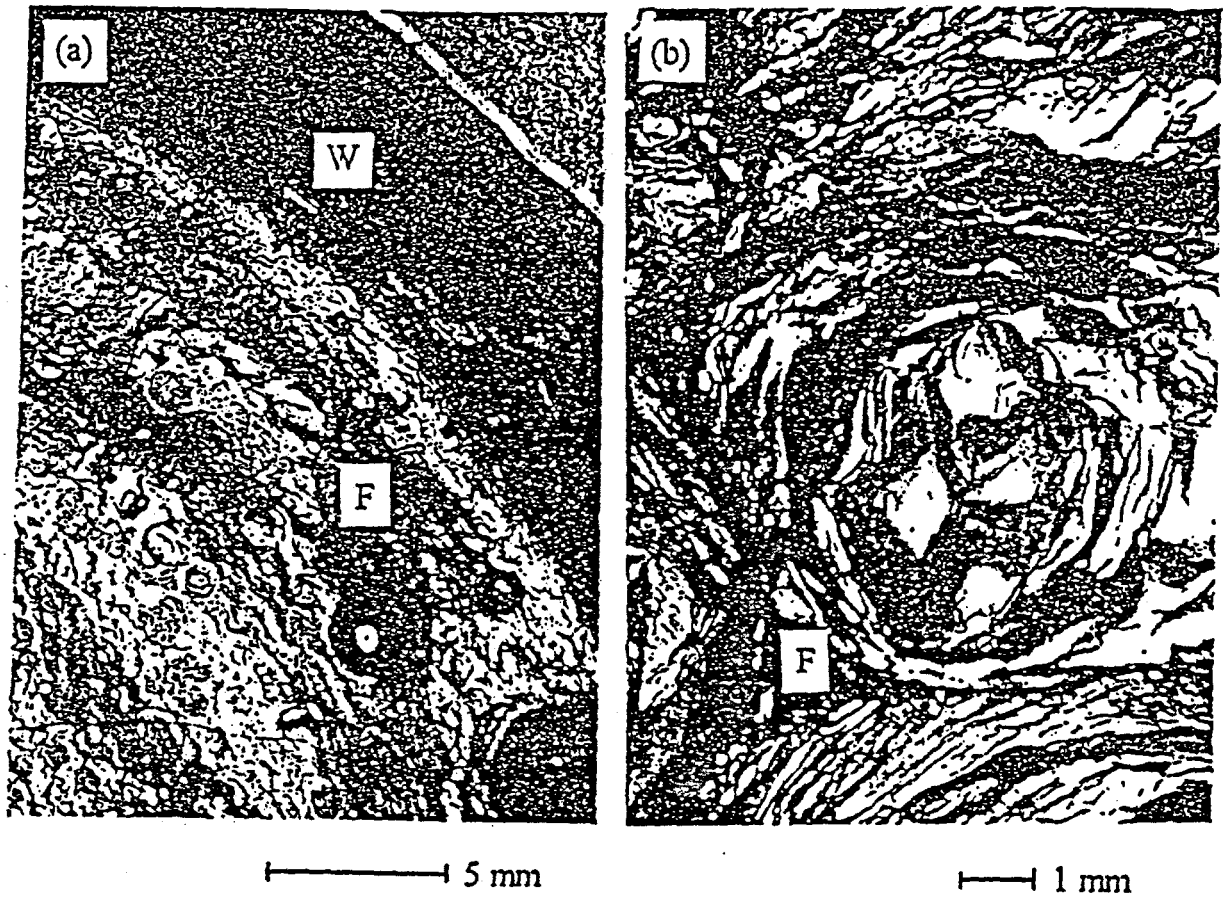

Figure 7. Optical micrographs shwoing morphology of melt foaming in PFP1-7 (a) and PFP1-4 (b) glasses (Both glasses were melted at 1150 °C for 60 min. F and S stand for melt foaming and segregated phase, respectively).

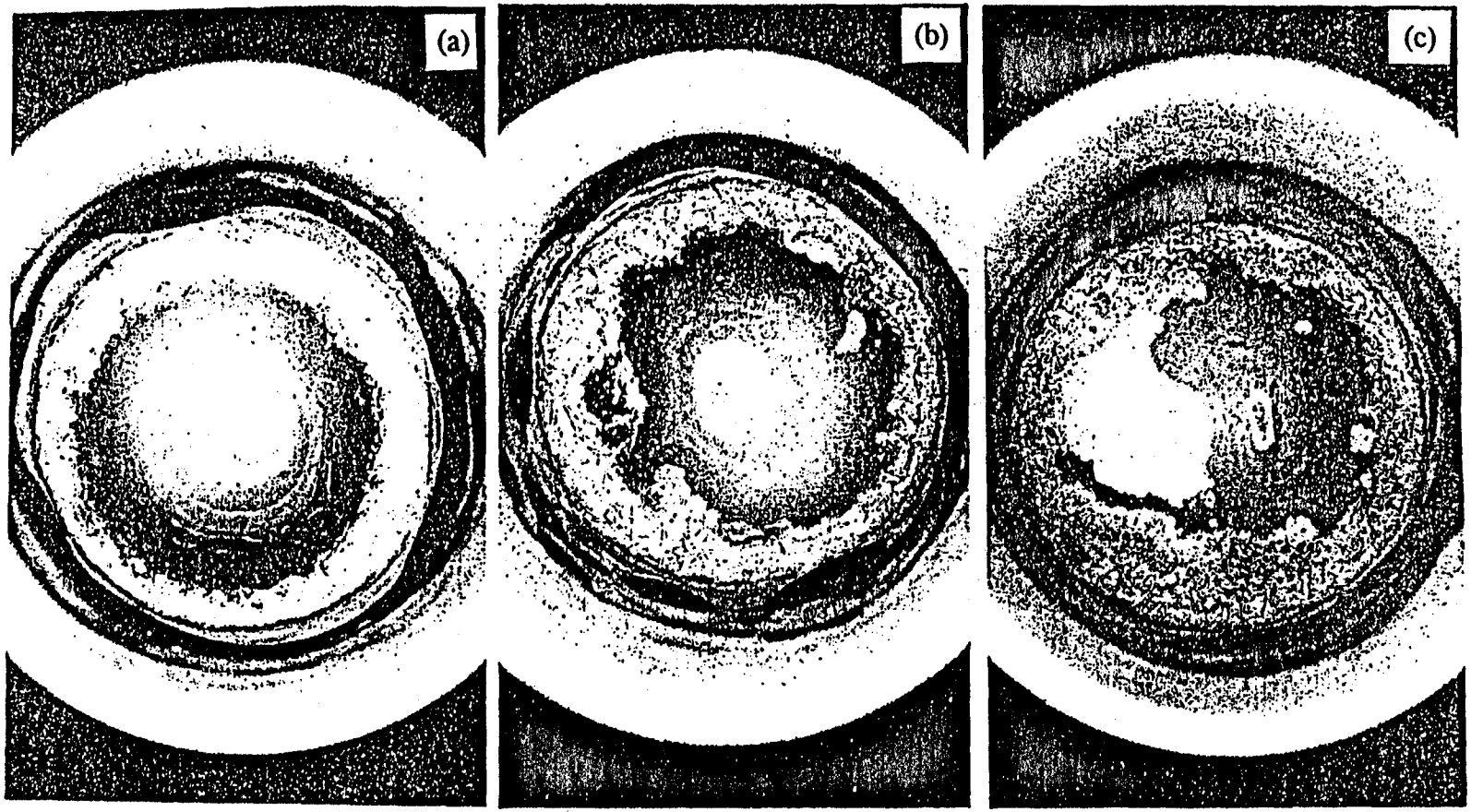

Figure 8. Optical micrographs shwoing morphology of the melt surface of WV182-4(a), WV182-8(b), and WV182-12(c) glasses melted at 1150 °C for 60 min (All glasses contained the same concentrations sulfate and phosphate, but different alumina contents).

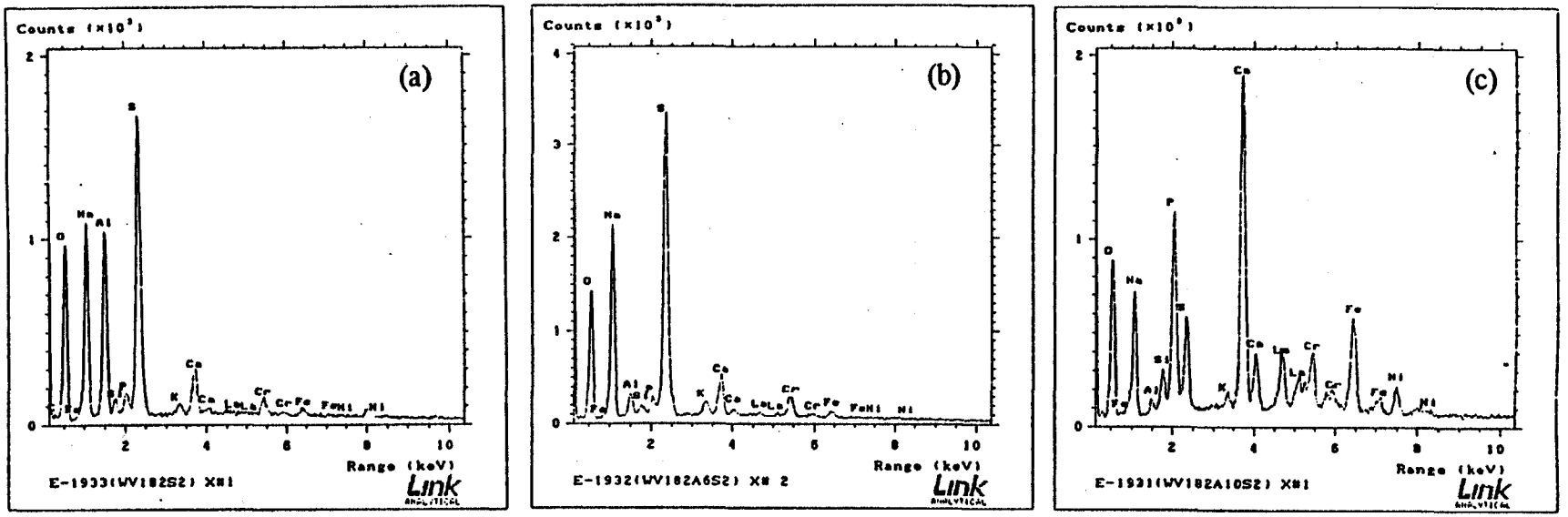

Figure 9. EDS elemental analyses in phase segregated areas shown in Figure 8 for WV182-4 (a), WV182-8 (b), and WV182-12 (c) glasses

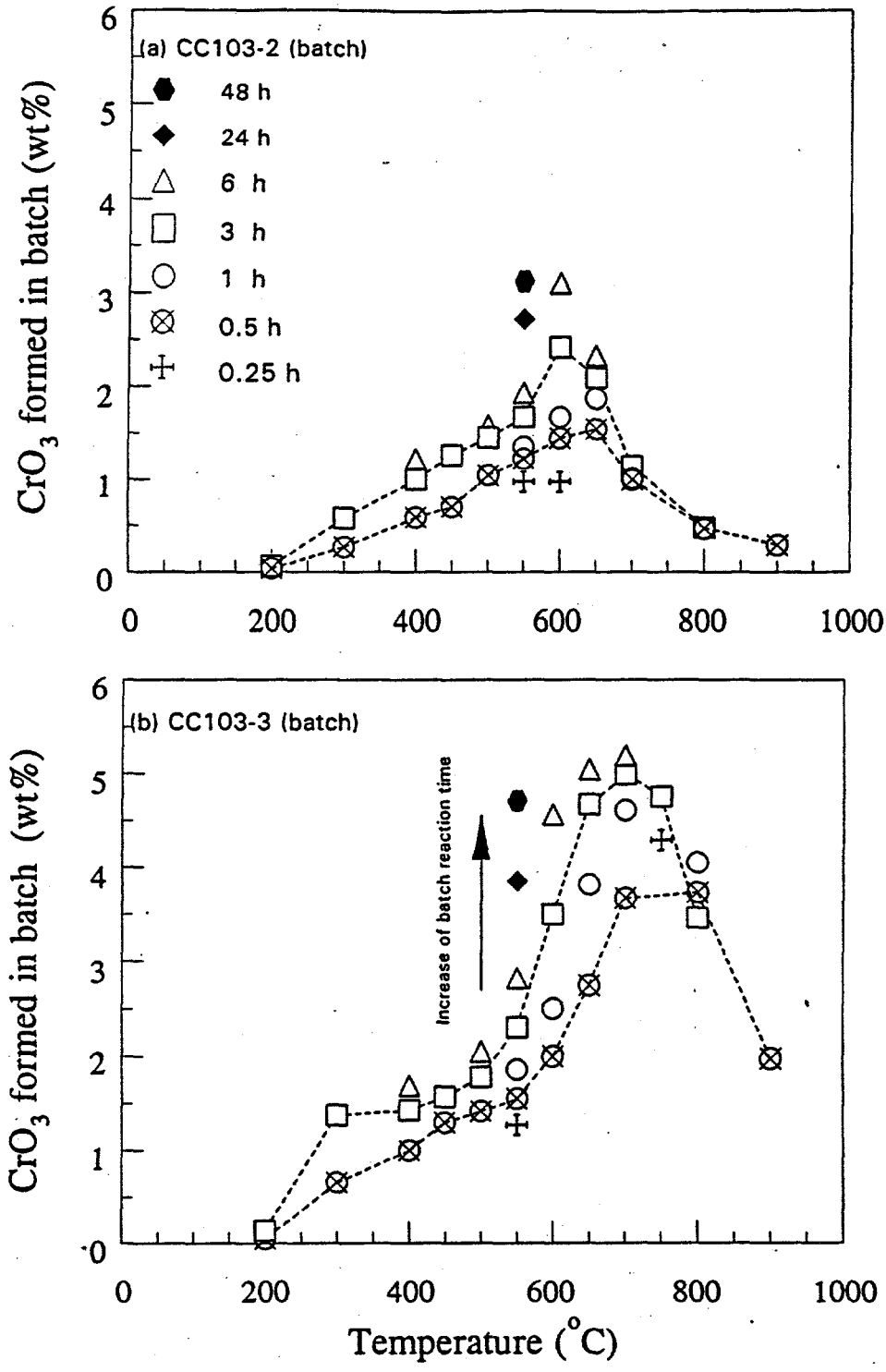

Figure 10. Chromate formation in batches CC103-2 and CC103-3 as a function of batch reaction temperature.

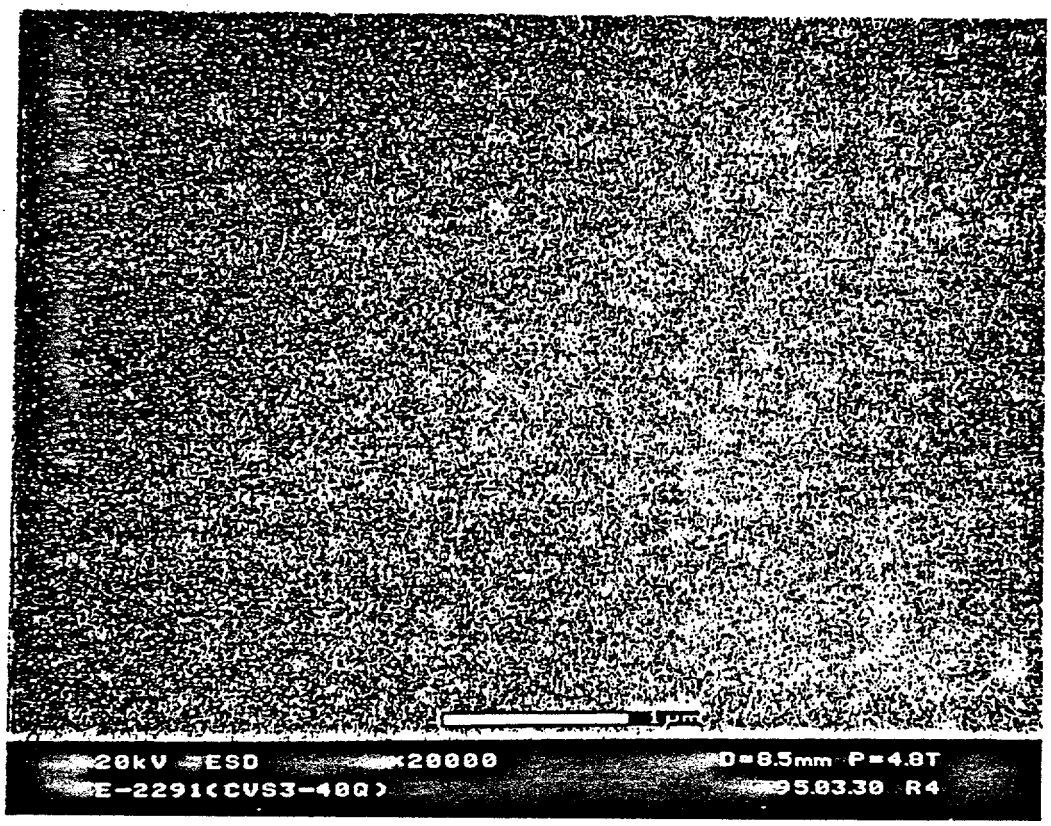

Figure 11. SEM micrograph of CVS3-40 glass with 9 wt% P_2O_5 revealing glass amorphous phase separation (Glass was melted at 1350°C for 2 hr).

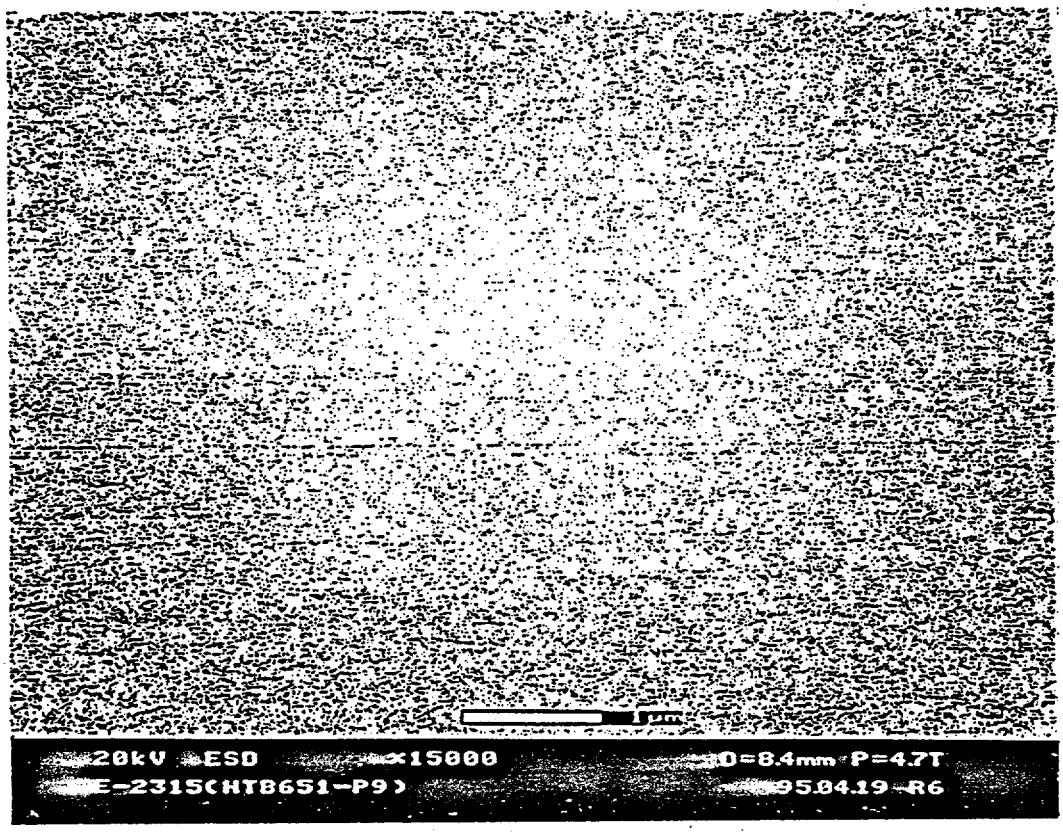

Figure 12. SEM micrograph of HTB651-4 glass with 9 wt% P_2O_5 revealing glass amorphous phase separation (Glass was melted at 1350°C for 2 hr).

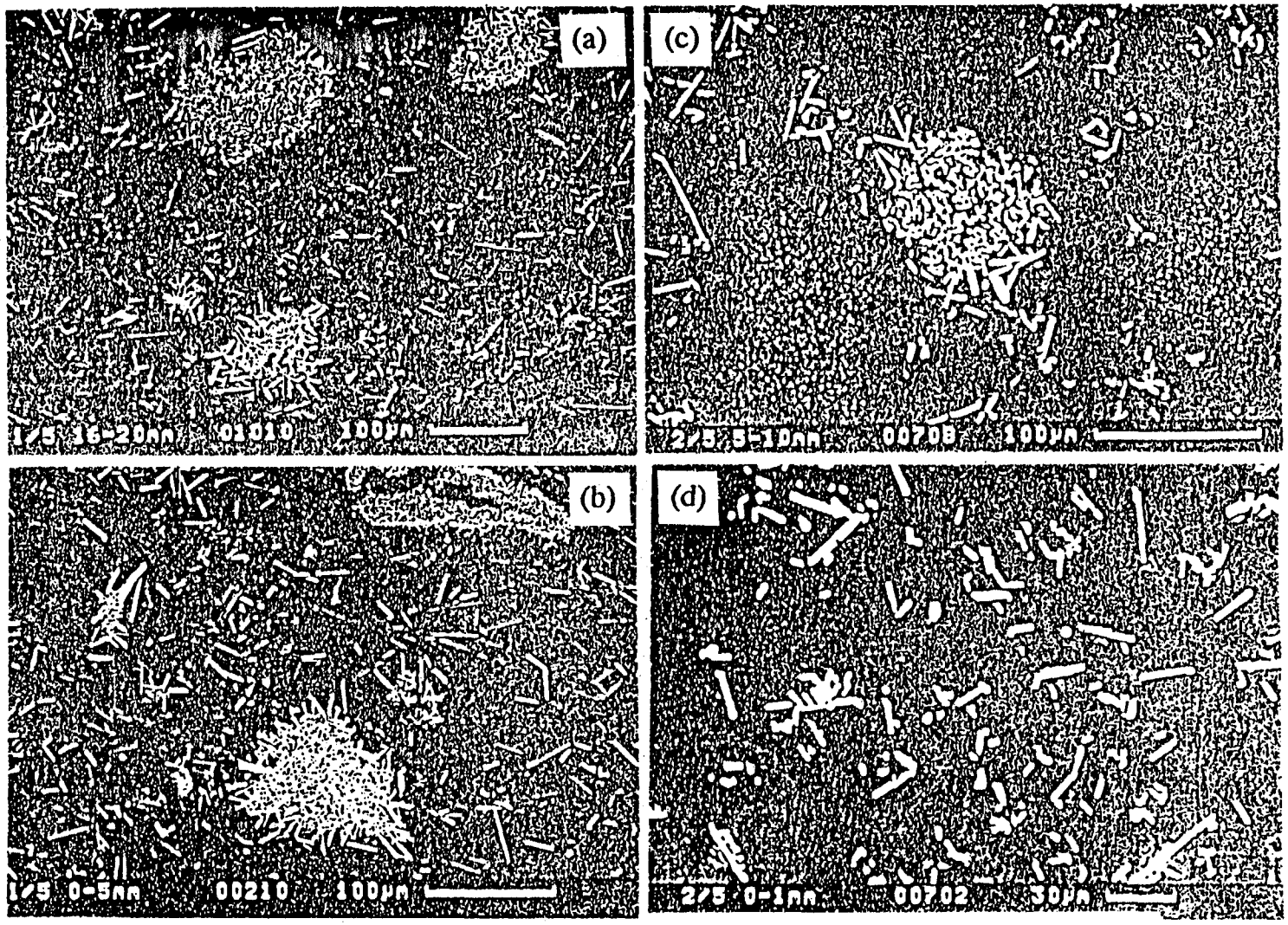

Figure 13. SEM micrographs showing crystal distributions in areas away from (a,c) and near (b,d) the bottom of the melts for CC103-2 and CC103-3 glasses (Glasses were melted at 1150°C and 1450°C, respectively).

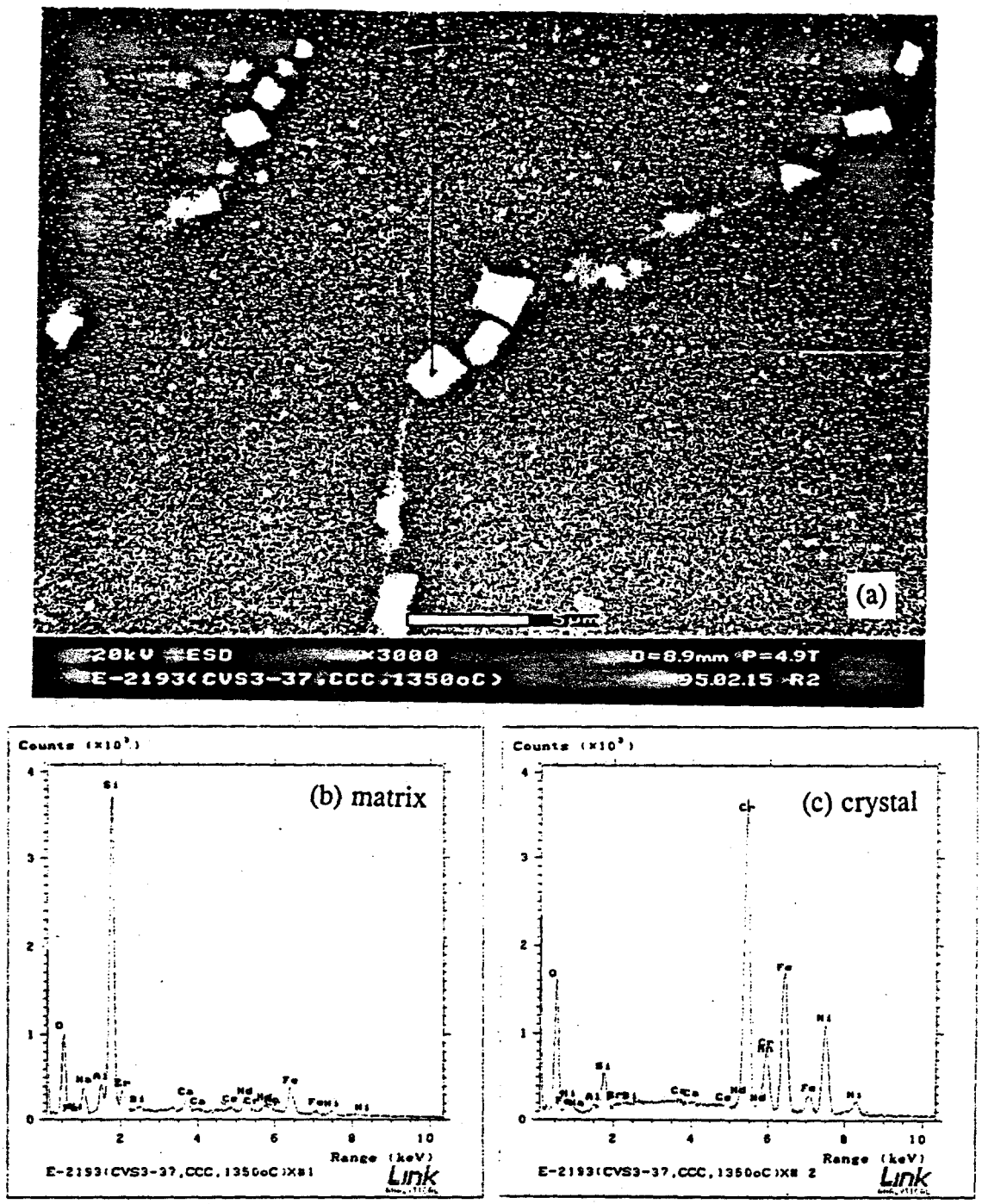

Figure 14. SEM micrograph showing glass amorphous phase separation (small white dots) (a) and EDS elemental analyses (b,c) of CCC-treated CVS3-37 glass with 3.0 wt% P_2O_5, revealing spinel crystals enriched in Cr, Fe, Mn, and Ni.

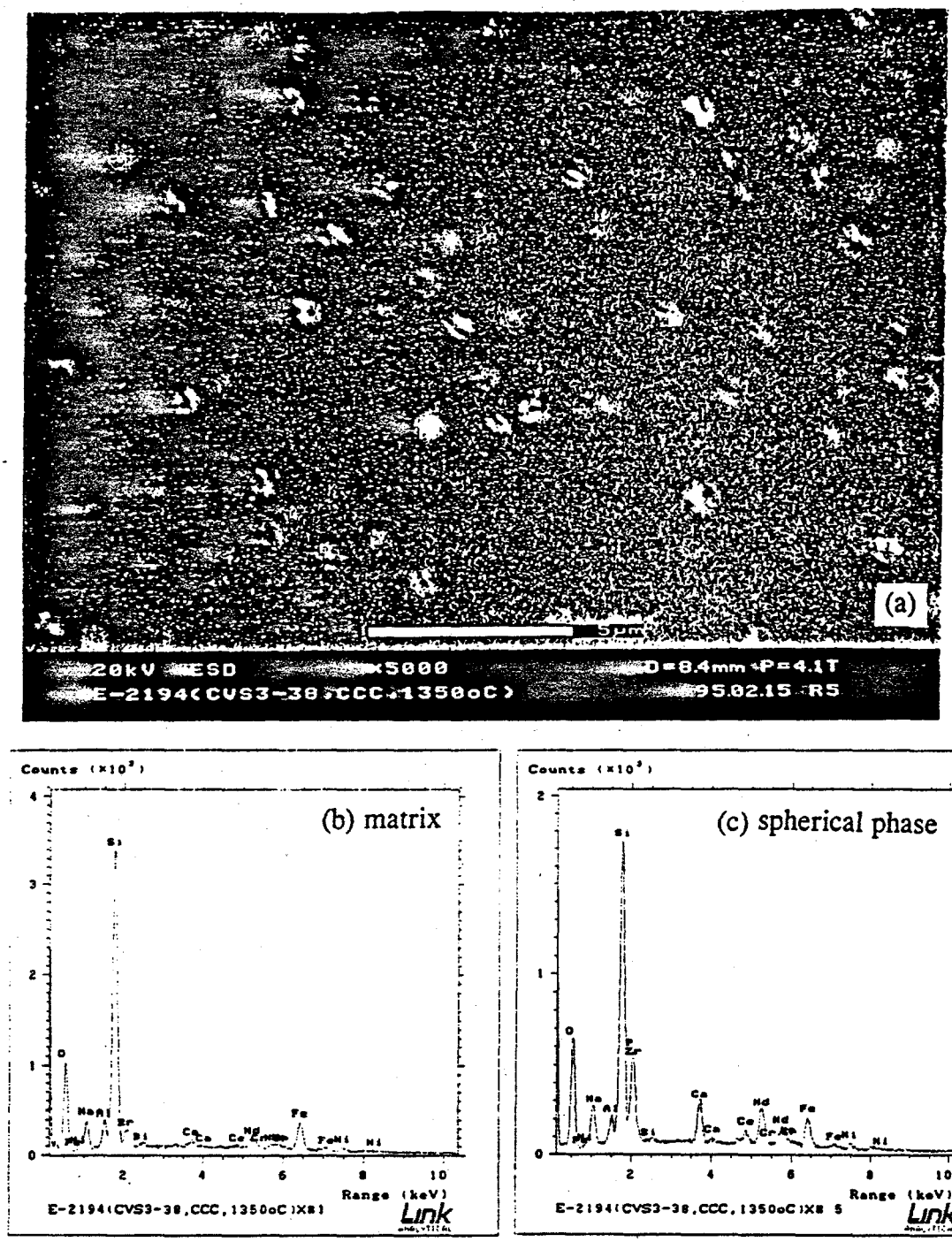

Figure 15. SEM micrograph (a) and EDS elemental analyses (b,c) of CCC-treated CVS3-38 glass with 5.0 wt% P_2O_5, revealing a spherical phase enriched in P, Ca, Ce, and Ni.

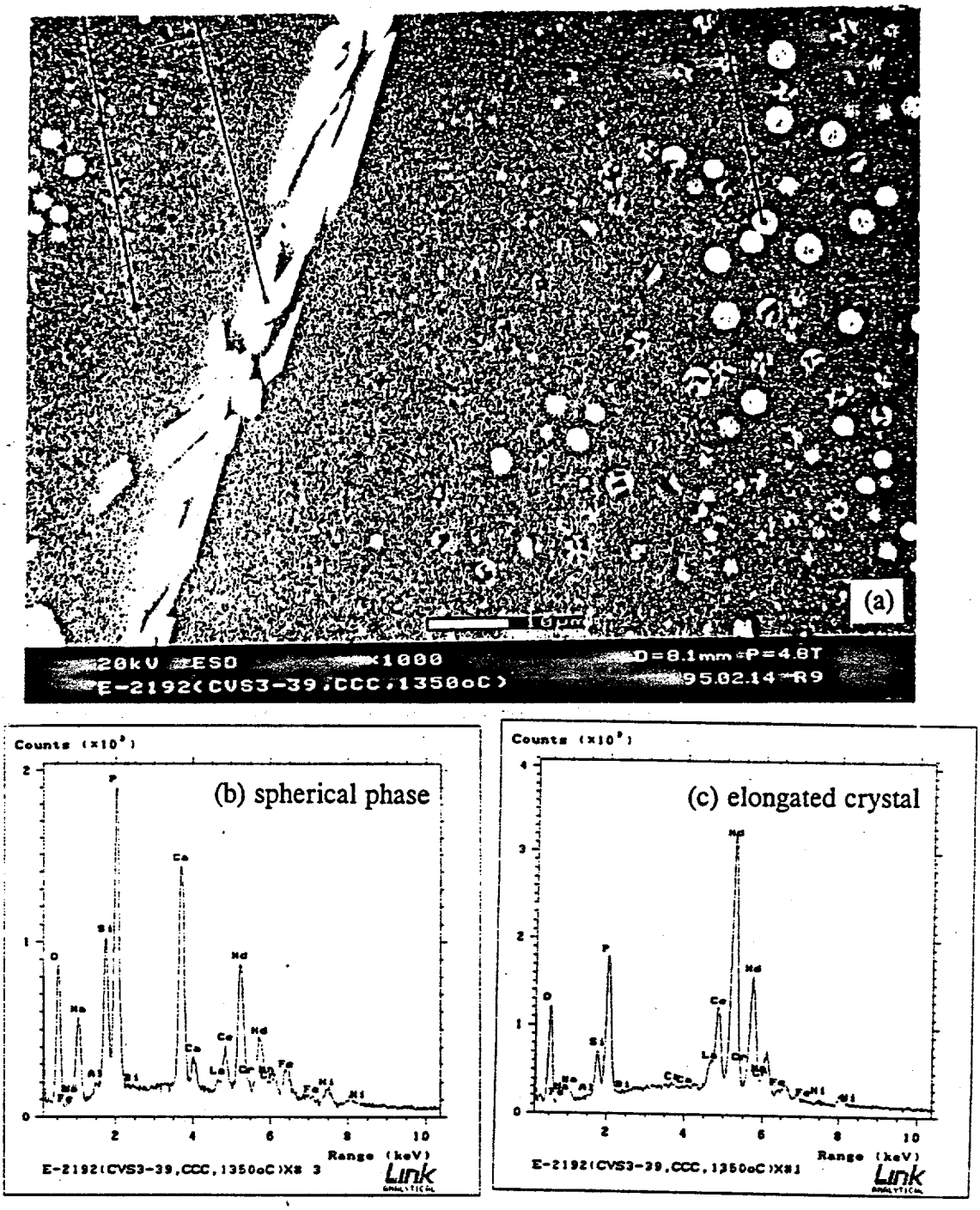

Figure 16. SEM micrograph (a) and EDS elemental analyses of CCC-treated CVS3-39 glass with 7.0 wt% P_2O_5, revealing a spherical phase enriched in P, Ca, Ce, Nd, Fe, and Ni (b) and elongated crystals enriched in P, Ce, and Nd (c).

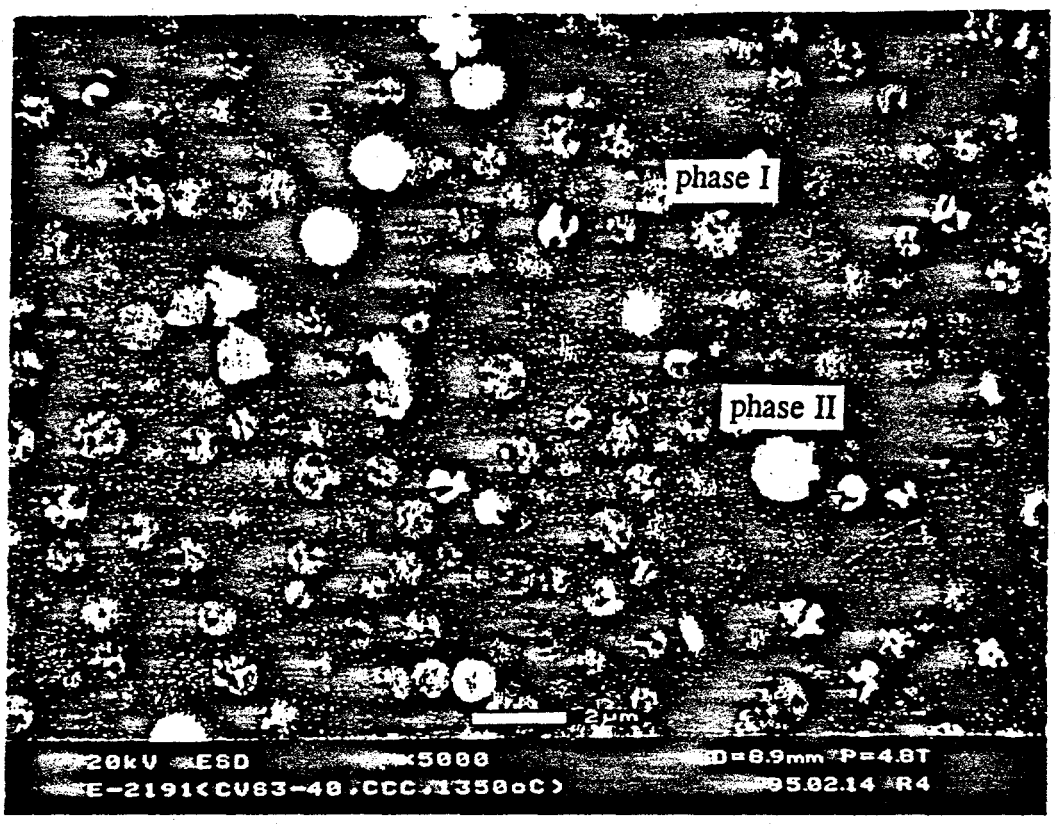

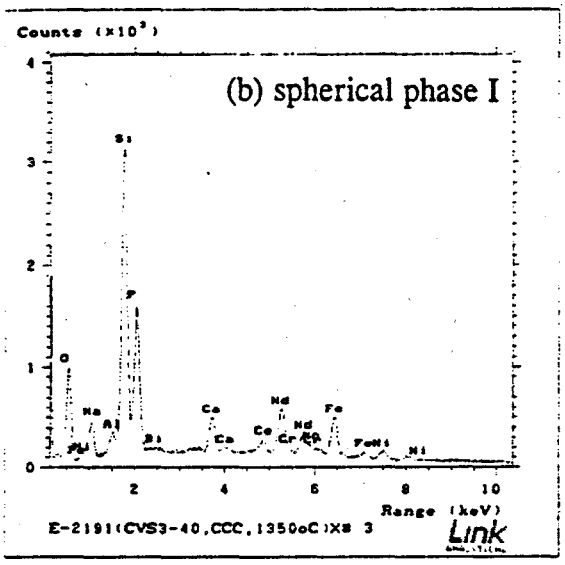

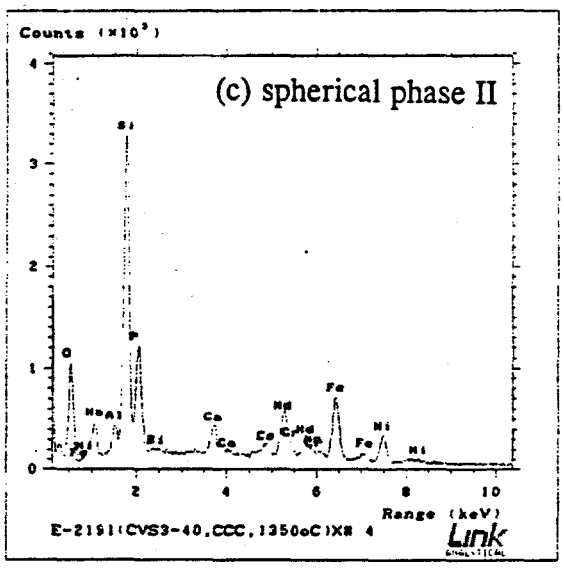

Figure 17. SEM micrograph (a), showing two spherical phases, and EDS elemental analyses (b,c) of CCC-treated CVS3-40 glass with 9.0 wt% P_2O_5, revealing both phases enriched in P, Ca, Ce, Nd, Fe, and Nd.

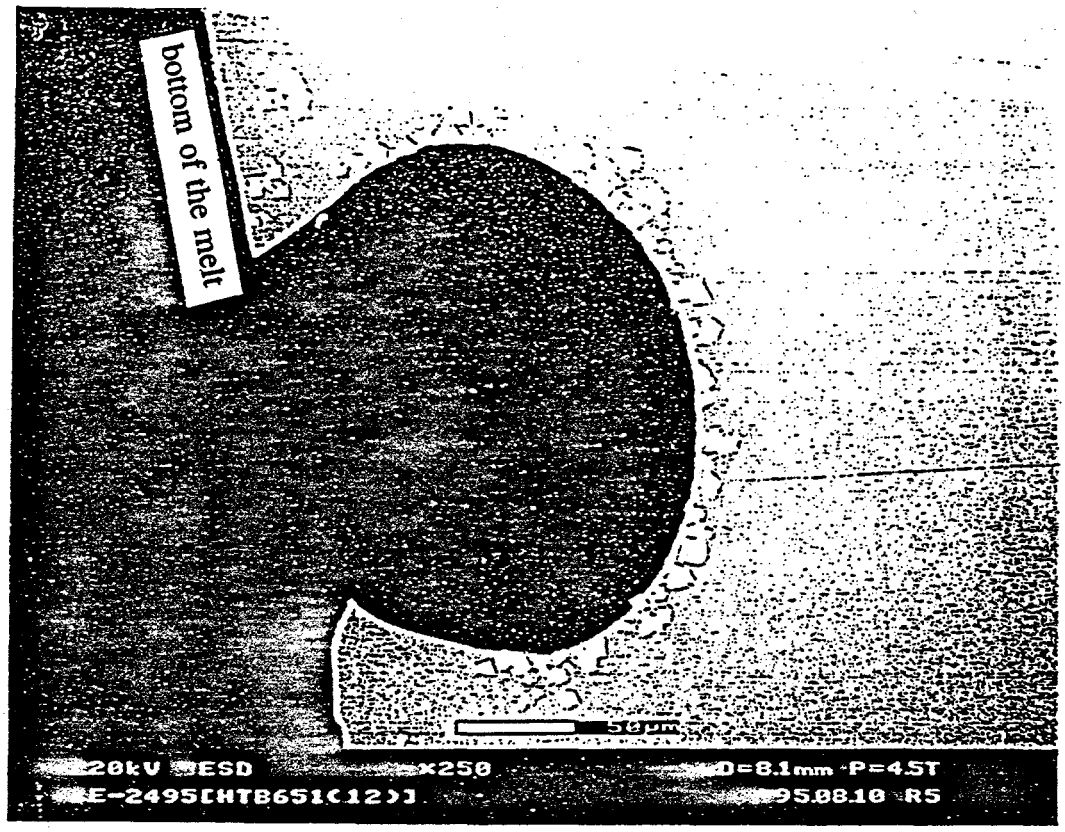

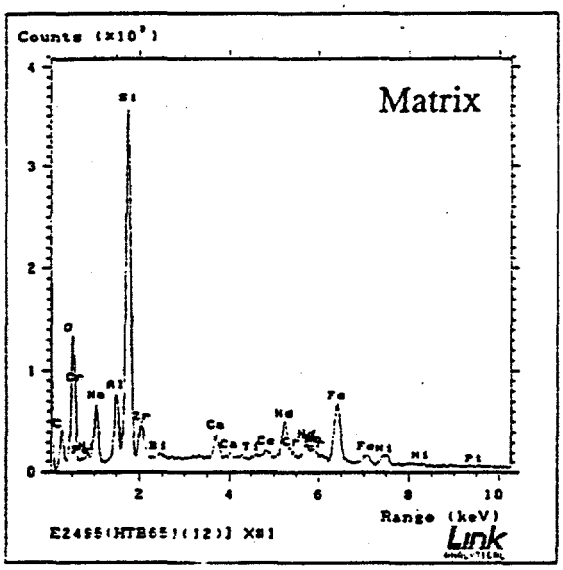

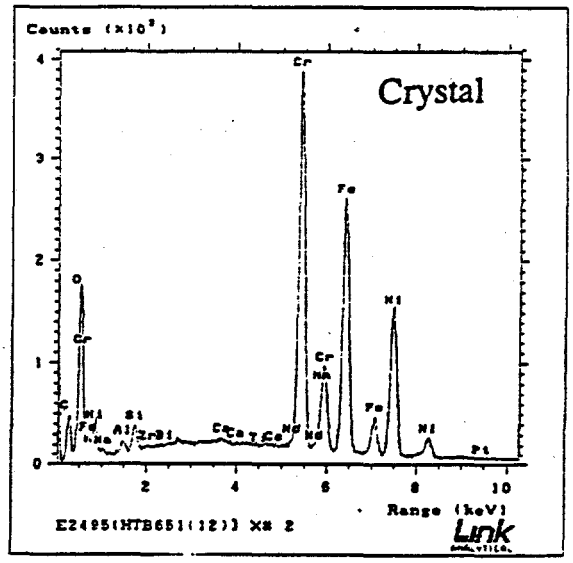

Figure 18. SEM micrograph and EDS elemental analyses of HTB651-6 glass with 0.8 wt% Cr_2O_3, revealing spinel crystals (high in Cr, Fe, Mn, Ni) surrounding a bubble at the bottom of the melt (Glass was melted at 1350°C for 2 hr and then heat-treated at 1245 °C for 24 hr in a closed Pt container).

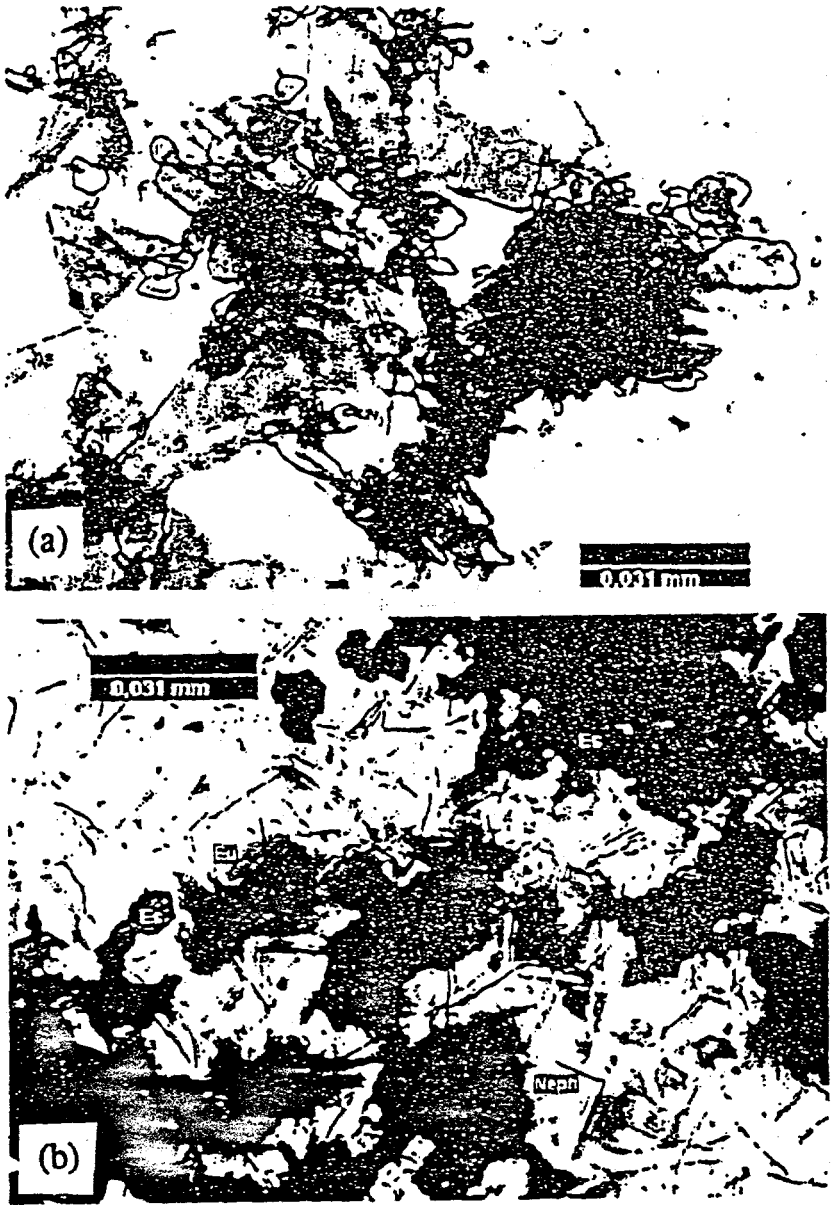

Figure 19. TEM micrographs of CCC-treated CC103-2 (a) and CC103-3 (b) glasses showing crystals of Cr_2O_3 (eskolait, Es) in both glasses, and $NaAlSiO_4$ (nepheline, Neph) and beta-$LiAlSiO_4$ (beta-eucryptite, Eu) in CC103-3 glass.

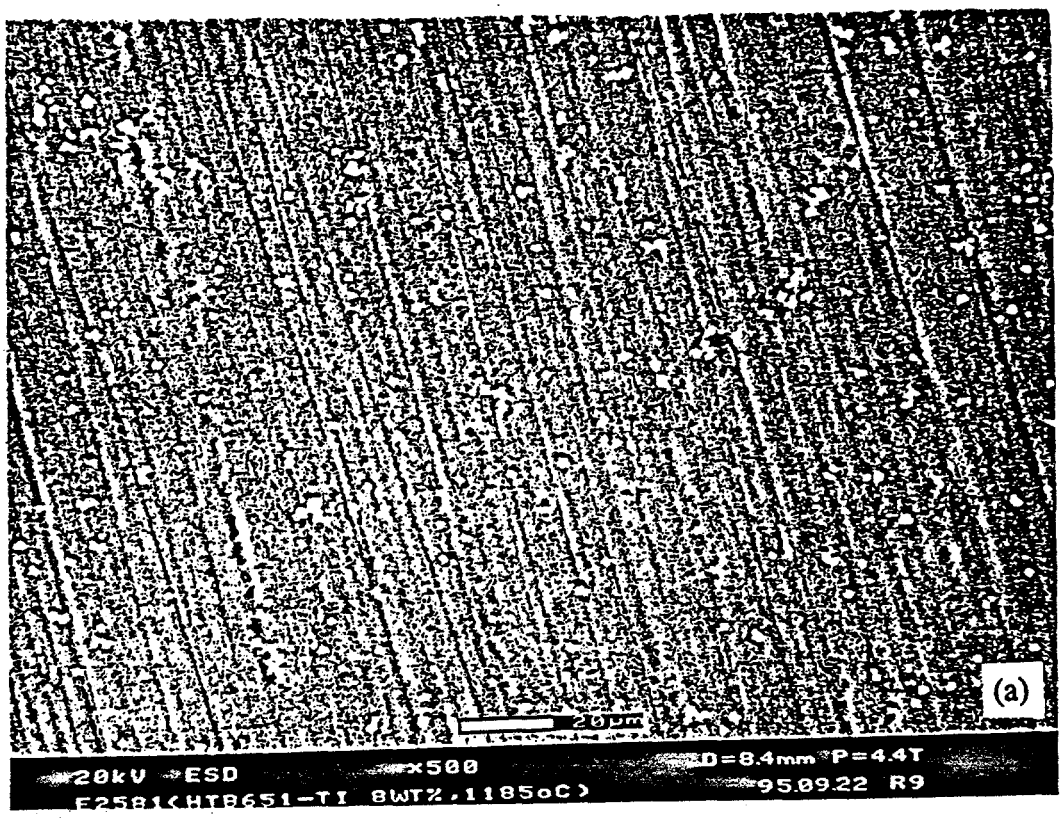

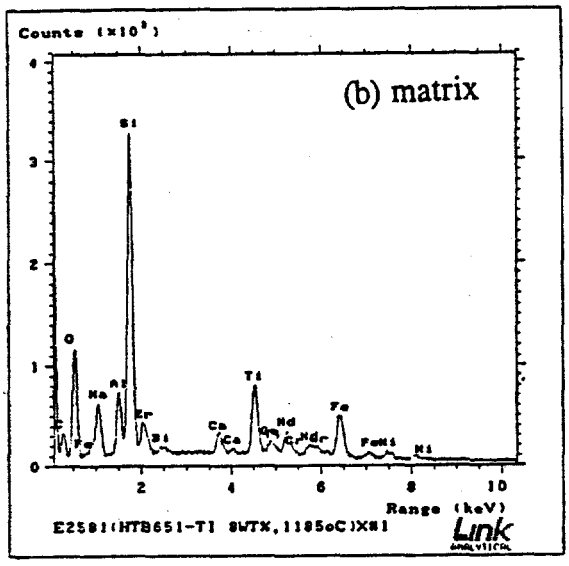

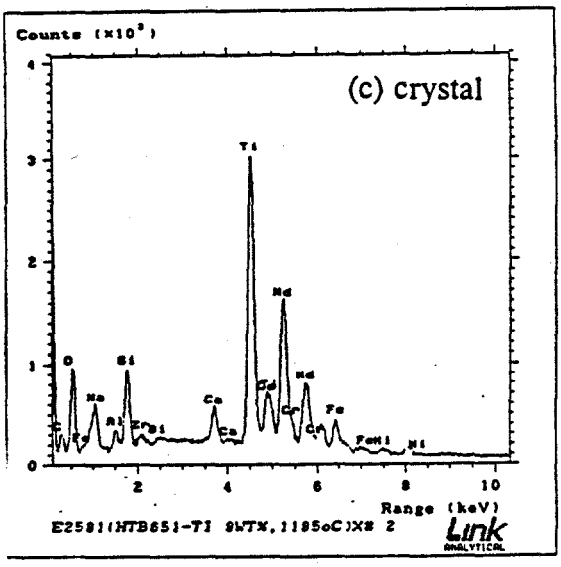

Figure 20. SEM micrograph (a) and EDS elemental analyses (b,c) of HTB651-10 glass with 5 wt% TiO_2, revealing precipitation of TiO_2 crystals from the melt (Glass was melted at 1350°C for 2 hr and then heat-treated at 1185°C for 24 hr in a closed Pt-container).

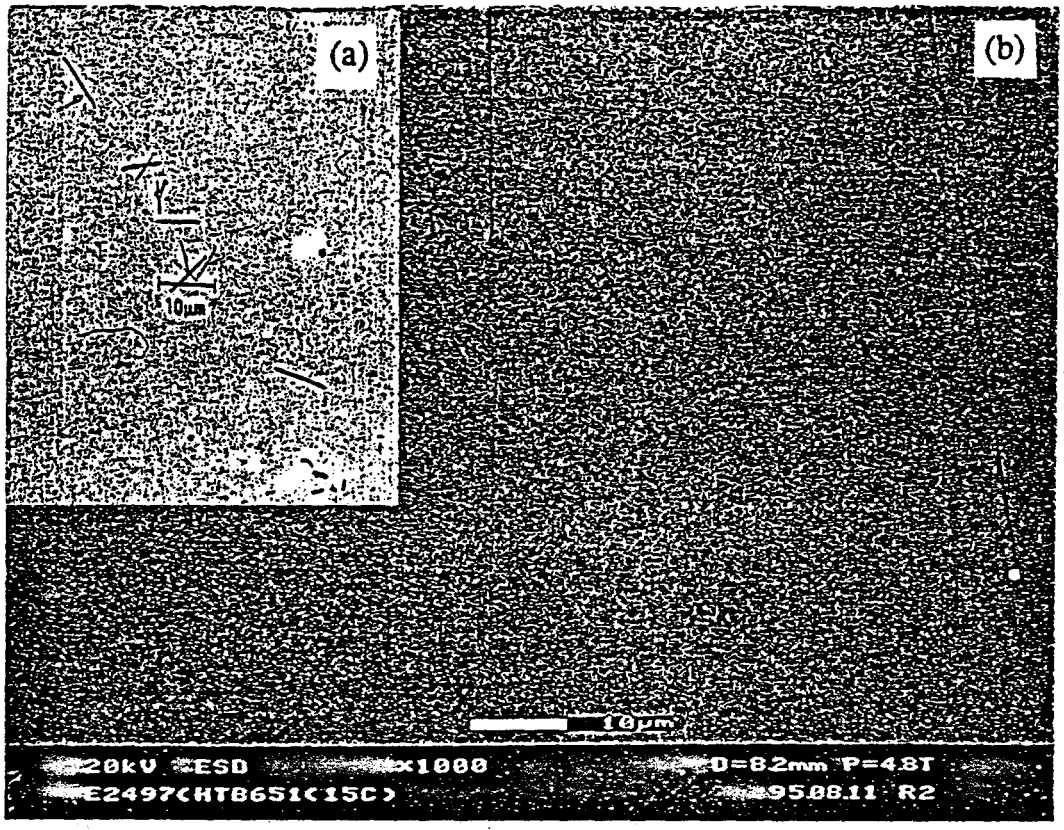

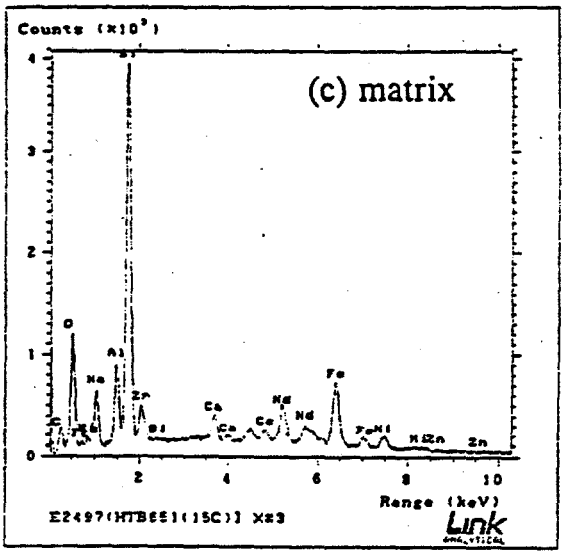

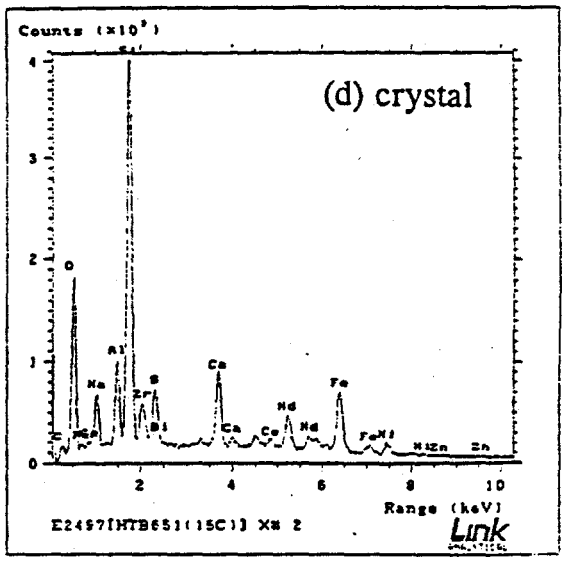

Figure 21. Optical (a) and SEM (b) micrographs and EDS elemental analyses (c,d) of HTB651-7 glass with 1 wt% TiO_2, revealing isolated crystals rich in Ca and S (Glass was melted at 1350°C for 2 hr and then heat-treated at 1339°C for 24 hr in a closed Pt container).

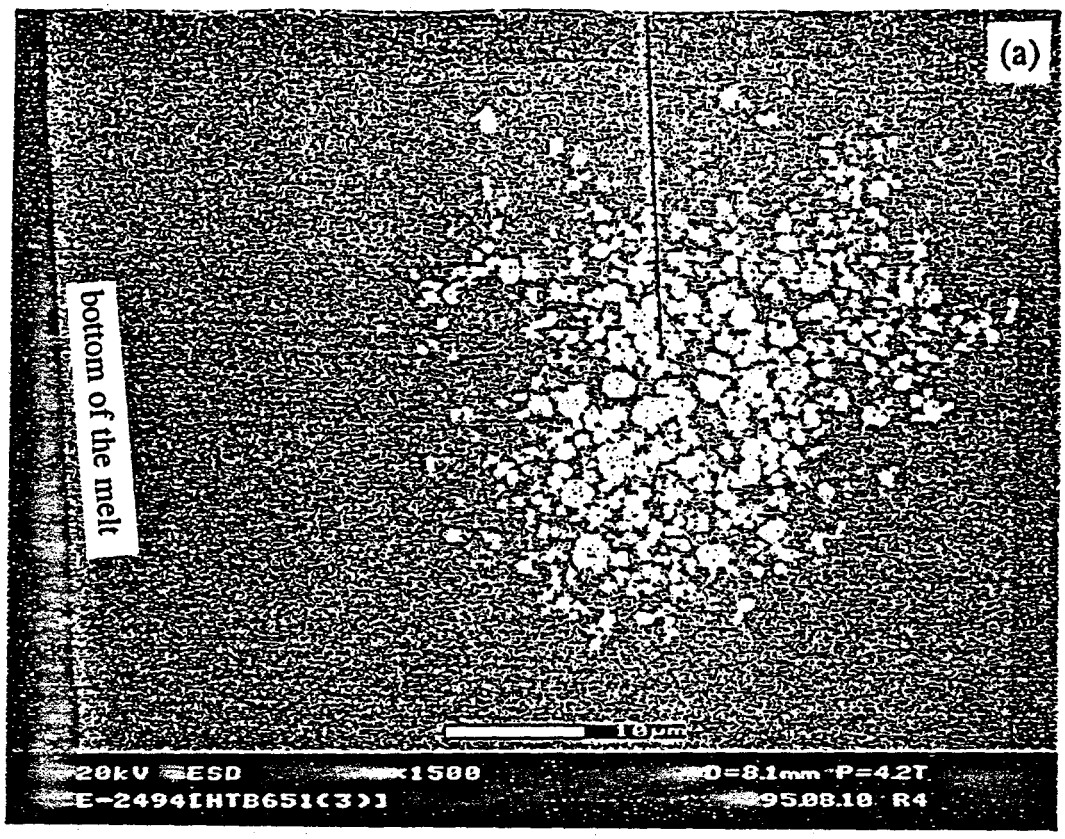

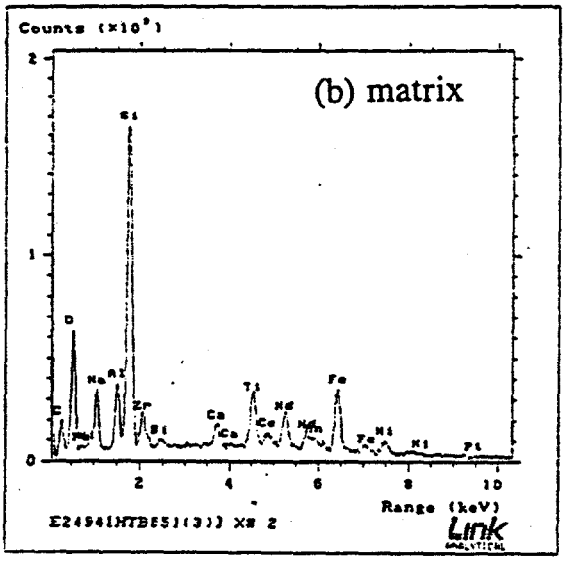

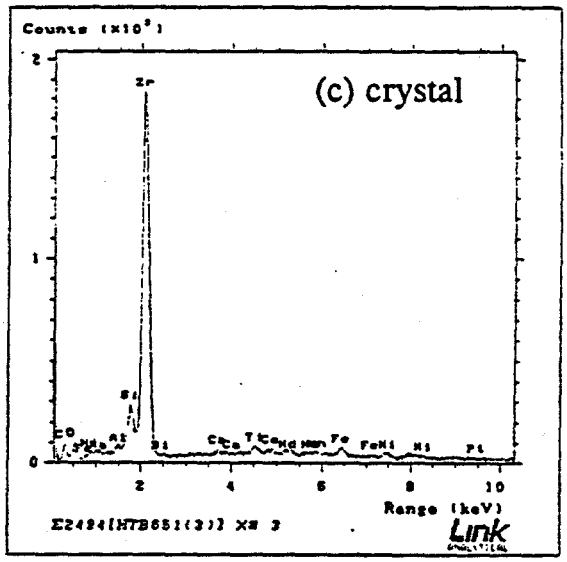

Figure 22. SEM micrograph (a) and EDS elemental analyeses (b,c) of HTB651-9 glass with 5 wt% TiO_2, revealing an isolated cluster of ZrO_2 particles near the bottom of the melt (Glass was melted at 1350 °C for 2 hr and then heat-treated at 1230 °C for 24 hr in a closed Pt container).

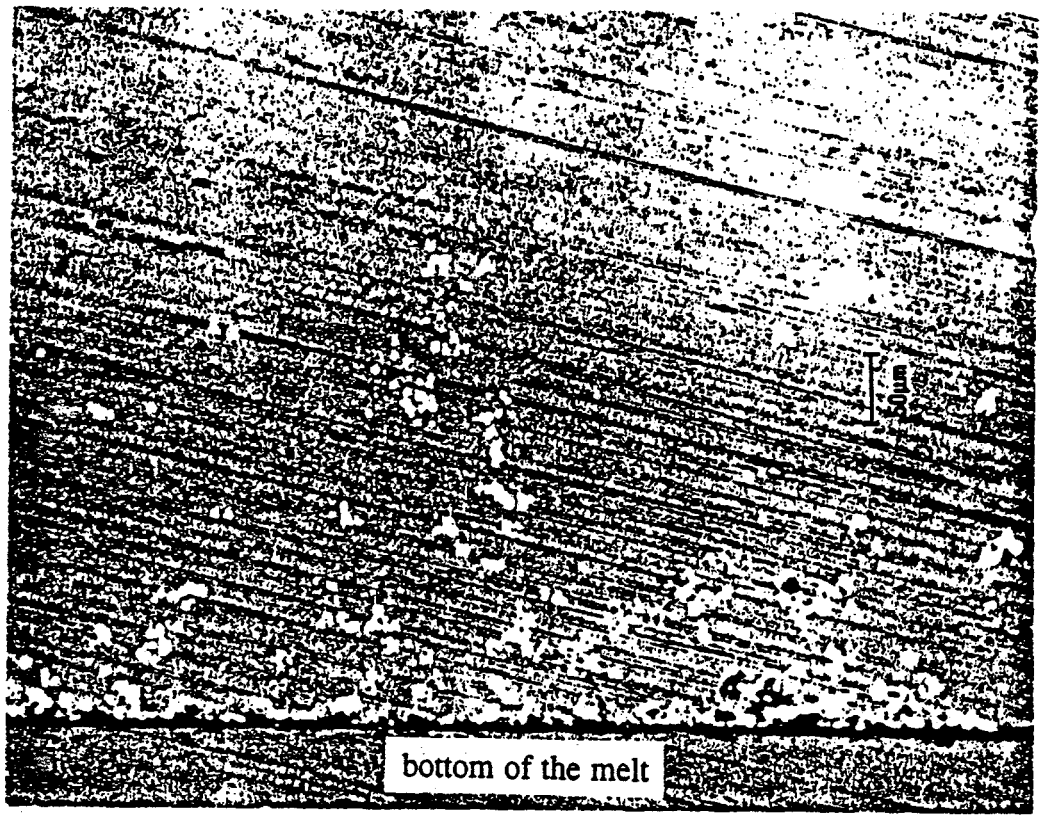

Figure 23. Optical micrograph of HTB651-12 glass with 5.0 wt% TiO_2 and 8.0 wt% ZrO_2, revealing settlement of ZrO_2 particles at the bottom of the melt (Glass was melted at 1350 °C for 2 hr and then heat-treated at 1328 °C for 24 hr in a closed Pt-container).

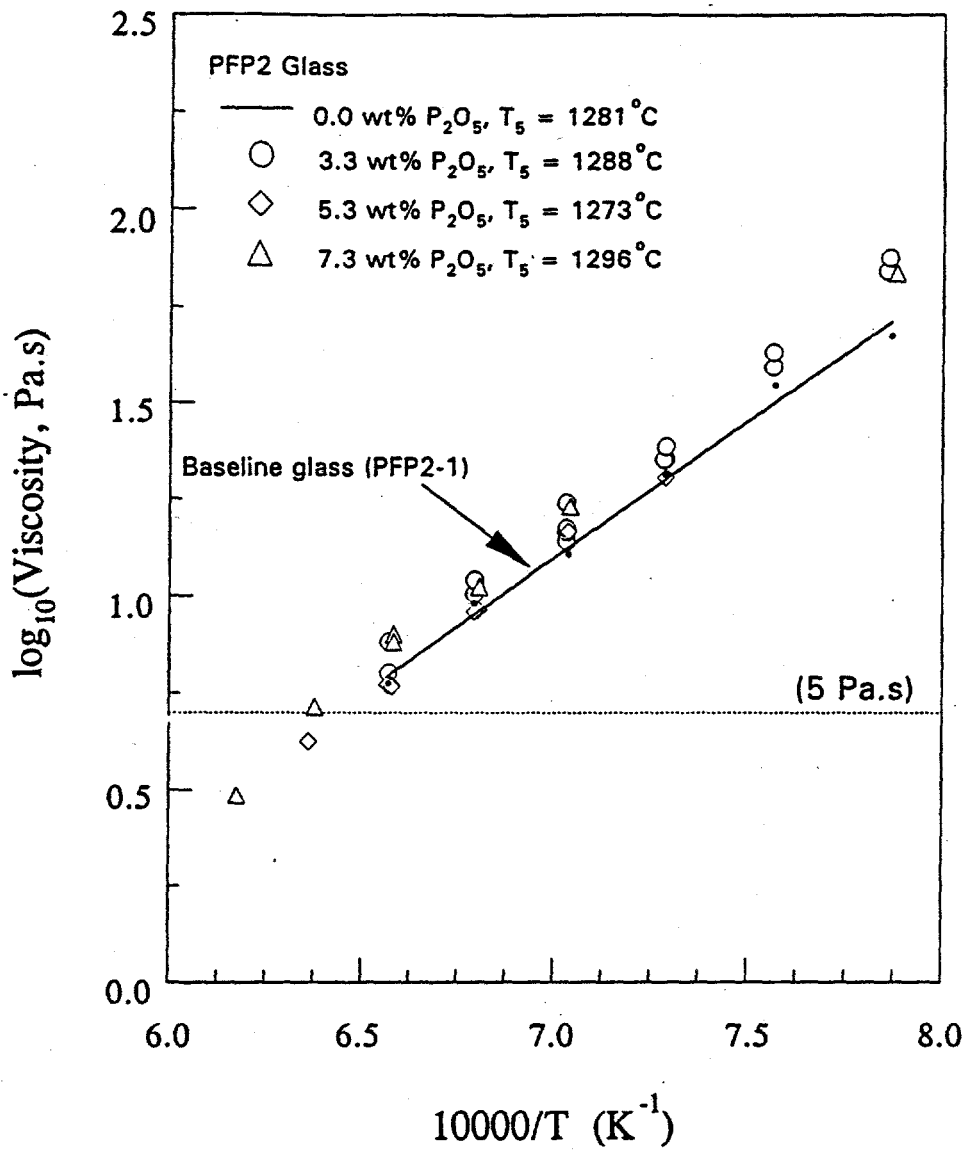

Figure 24. Measured glass melt viscosity as a fucntion of temperature for PFP2 glasses with various concentrations of P_2O_5 (T_5 is the estimated tempearture at which the glass melt viscosity is 5 Pa.s).

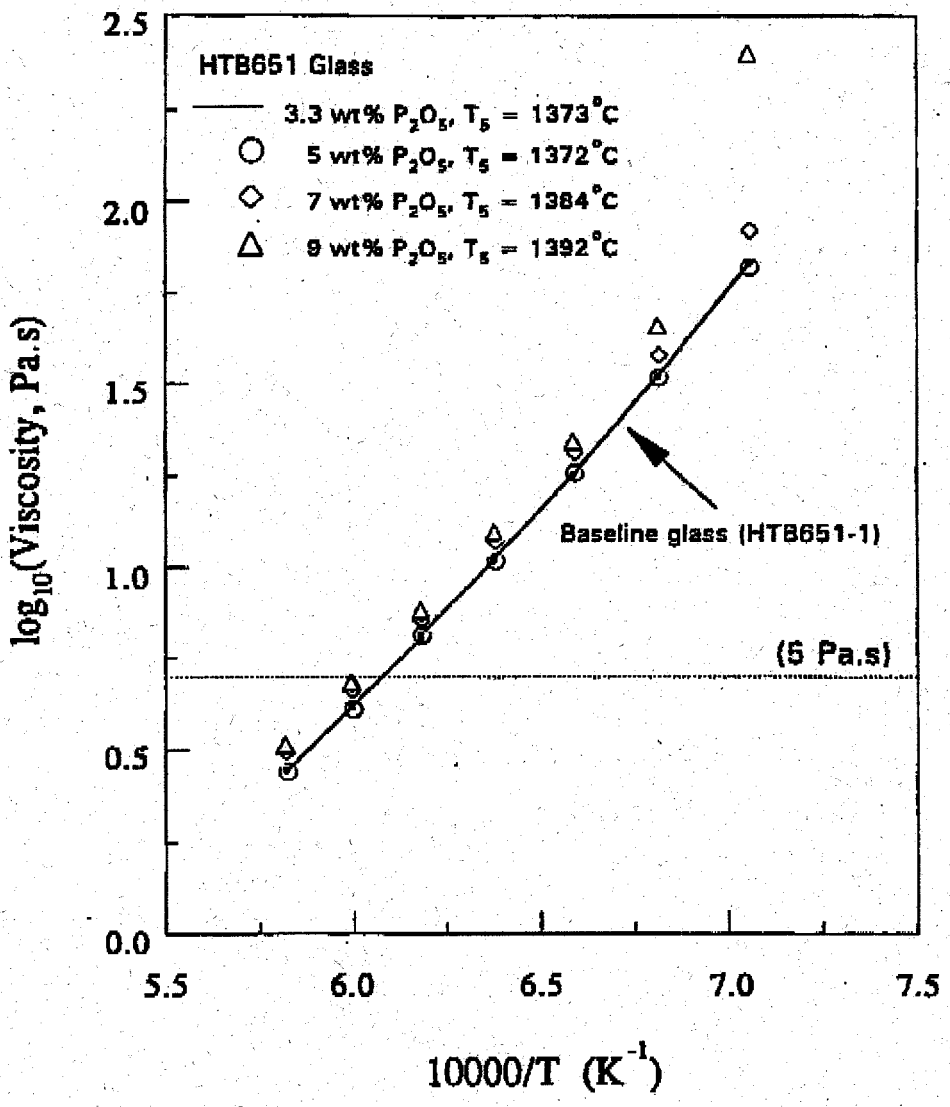

Figure 25. Measured glass melt viscosity as a fucntion of temperature for HTB651 glasses with various concentrations of P_2O_5 (T_5 is the estimated tempearture at which the glass melt viscosity is 5 Pa.s).

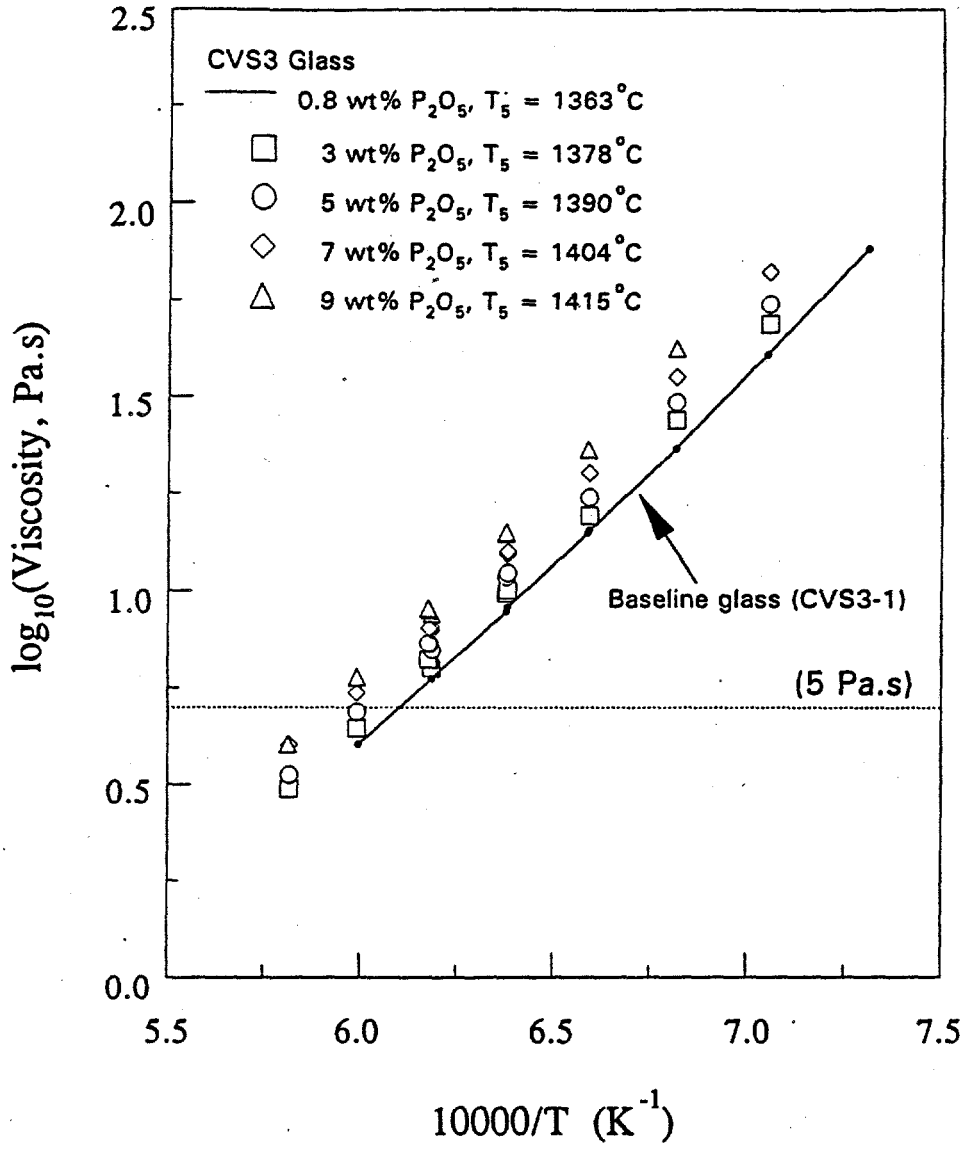

Figure 26. Measured glass melt viscosity as a fucntion of temperature for CVS3 glasses with various concentrations of P_2O_5 (T_5 is the estimated tempearture at which the glass melt viscosity is 5 Pa.s).

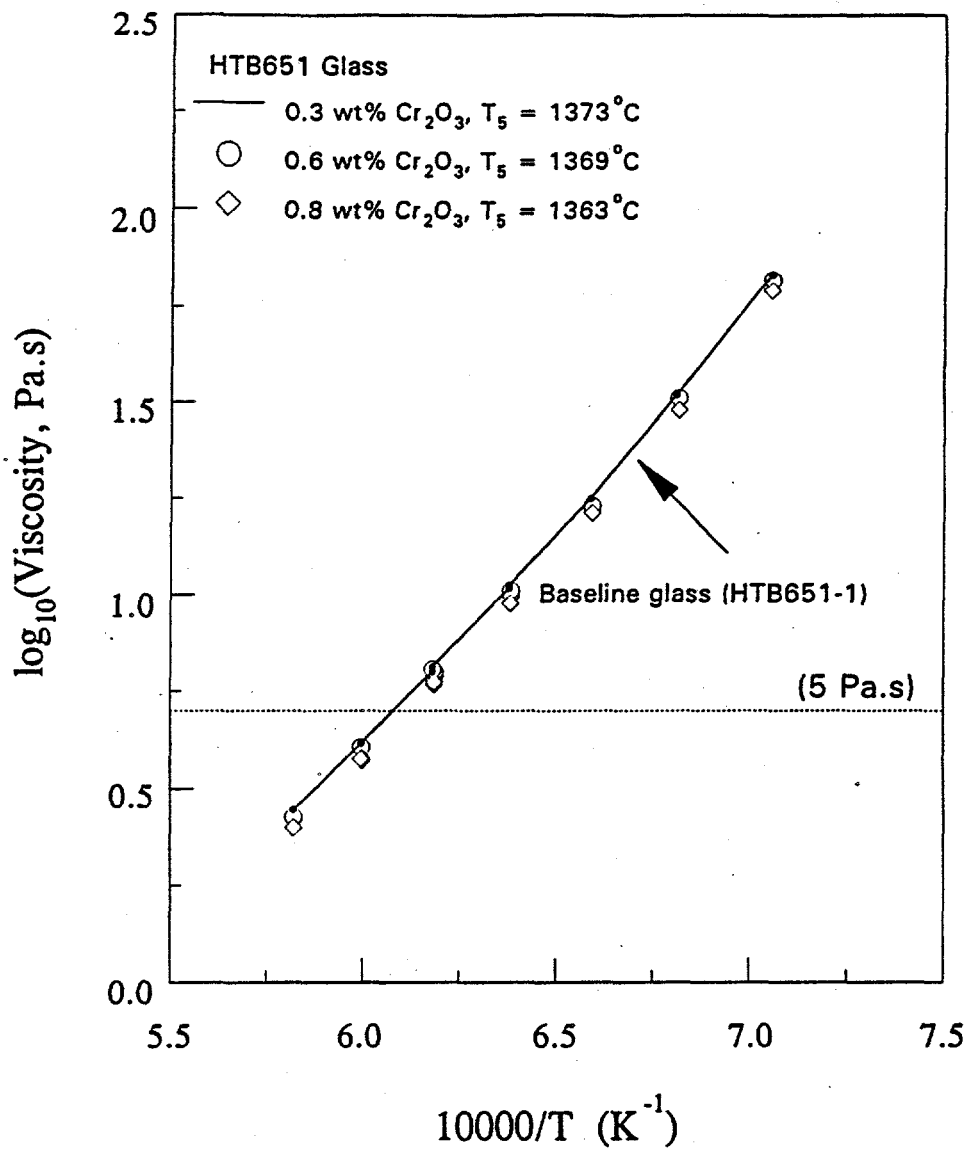

Figure 27. Measured glass melt viscosity as a fucntion of temperature for HTB651 glasses with various concentrations of Cr_2O_3 (T_5 is the estimated tempearture at which the glas melt viscosity is 5 Pa.s).

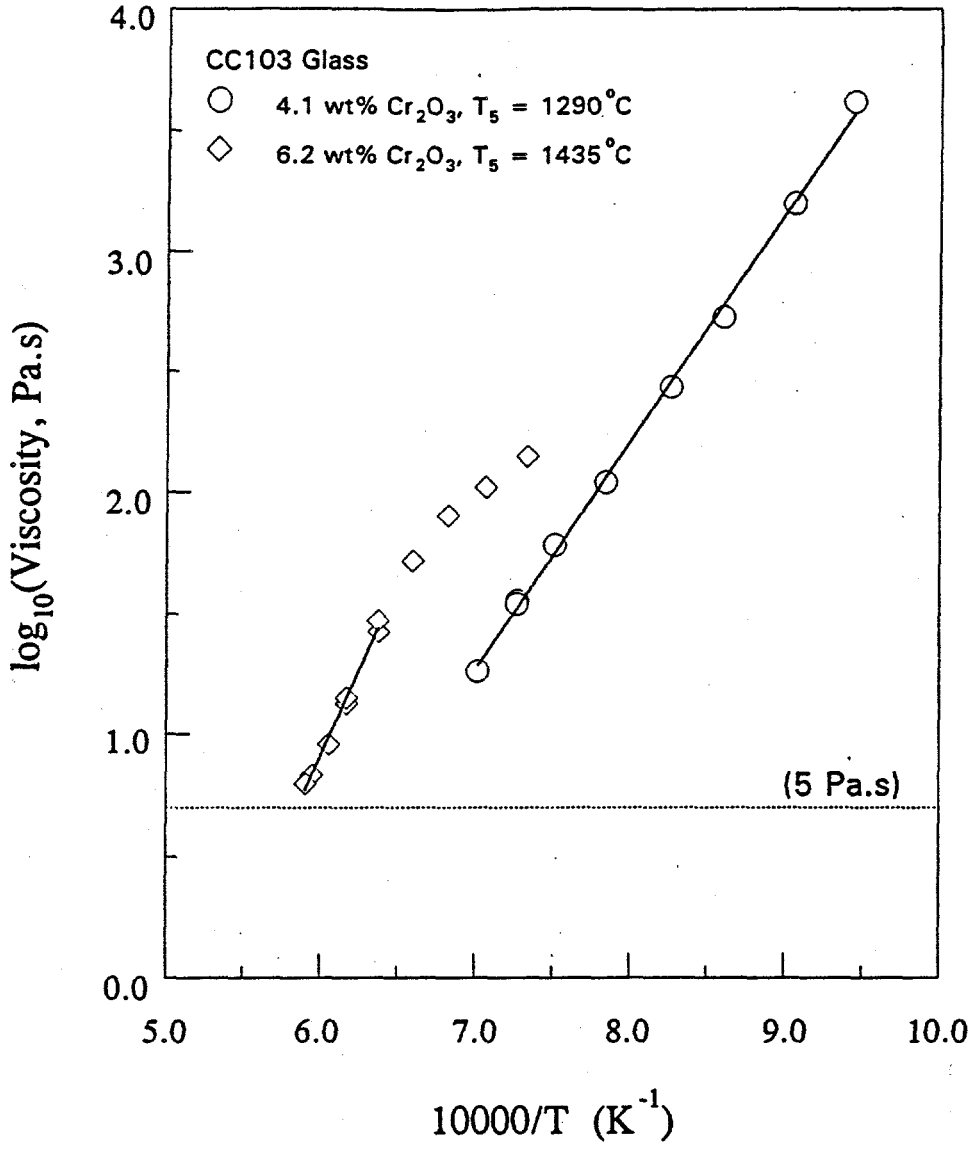

Figure 28. Measured glass melt viscosity as a fucntion of temperature for CC103-2 and CC103-3 glasses with two different levels of Cr_2O_3 (T_5 is the estimated temperature at which the glass melt viscosity is 5 Pa.s).

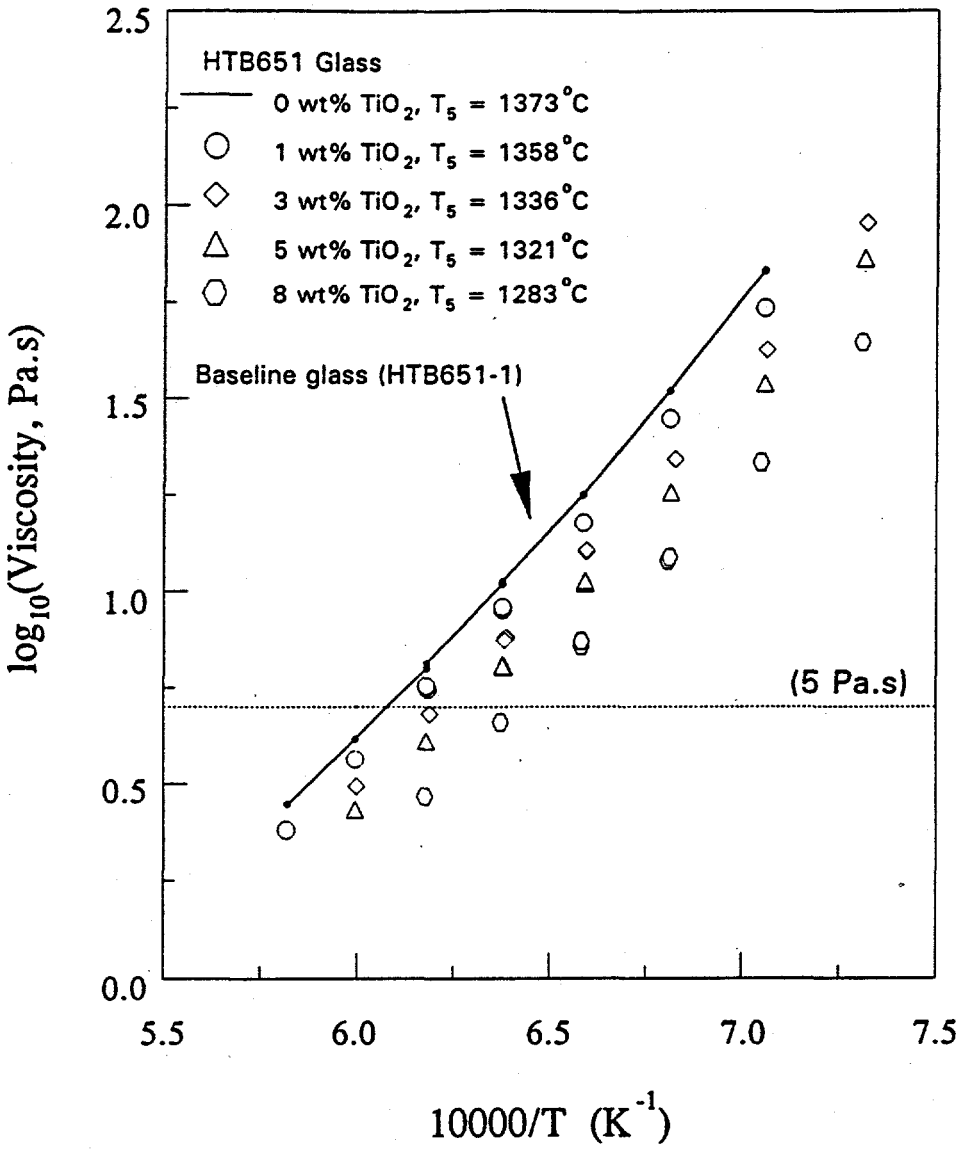

Figure 29. Measured glass melt viscosity as a fucntion of temperature for HTB651 glasses with various concentrations of TiO_2 (T_5 is the estimated tempearture at which the glass melt viscosity is 5 Pa.s).

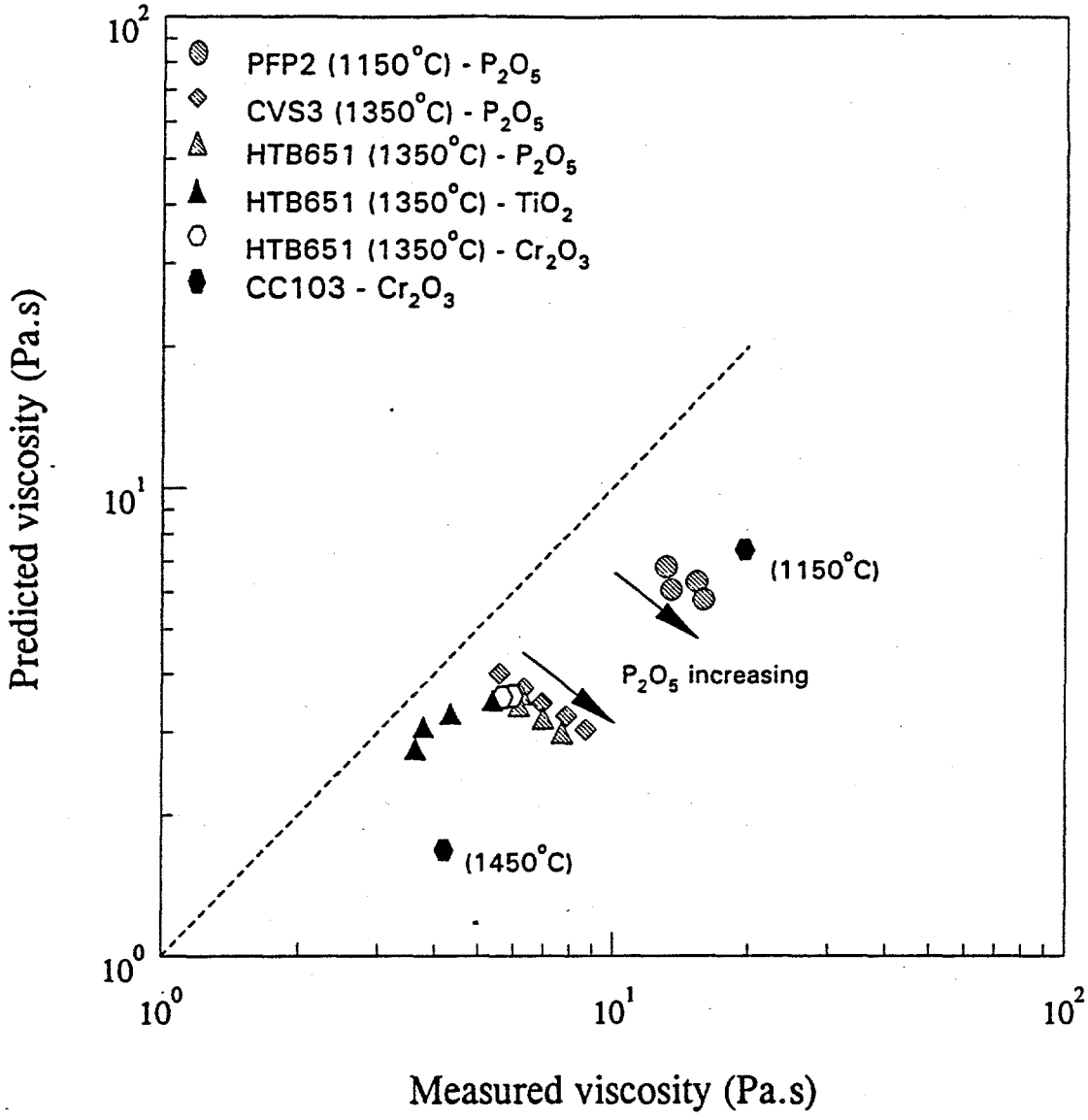

Figure 30. A comparison between the measured and the predicted glass melt viscosities at glass processing temperature for various HLW glasses.

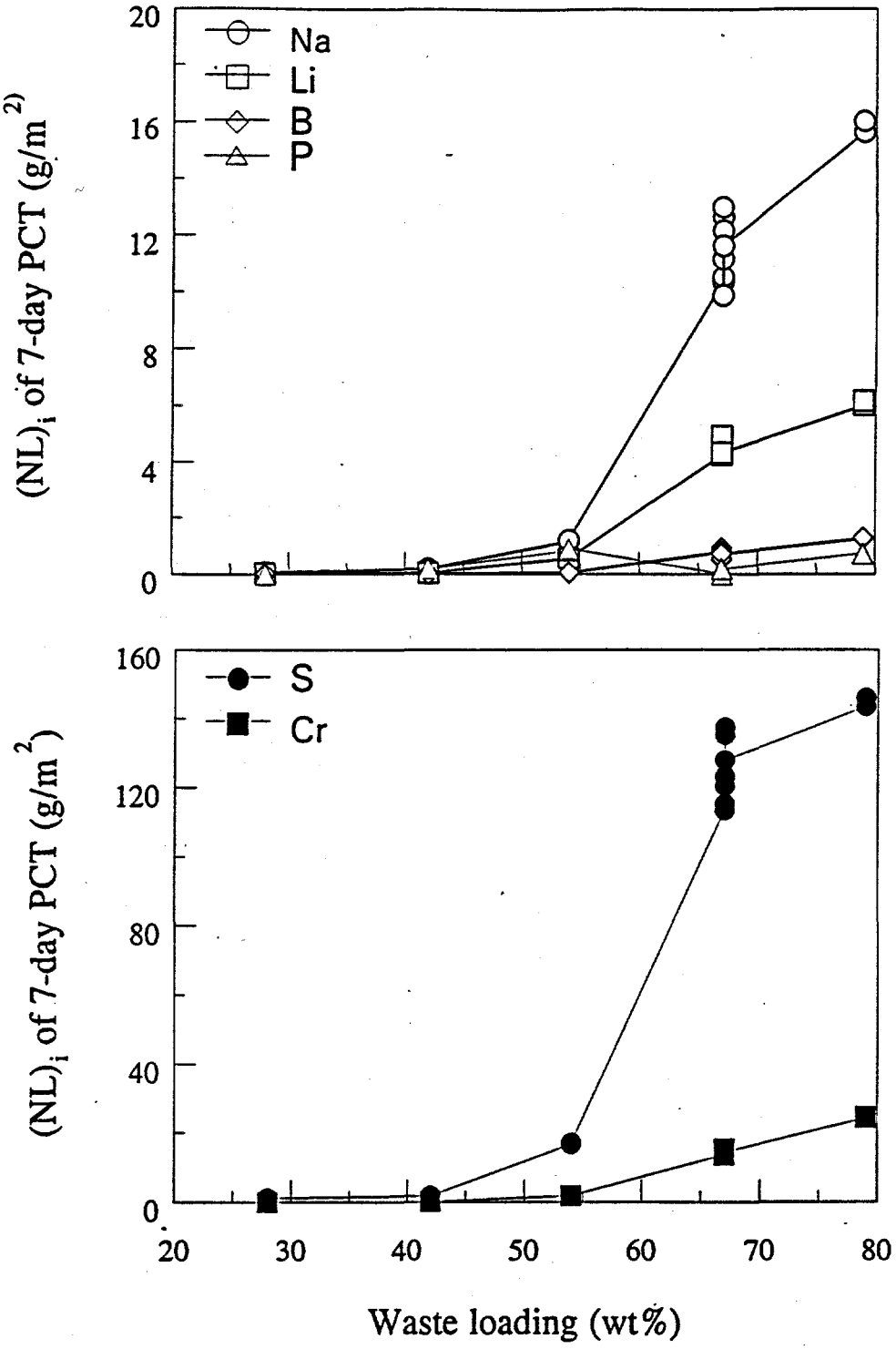

Figure 31. Normalized elemental mass losses of CCW1 glasses as a function of waste loading (Data were determined after 7-day PCT in deionized water at 90°C).

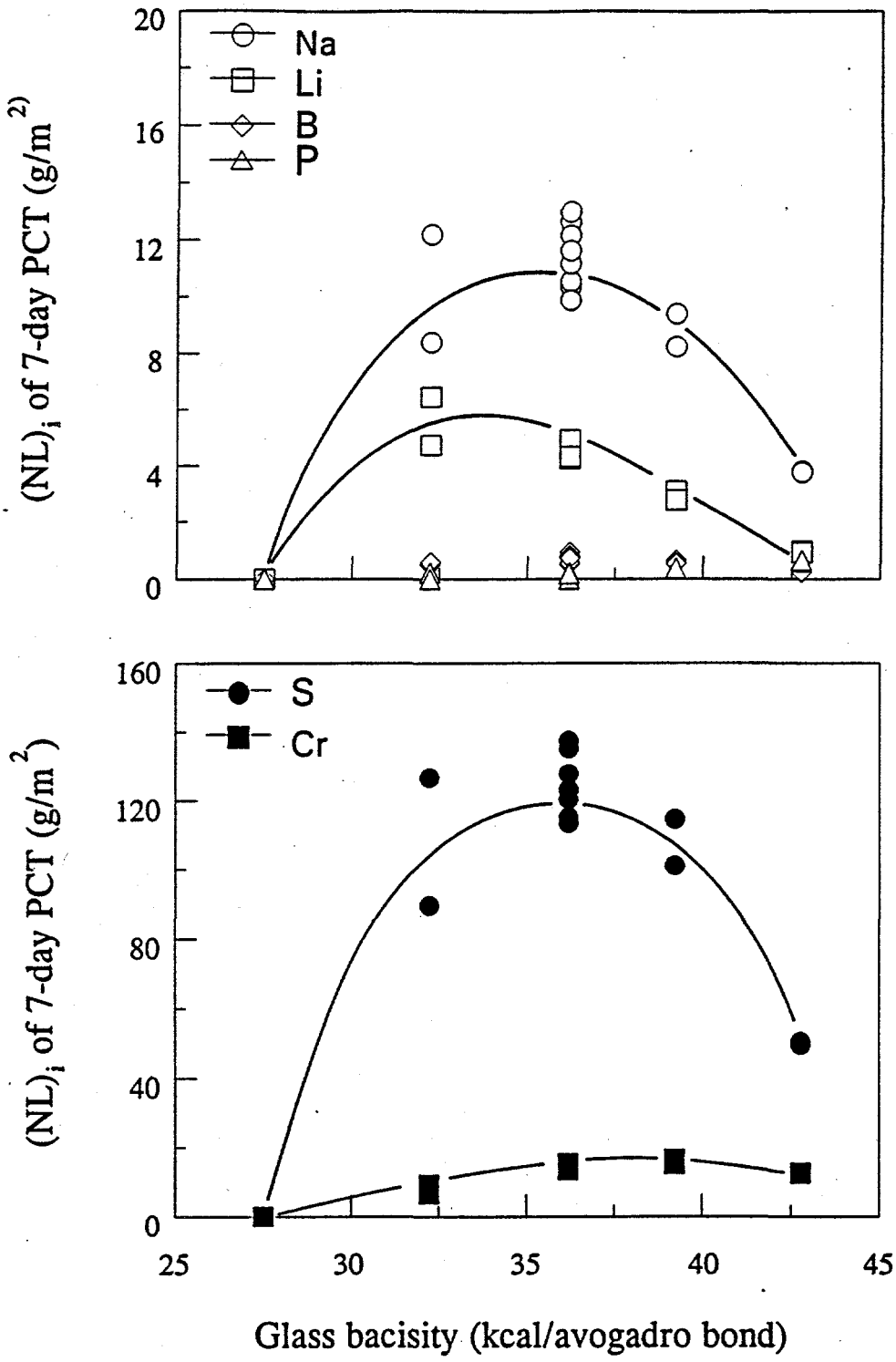

Figure 32. Normalized elemental mass losses of CCW2 glasses as a function of glass basicity (Data were determined after 7-day PCT in deionized water at 90°C).

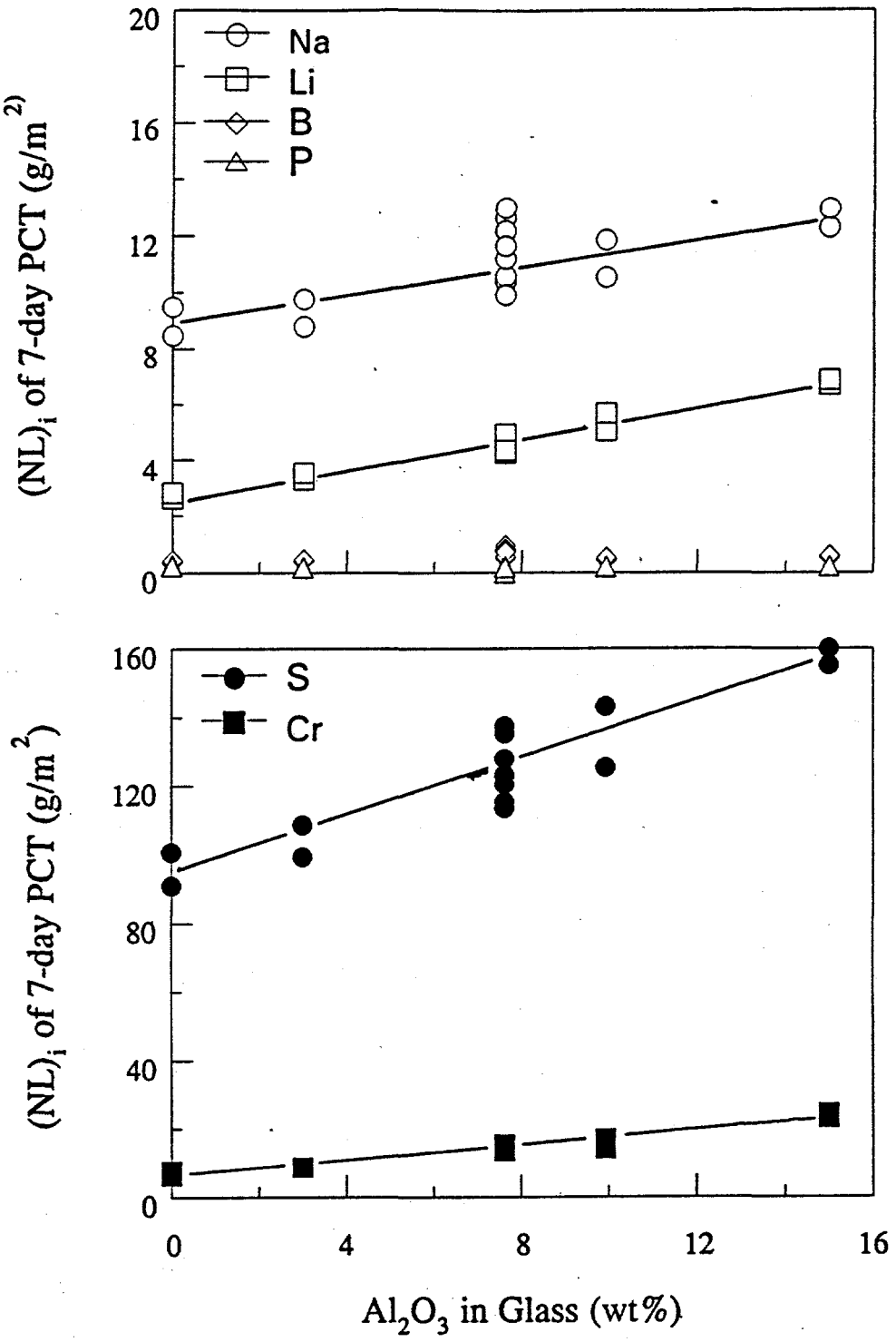

Figure 33. Normalized elemental mass losses of CCW3 glasses as a function of alumina content in glass (Data were determined after 7-day PCT in deionized water at 90°C).

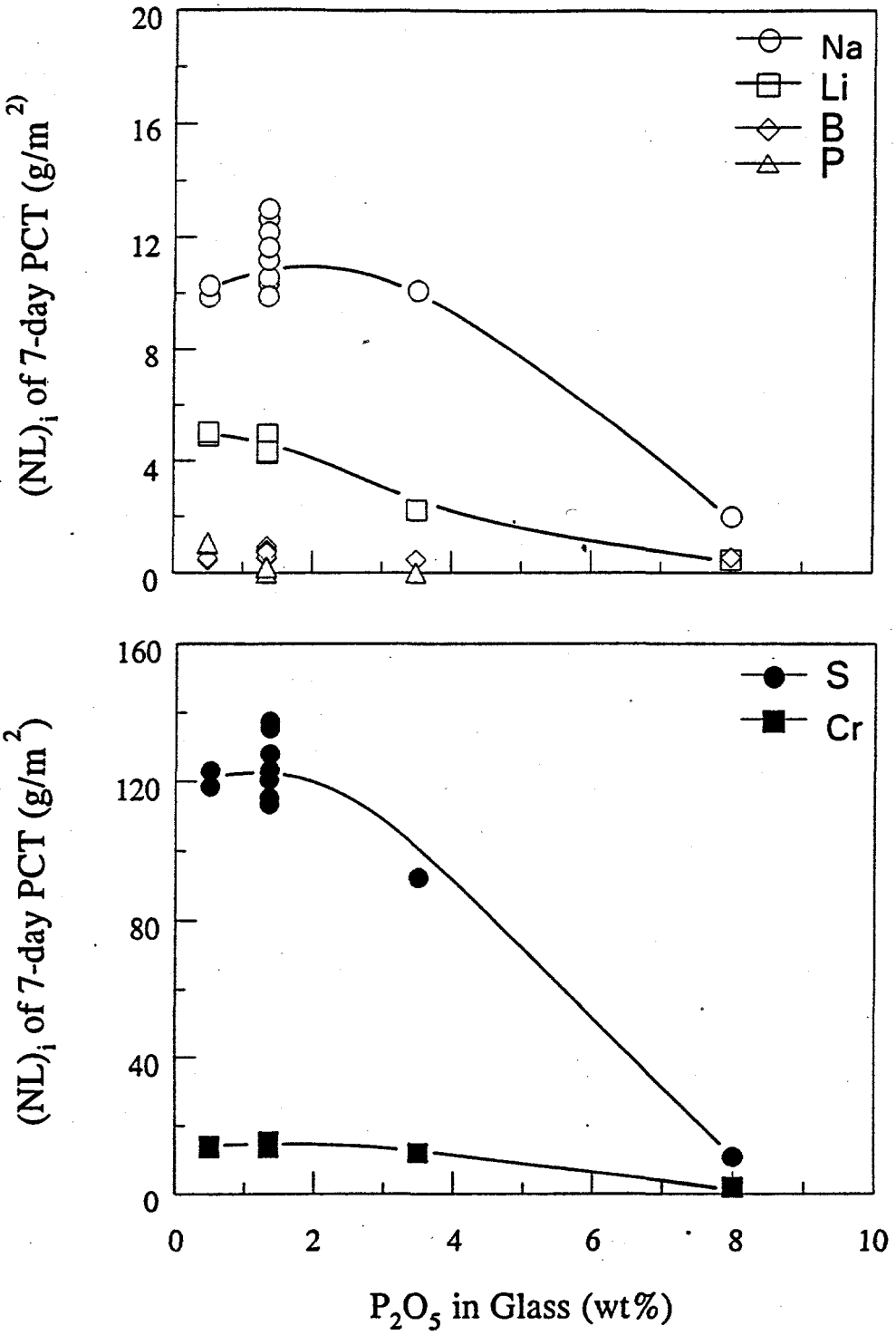

Figure 34. Normalized elemental mass losses of CCW4 glasses as a function of phosphate content in glass (Data were determined after 7-day PCT in deionized water at 90°C).

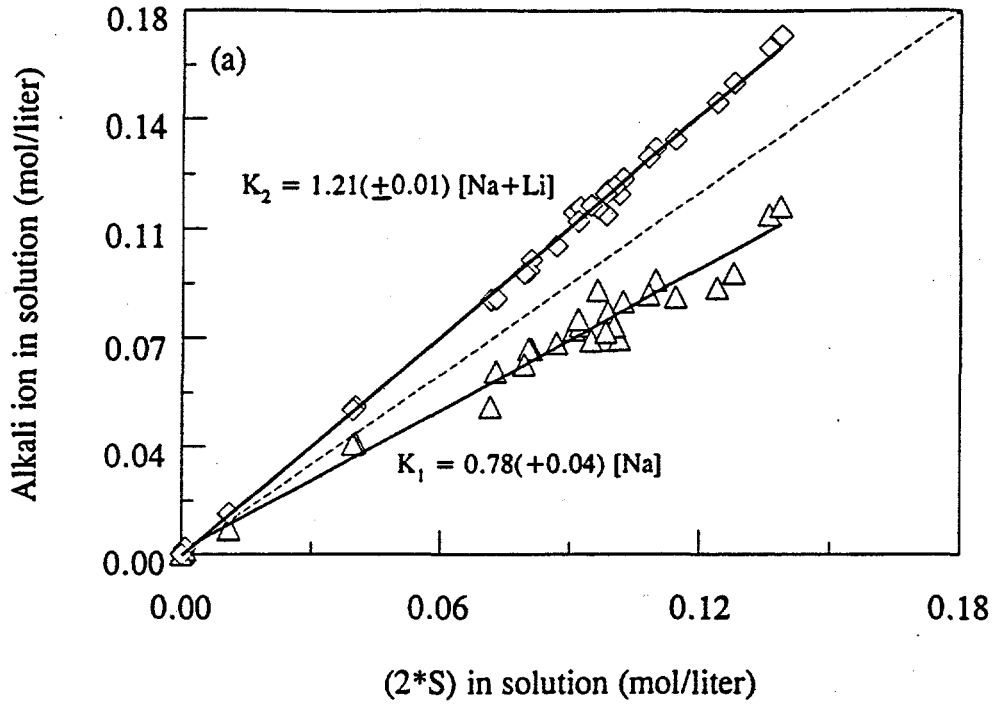

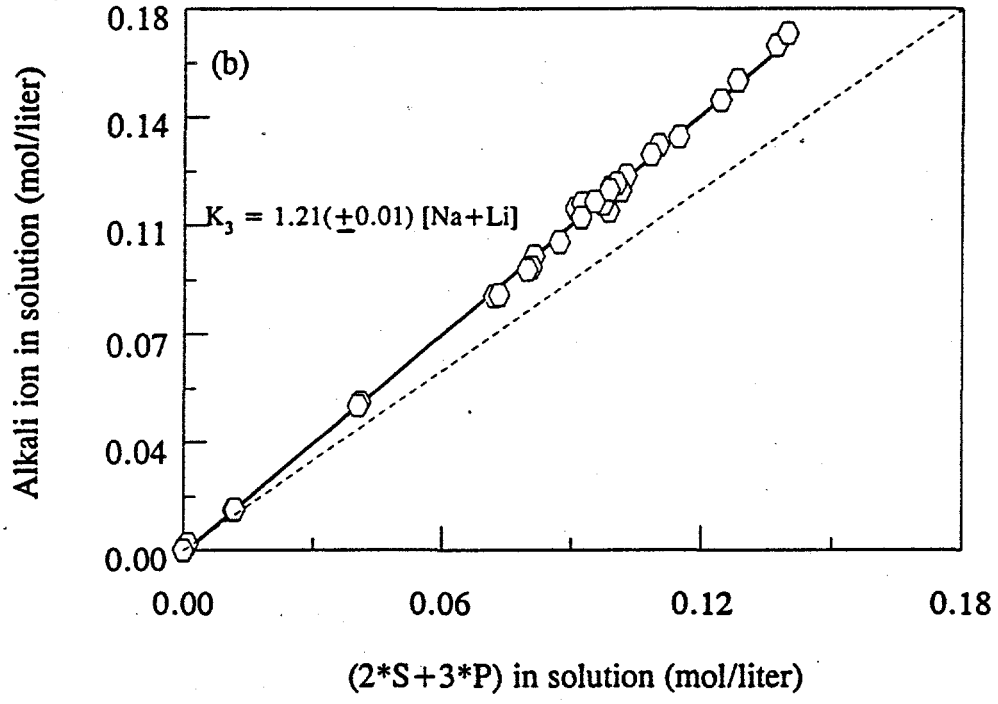

Figure 35. Relationship between released sulfur or sulfur plus phosphorous and released sodium or sodium plus lithium in solution for all CCW glasses (after 7-day PCT).

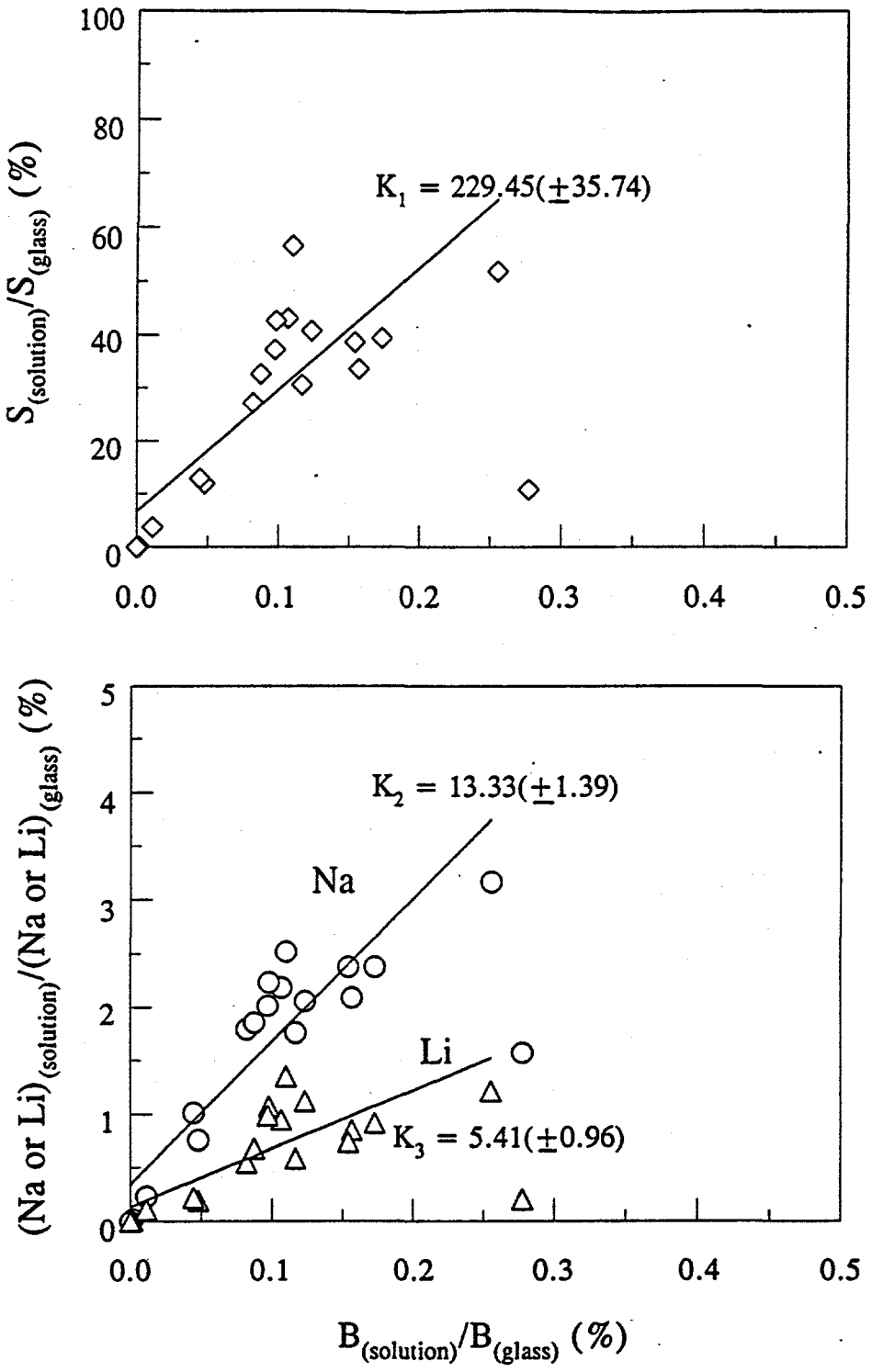

Figure 36. Comparisons between relative releases of sulfur, sodium, and lithium and that of boron for all CCW glasses (after 7-day PCT).

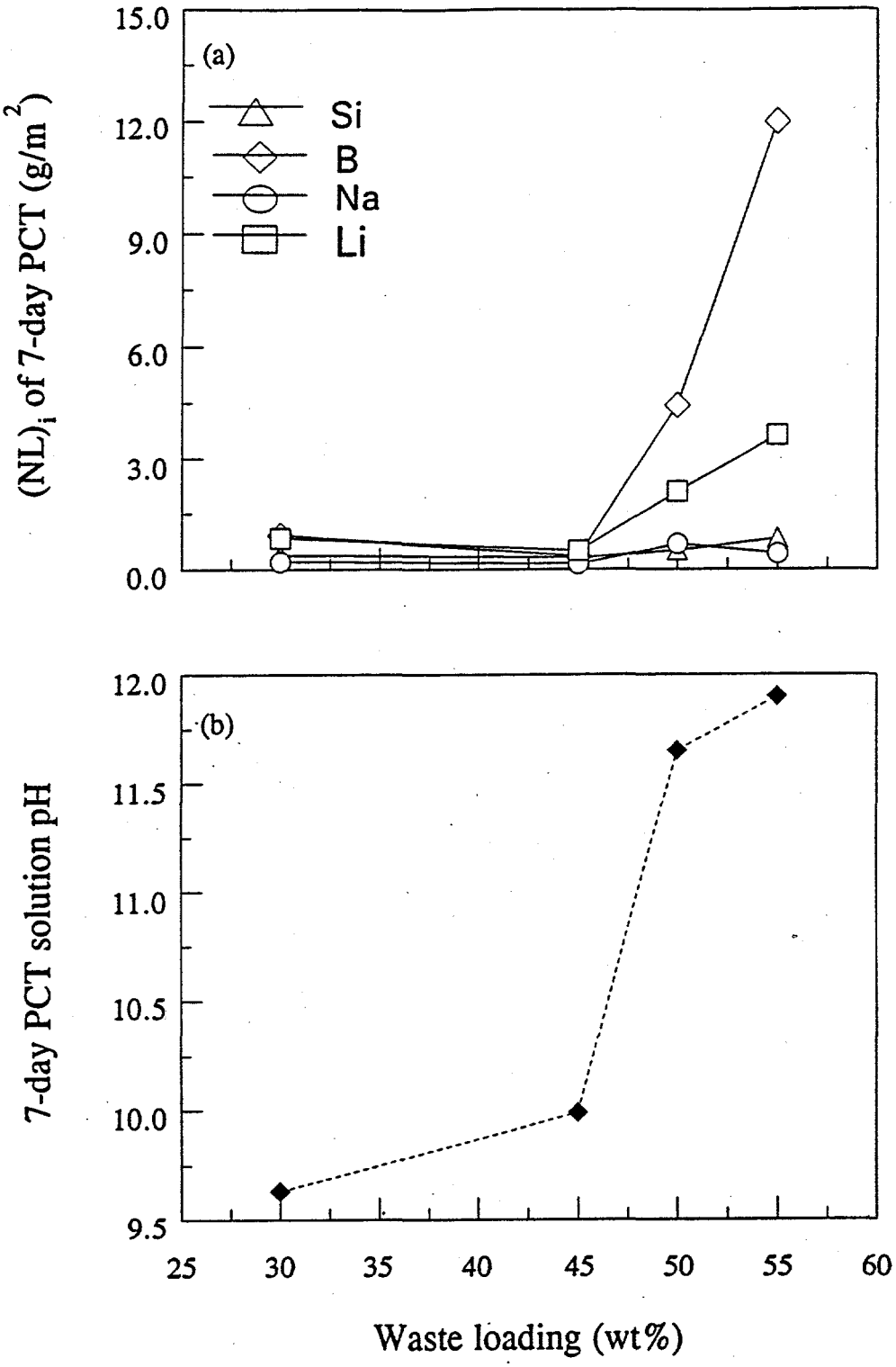

Figure 37. Normalized elemental mass losses (a) and solution pH values (b) of CC103 glasses as a function of waste loading (Data were determined after 7-day PCT in deionized water at 90°C).

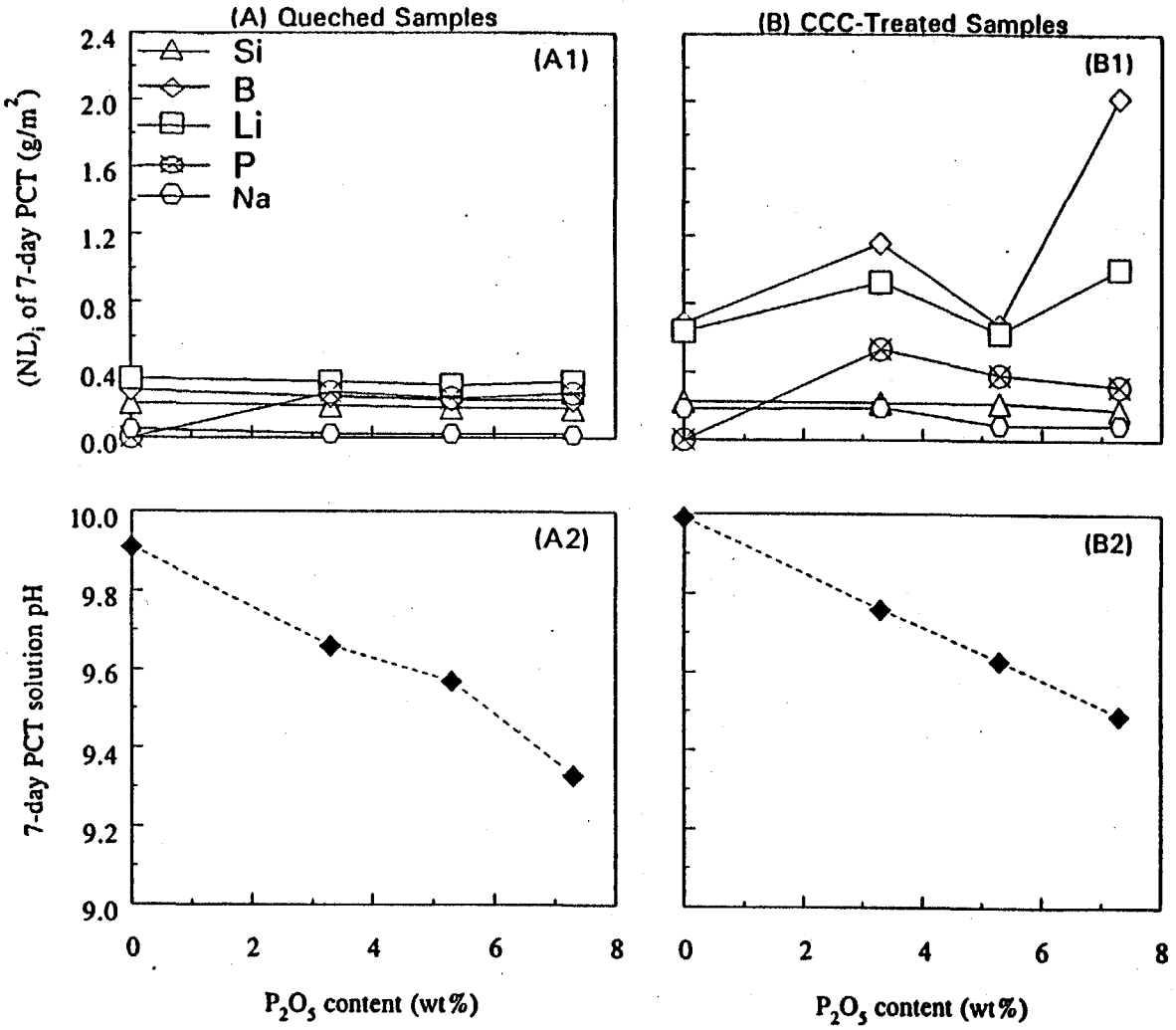

Figure 38. Normalized elemental mass losses and solution pH for quenched (A1,A2) and CCC-treated (B1,B2) PFP2 glasses as a function of phosphate content in glass (Data were determined after 7-day PCT in deionized water at 90°C).

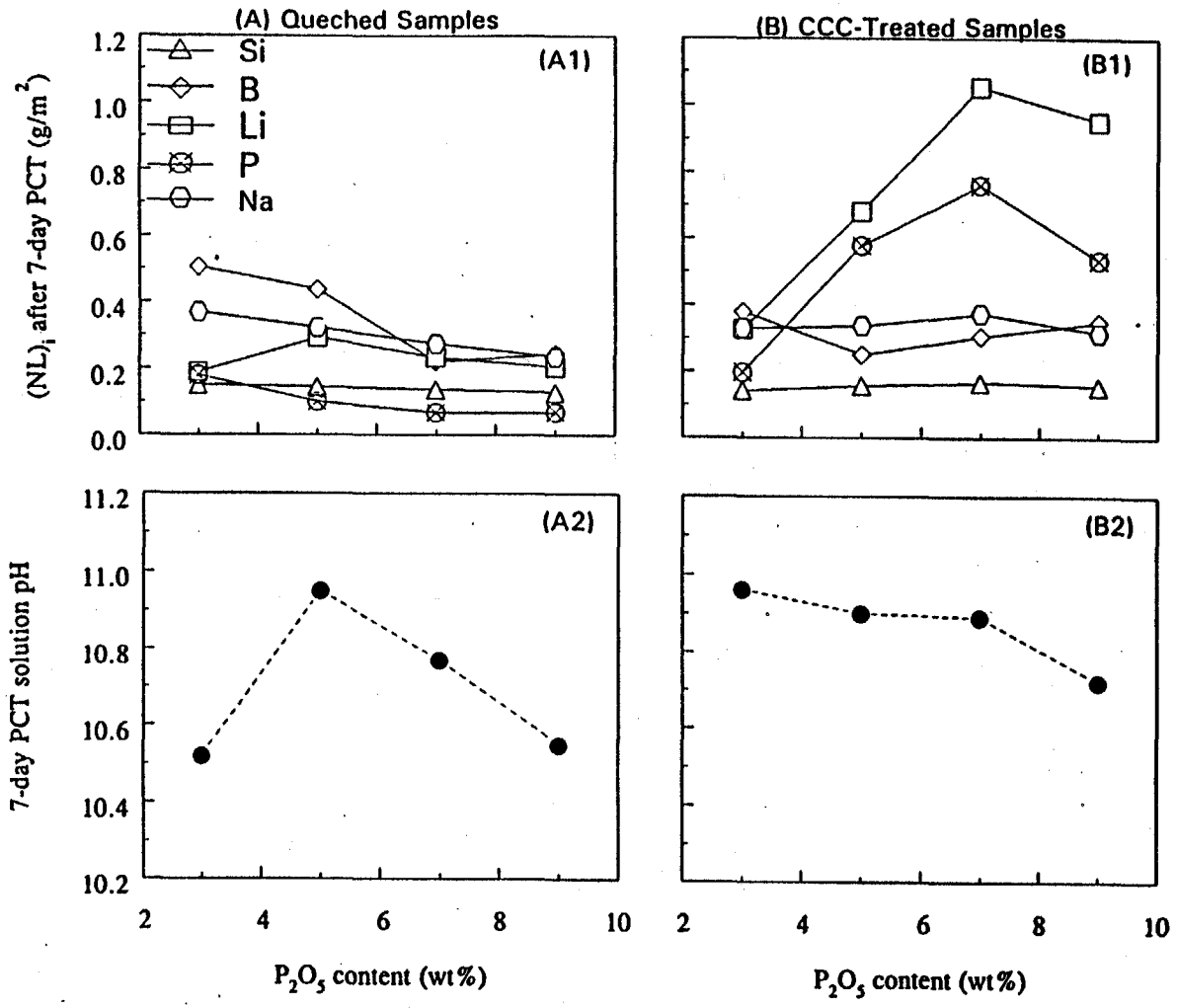

Figure 39. Normalized elemental mass losses and solution pH for quenched (A1,A2) and CCC-treated (B1,B2) CVS3 glasses as a function of phosphate content in glass (Data were determined after 7-day PCT in deionized water at 90°C).

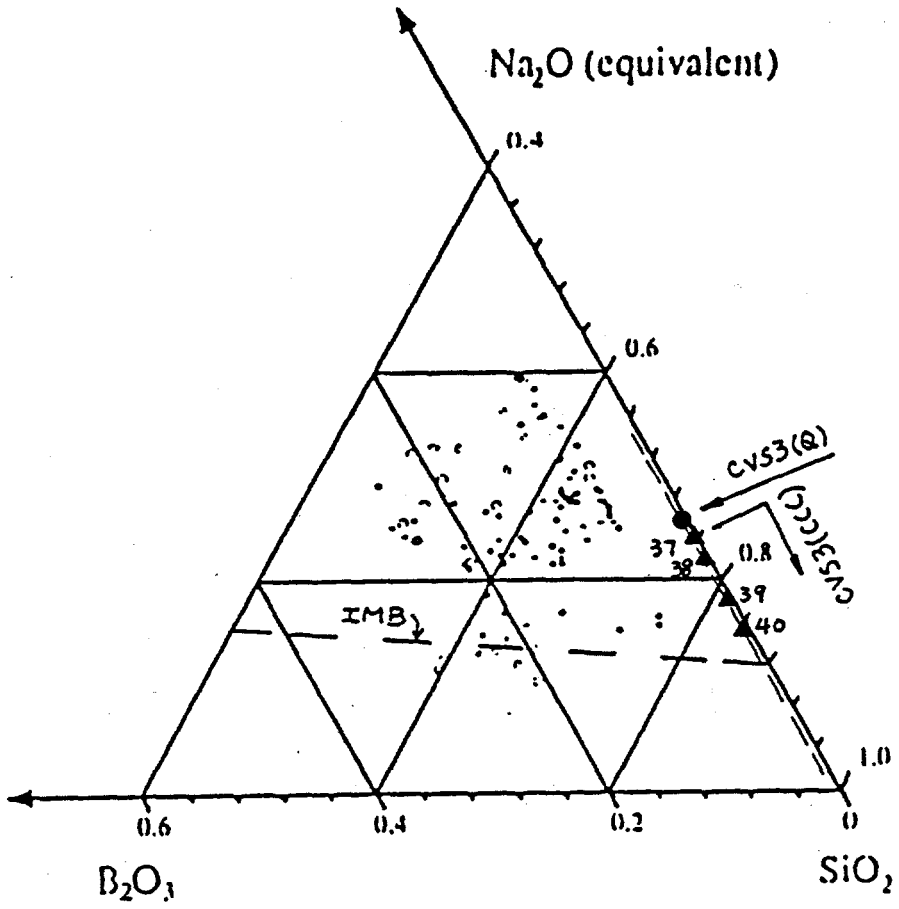

Figure 40. Normalized submixture of $(Na_2O)_{equivalent}$-SiO_2 -B_2O_3 glass system (after Peeler and Hrma, 1994), showing that the residual glass submixture compositions move toward the glass immissibility boundary (IMB) when more phosphate-bearing crystals precipitate in glass (for CCC-treated CVS3 glasses from -37 to -40).

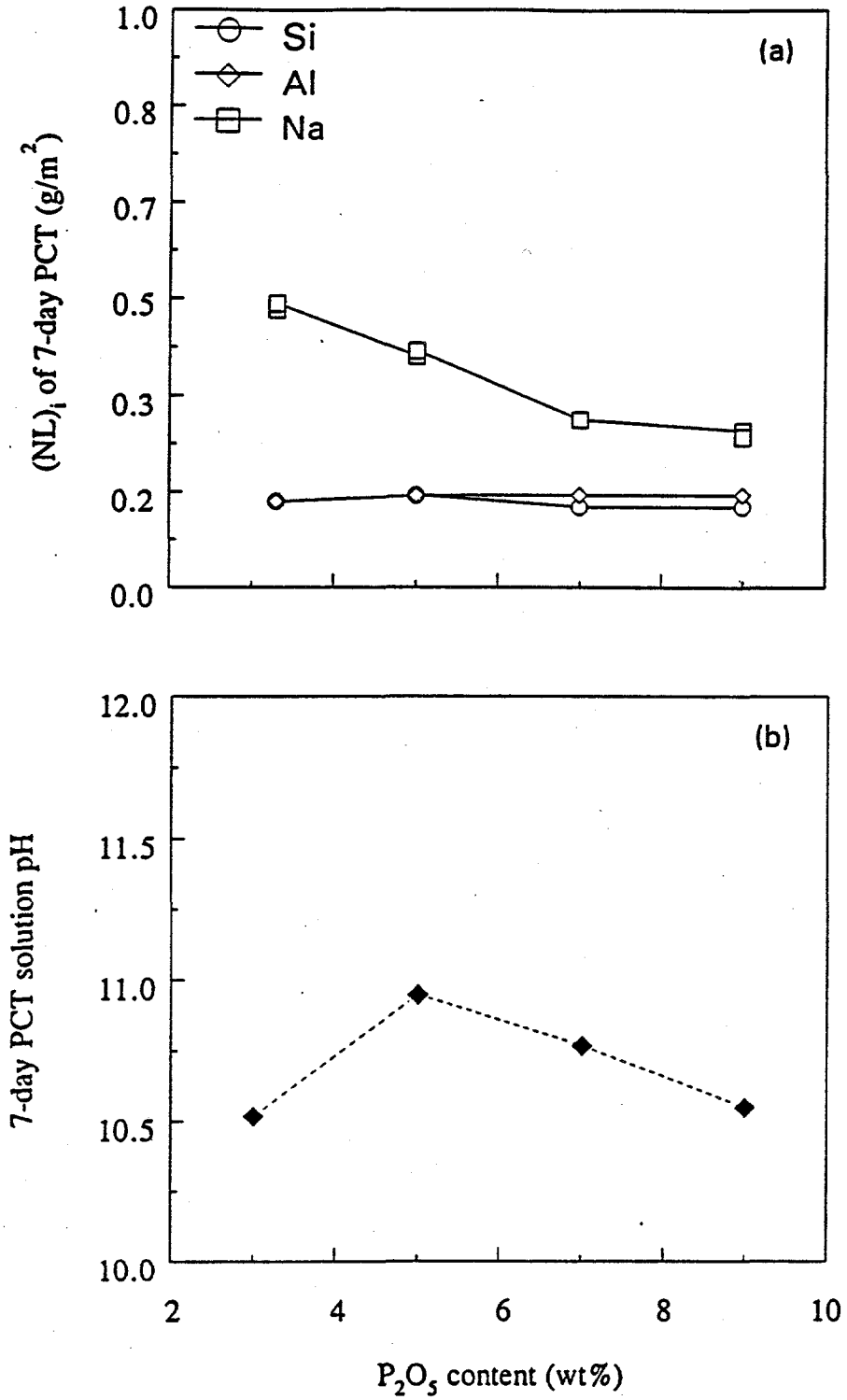

Figure 41. Normalized elemental mass losses (a) and solution pH (b) for HTB651 glasses as a function of phosphate content in glass (Data were determined after 7-day PCT in deionized water at 90°C).

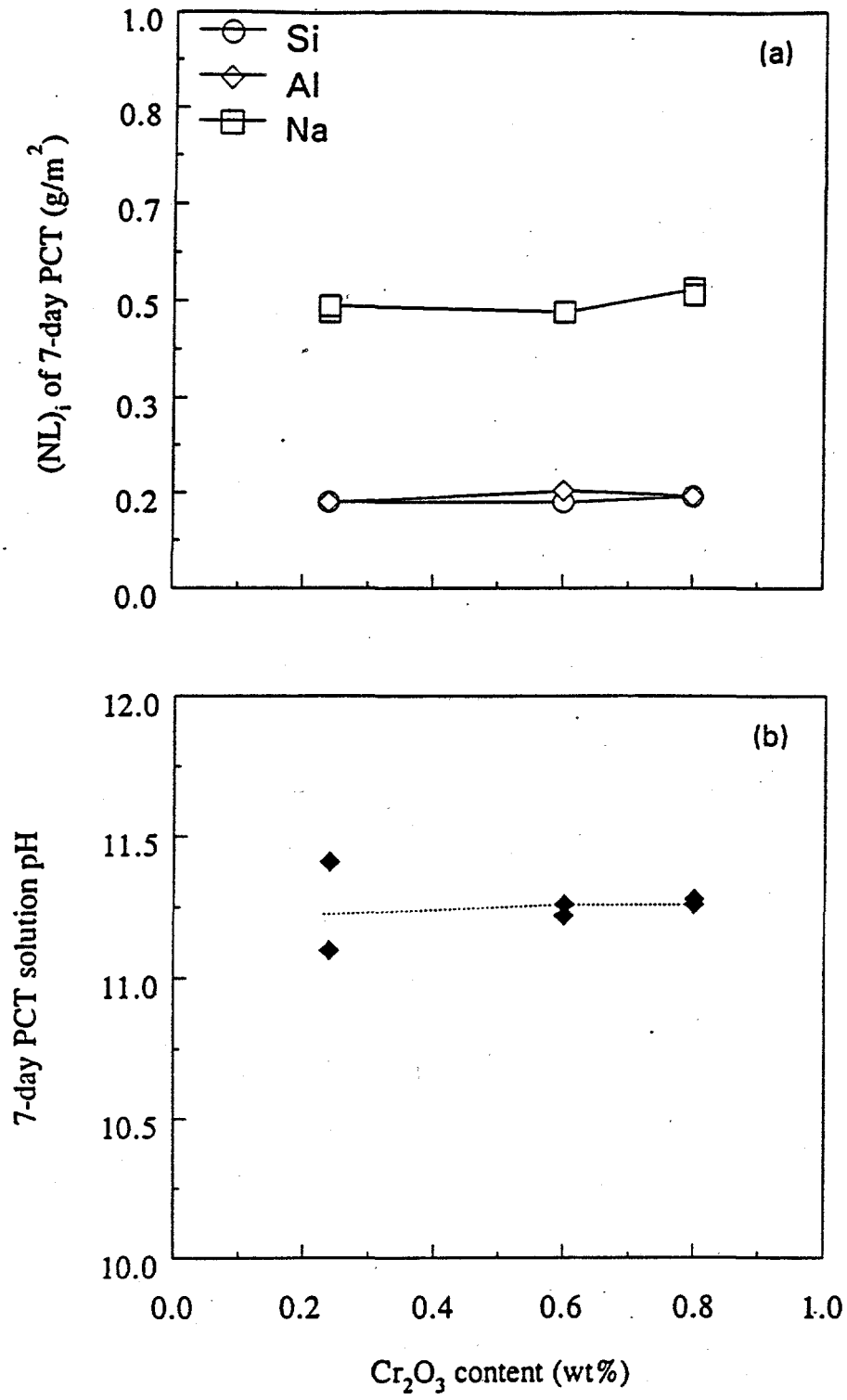

Figure 42. Normalized elemental mass losses (a) and solution pH (b) for HTB651 glasses as a function of chrome content in glass (Data were determined after 7-day PCT in deionized water at 90°C).

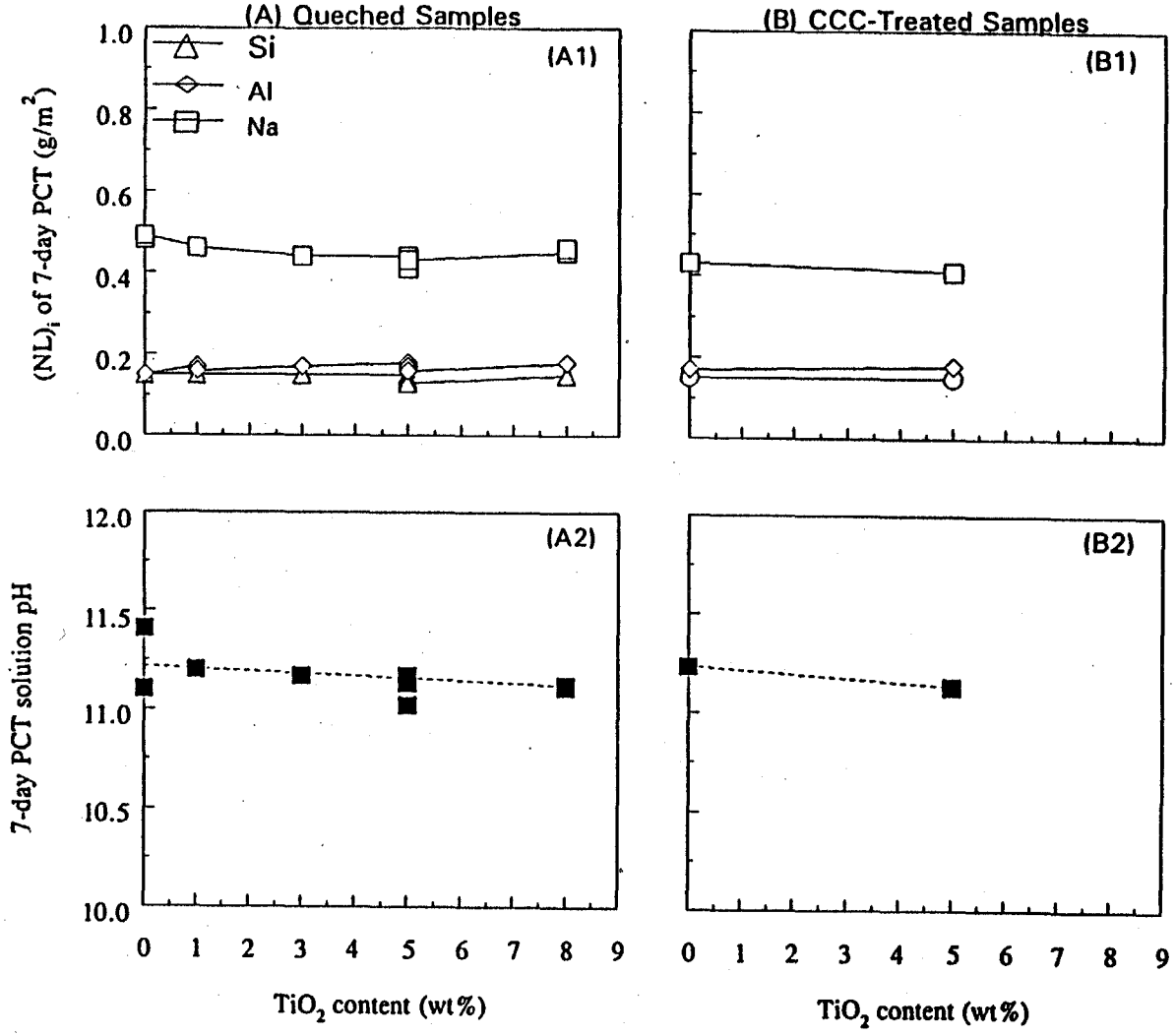

Figure 43. Normalized elemental mass losses and solution pH for quenched (A1,A2) and CCC-treated (B1,B2) HTB651 glasses as a function of titania content in glass (Data were determined after 7-day PCT in deionized water at 90 °C).

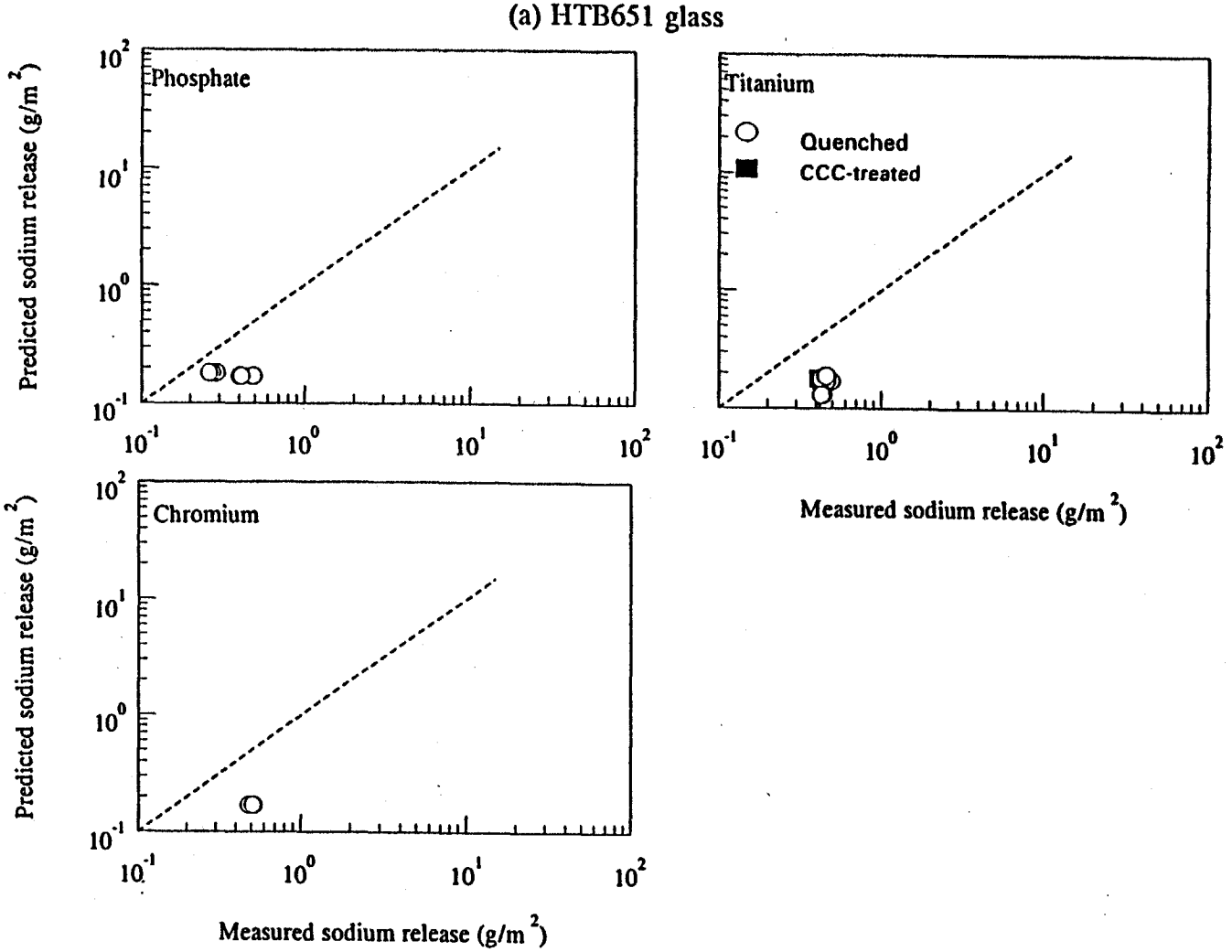

Figure 44. Comparisons between the measured and the predicted sodium and boron normalized releases after 7-day PCT for HTB651 (a), CVS3 (b), CCW (c), CC103 (d) and PFP2 (e) glasses (after 7-day PCT).

(b) CVS3 glass

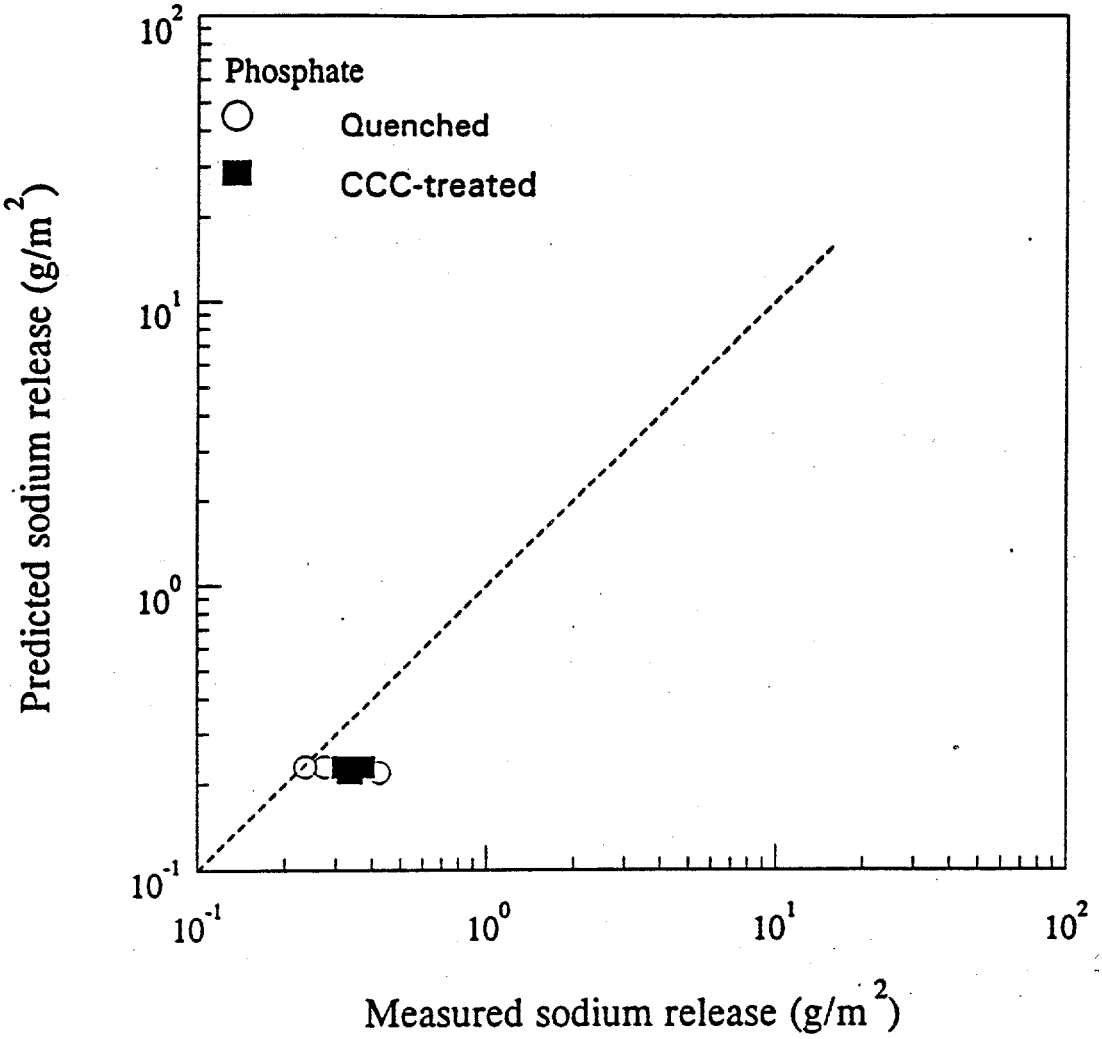
Phosphate
Quenched
CCC-treated
Predicted sodium release (g/m^2)
Measured sodium release (g/m^2)
10^2
10^1
10^0
10^{-1}
10^{-1}
10^0
10^1
10^2

(c) CCW glass

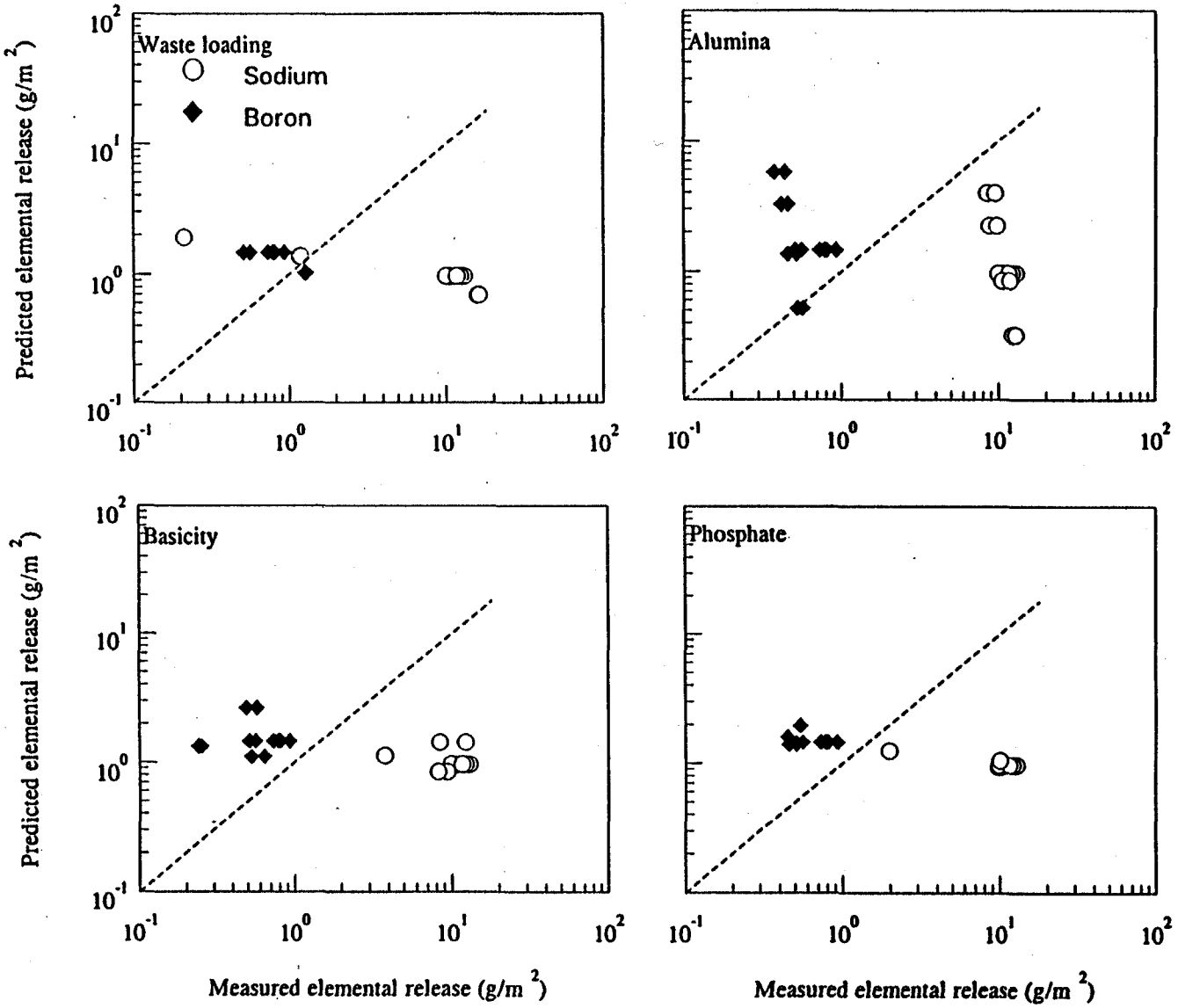
Waste loading
Sodium
Boron
Alumina
Basicity
Phosphate
Predicted elemental release (g/m 2)
Predicted elemental release (g/m 2)
Measured elemental release (g/m 2)
Measured elemental release (g/m 2)
10^2
10^1
10^0
10^-1

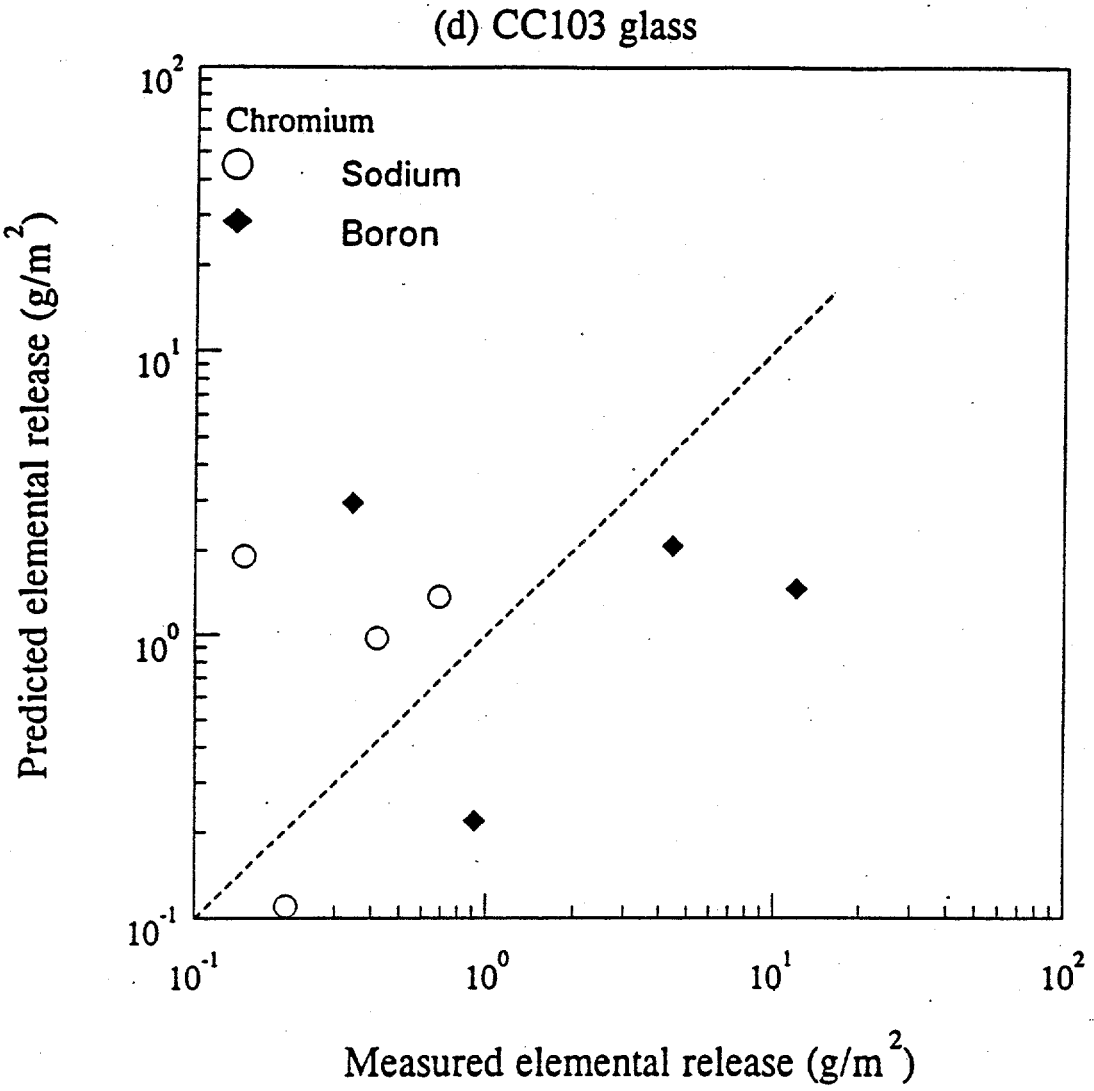
(d) CC103 glass
Chromium
Sodium
Boron
Predicted elemental release (g/m^2)
Measured elemental release (g/m^2)
10^2
10^1
10^0
10^{-1}
10^{-1}
10^0
10^1
10^2

(e) PFP2 glass

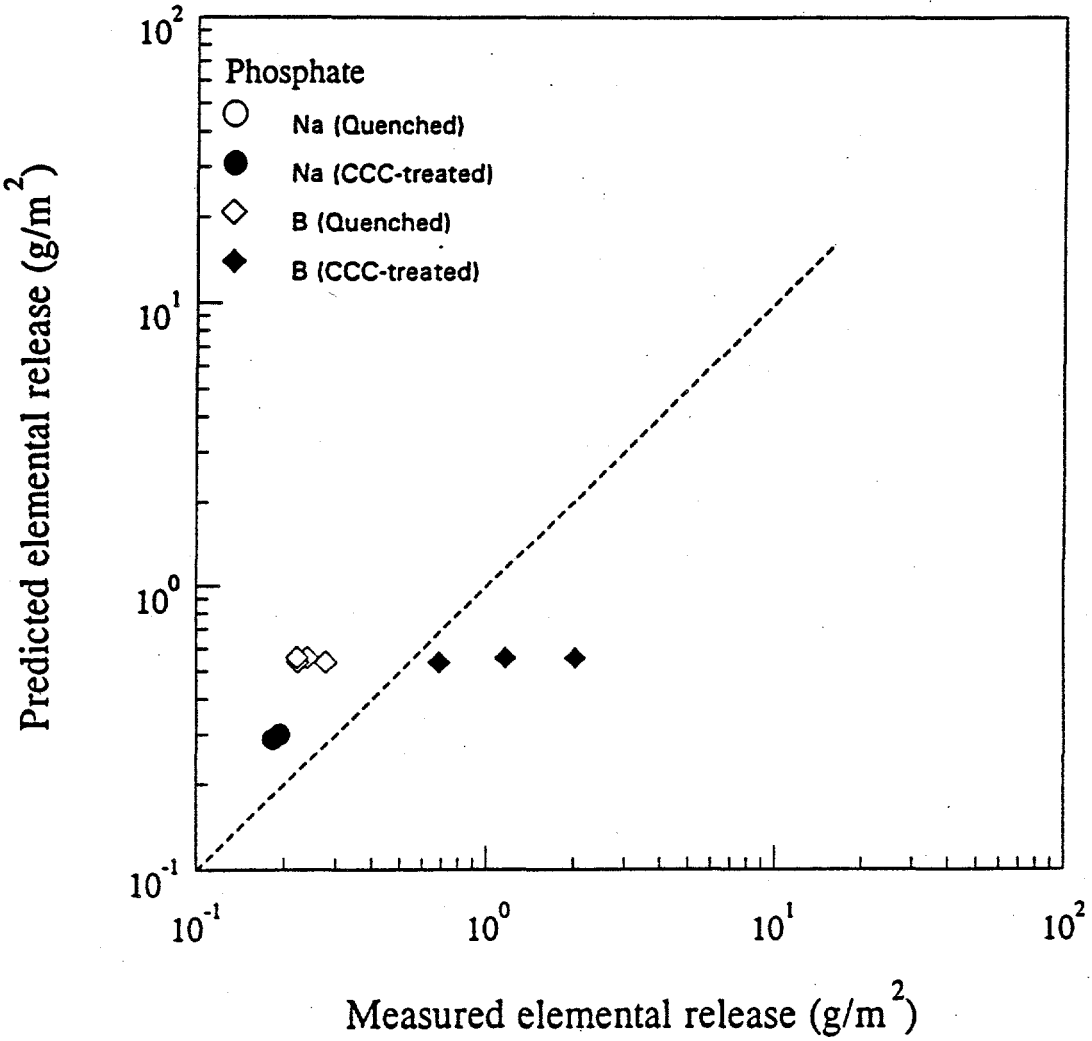
Phosphate
Na (Quenched)
Na (CCC-treated)
B (Quenched)
B (CCC-treated)
Predicted elemental release (g/m^2)
Measured elemental release (g/m^2)
10^2
10^1
10^0
10^{-1}
10^{-1}
10^0
10^1
10^2

Appendix A

Nominal Compositions (wt%) of HWVP Wastes

Appendix A Nominal Compositions (wt%) of HWVP Wastes

Component	CCW	PFP1	PFP2	DST/SST	CC103-SY92SW	Raw Materials
SiO2	69.09	1.90	1.91	10.68	1.69	SiO2
B2O3	0.00	0.25	0.25	0.08	0.00	H3BO3
Na2O	9.88	14.90	14.95	27.02	20.82	Na2CO3
Li2O	0.00	0.00	0.00	0.00	0.00	Li2CO3
CaO	0.28	3.00	3.01	2.20	0.62	CaCO3
MgO	0.18	1.06	1.06	0.08	0.06	MgO
Fe2O3	1.13	12.70	12.74	11.75	4.66	Fe2O3
Al2O3	11.40	30.70	30.80	13.88	54.04	Al2O3
ZrO2	0.08	0.20	0.20	7.56	0.07	ZrO2
Ag2O	0.00	0.08	0.00	0.00	0.00	Ag2O
Bi2O3	0.00	0.00	0.00	2.08	0.00	Bi2O3
CdO	0.00	0.40	0.40	0.10	0.00	CdO
CeO2	0.00	0.42	0.43	2.92	0.00	CeO2
Cl	1.31	0.21	0.00	0.00	0.41	NaCl
Cr2O3	0.43	8.58	8.61	0.48	13.81	Cr2O3
CuO	0.00	0.57	0.58	0.00	0.00	CuO
F	0.73	0.40	0.40	0.59	0.09	NaF
K2O	0.00	0.06	0.08	0.24	0.25	K2CO3
La2O3	0.15	0.20	0.20	0.46	0.07	La2O3
MnO2	0.52	5.39	5.41	1.59	1.37	MnO2
MoO3	0.23	0.10	0.10	0.08	0.36	MoO3
Nd2O3	0.00	0.93	0.93	9.33	0.20	Nd2O3
NiO	0.19	1.80	0.30	2.43	0.30	NiO
P2O5	2.01	11.83	11.84	5.03	0.36	NaPO3
PbO2	0.00	0.49	0.50	0.00	0.00	PbO2
PdO	0.00	0.50	0.50	0.38	0.00	PdO
Rh2O3	0.00	0.21	0.21	0.00	0.00	Rh2O3
RuO2	0.00	0.21	0.21	0.05	0.00	RuO2
Sb2O3	0.00	0.15	0.15	0.00	0.00	Sb2O3
SeO2	0.00	0.00	1.15	0.00	0.00	SeO2
SrO	0.00	0.00	0.00	0.44	0.00	SrCO3
SO3	2.39	2.49	2.50	0.36	0.19	Na2SO4
TeO2	0.00	0.17	0.18	0.00	0.00	TeO2
TiO2	0.00	0.10	0.10	0.00	0.00	TiO2
WO3	0.00	0.00	0.00	0.19	0.00	WO3
ZnO	0.00	0.00	0.00	0.00	0.62	ZnO
Total	100.00	100.00	100.00	100.00	100.00	

Appendix B

Nominal Compositions (wt%) of HLW Glasses

Appendix B1 Nominal Composition (wt%) of CCW Glasses

Series	Waste Loading					Basicity				Alumina				Phosphate		
Glass ID	CCW1-1	CCW1-2	CCW1-3	CCW1-4	CCW1-5	CCW2-1	CCW2-2	CCW2-3	CCW2-4	CCW3-1	CCW3-2	CCW3-3	CCW3-4	CCW4-1	CCW4-2	CCW4-3
WL (%)	28.0	42.0	54.0	67.0	79.0	67.0	67.0	67.0	67.0	67.0	67.0	67.0	67.0	67.0	67.0	67.0
SiO2	63.51	61.23	59.16	57.09	55.02	48.24	51.82	60.02	60.53	66.10	62.73	52.26	46.57	57.92	54.92	50.42
B2O3	12.59	11.96	11.40	10.82	10.25	27.00	19.43	5.11	1.02	9.44	9.80	13.35	13.97	10.83	10.83	10.83
Na2O	11.17	11.17	11.17	11.17	11.17	6.62	9.09	12.89	15.11	11.17	11.17	11.17	11.17	11.17	11.17	11.17
Li2O	6.84	6.84	6.84	6.84	6.84	4.05	5.57	7.89	9.25	6.84	6.84	6.84	6.84	6.84	6.84	6.84
CaO	0.08	0.12	0.15	0.19	0.22	0.19	0.19	0.19	0.19	0.19	0.19	0.19	0.19	0.19	0.19	0.19
MgO	0.05	0.08	0.10	0.12	0.14	0.12	0.12	0.12	0.12	0.12	0.12	0.12	0.12	0.12	0.12	0.12
Fe2O3	0.32	0.47	0.61	0.76	0.90	0.76	0.76	0.76	0.76	0.76	0.76	0.76	0.76	0.76	0.76	0.76
Al2O3	3.19	4.77	6.20	7.63	9.06	7.64	7.64	7.64	7.64	0.00	3.00	9.93	15.00	7.64	7.64	7.64
ZrO2	0.02	0.03	0.04	0.05	0.06	0.05	0.05	0.05	0.05	0.05	0.05	0.05	0.05	0.05	0.05	0.05
Others	2.23	3.33	4.33	5.33	6.33	5.33	5.33	5.33	5.33	5.33	5.33	5.33	5.33	4.49	7.49	11.99
Total	100.00	100.00	100.00	100.00	100.00	100.00	100.00	100.00	100.00	100.00	100.00	100.00	100.00	100.00	100.00	100.00
Others																
Cl	0.37	0.55	0.71	0.88	1.04	0.88	0.88	0.88	0.88	0.88	0.88	0.88	0.88	0.88	0.88	0.88
Cr2O3	0.12	0.18	0.23	0.29	0.34	0.29	0.29	0.29	0.29	0.29	0.29	0.29	0.29	0.29	0.29	0.29
Cs2O	0.00	0.00	0.00	0.00	0.00	0.00	0.00	0.00	0.00	0.00	0.00	0.00	0.00	0.00	0.00	0.00
F	0.20	0.31	0.40	0.49	0.58	0.49	0.49	0.49	0.49	0.49	0.49	0.49	0.49	0.49	0.49	0.49
La2O3	0.04	0.06	0.08	0.10	0.12	0.10	0.10	0.10	0.10	0.10	0.10	0.10	0.10	0.10	0.10	0.10
MnO2	0.15	0.22	0.28	0.35	0.41	0.35	0.35	0.35	0.35	0.35	0.35	0.35	0.35	0.35	0.35	0.35
MoO3	0.06	0.10	0.13	0.15	0.18	0.15	0.15	0.15	0.15	0.15	0.15	0.15	0.15	0.15	0.15	0.15
NiO	0.05	0.08	0.10	0.13	0.15	0.13	0.13	0.13	0.13	0.13	0.13	0.13	0.13	0.13	0.13	0.13
P2O5	0.56	0.84	1.09	1.35	1.60	1.35	1.35	1.35	1.35	1.35	1.35	1.35	1.35	0.50	3.50	8.00
SO3	0.67	1.00	1.30	1.60	1.90	1.60	1.60	1.60	1.60	1.60	1.60	1.60	1.60	1.60	1.60	1.60
Subtaotal	0.49	3.33	4.33	5.33	6.33	5.33	5.33	5.33	5.33	1.17	1.17	1.17	1.17	1.17	1.17	1.17
Viscosity (Pa.s)	5.75	5.70	5.65	5.61	5.56	4.00	4.00	6.00	4.00	6.00	6.00	4.00	4.00	6.09	4.54	2.92
Melting Temp (C)	1150	1150	1150	1150	1150	1150	1150	1150	1150	1150	1150	1150	1150	1150	1150	1150
Glass Basicity	32.32	33.68	34.93	36.20	37.48	27.52	32.24	39.24	42.79	35.40	35.73	36.29	36.88	36.11	36.45	36.97

Appendix B2 Nominal Composition (wt%) of PFP1 Glasses

Glass ID	PFP1-1	PFP1-2	PFP1-3	PFP1-4	PFP1-5	PFP1-6	PFP1-7
WL (%)	40.0	40.0	40.0	40.0	40.0	40.0	40.0
SiO2	39.56	41.12	41.87	37.11	37.85	38.97	43.09
B2O3	6.40	5.50	4.36	22.05	20.91	19.19	12.86
Na2O	19.36	18.49	18.49	5.96	5.96	5.96	5.96
Li2O	1.50	1.70	2.10	1.70	2.10	2.70	4.90
CaO	1.20	1.20	1.20	1.20	1.20	1.20	1.20
MgO	0.42	0.42	0.42	0.42	0.42	0.42	0.42
Fe2O3	5.08	5.08	5.08	5.08	5.08	5.08	5.08
Al2O3	12.28	12.28	12.28	12.28	12.28	12.28	12.28
ZrO2	0.08	0.08	0.08	0.08	0.08	0.08	0.08
Others	14.12	14.10	14.12	14.10	14.10	14.10	14.10
Total	100.00	100.00	100.00	100.00	100.00	100.00	100.00
Others							
Ag2O	0.03	0.03	0.03	0.03	0.03	0.03	0.03
CdO	0.16	0.16	0.16	0.16	0.16	0.16	0.16
CeO2	0.17	0.17	0.17	0.17	0.17	0.17	0.17
Cl	0.08	0.08	0.08	0.08	0.08	0.08	0.08
Cr2O3	3.44	3.43	3.43	3.43	3.43	3.43	3.43
CuO	0.23	0.23	0.23	0.23	0.23	0.23	0.23
F	0.16	0.16	0.16	0.16	0.16	0.16	0.16
K2O	0.03	0.03	0.03	0.03	0.03	0.03	0.03
La2O3	0.08	0.08	0.08	0.08	0.08	0.08	0.08
MnO2	2.16	2.16	2.16	2.16	2.16	2.16	2.16
MoO3	0.04	0.04	0.04	0.04	0.04	0.04	0.04
Nd2O3	0.37	0.37	0.37	0.37	0.37	0.37	0.37
NiO	0.72	0.71	0.71	0.71	0.71	0.71	0.71
P2O5	4.73	4.72	4.72	4.72	4.72	4.72	4.72
PbO2	0.20	0.19	0.19	0.19	0.19	0.19	0.19
PdO	0.20	0.20	0.20	0.20	0.20	0.20	0.20
Rh2O3	0.09	0.08	0.08	0.08	0.08	0.08	0.08
RuO2	0.09	0.08	0.08	0.08	0.08	0.08	0.08
SO3	1.00	1.00	1.00	1.00	1.00	1.00	1.00
Sb2O3	0.06	0.06	0.06	0.06	0.06	0.06	0.06
TeO2	0.07	0.07	0.07	0.07	0.07	0.07	0.07
TiO2	0.04	0.04	0.04	0.04	0.04	0.04	0.04
Subotal	14.12	14.10	14.12	14.10	14.10	14.10	14.10
Viscosity (Pa.s)	6.00	7.48	7.48	7.48	7.48	7.48	7.48
Melting Temp. (C)	1150	1150	1150	1150	1150	1150	1150

Appendix B3 Nominal Composition (wt%) of PFP2 Glasses

Glass ID	PFP2-1	PFP2-2	PFP2-3	PFP2-4	PFP2-5
WL (%)	28.0	28.0	28.0	28.0	28.0
SiO2	54.04	52.18	51.10	52.34	50.02
B2O3	14.11	13.63	13.34	13.67	13.06
Na2O	4.36	4.21	4.12	4.22	4.03
Li2O	7.44	7.18	7.03	7.21	6.89
CaO	0.88	0.85	0.83	0.85	0.81
MgO	0.31	0.30	0.29	0.30	0.29
Fe2O3	3.71	3.59	3.51	3.60	3.44
Al2O3	8.98	8.67	8.49	8.70	8.31
ZrO2	0.06	0.06	0.06	0.06	0.05
Others	6.11	9.35	11.22	9.06	13.10
Total	100.00	100.00	100.00	100.00	100.00
CeO2	0.12	0.12	0.12	0.12	0.11
CdO	0.11	0.11	0.11	0.11	0.11
CuO	0.16	0.16	0.16	0.16	0.16
Cr2O3	2.51	2.42	2.37	0.00	2.32
F	0.11	0.11	0.11	0.11	0.11
La2O3	0.06	0.06	0.06	0.06	0.05
MnO2	1.24	1.24	1.22	1.25	1.19
MoO3	0.03	0.03	0.03	0.03	0.03
Nd2O3	0.18	0.18	0.18	0.18	0.17
NiO	0.08	0.08	0.08	0.08	0.08
P2O5	0.00	3.33	5.33	5.46	7.33
PbO2	0.13	0.13	0.13	0.13	0.13
PdO	0.14	0.14	0.14	0.14	0.13
Rh2O3	0.06	0.06	0.06	0.06	0.06
RuO2	0.10	0.10	0.10	0.10	0.10
SO3	0.70	0.70	0.69	0.70	0.67
SeO2	0.33	0.32	0.32	0.33	0.31
TiO2	0.03	0.03	0.03	0.03	0.03
Subtotal	6.11	9.35	11.22	9.06	13.10
Viscosity (Pa.s)	6.79	6.31	6.06	6.34	5.78
Melting Temp (°C)	1150	1150	1150	1150	1150

Appendix B4 Nominal Composition (wt%) of WV182 Glasses

Glass ID	WV182-1	WV182-2	WV182-3	WV182-4	WV182-5	WV182-6	WV182-7	WV182-8	WV182-9	WV182-10	WV182-11	WV182-12
WL (%)	--	--	--	--	--	--	--	--	--	--	--	--
SiO2	43.75	42.97	42.59	42.20	40.36	39.64	39.29	38.93	36.36	35.72	35.39	35.07
B2O3	13.45	13.21	13.09	12.97	13.45	13.21	13.09	12.97	13.45	13.21	13.09	12.97
Na2O	14.95	15.46	15.71	15.97	14.95	15.46	15.71	15.97	14.95	15.46	15.71	15.97
Li2O	0.04	0.04	0.04	0.04	0.04	0.04	0.04	0.04	0.04	0.04	0.04	0.04
CaO	2.88	2.83	2.80	2.78	2.88	2.83	2.80	2.78	2.88	2.83	2.80	2.78
MgO	0.2	0.20	0.19	0.19	0.2	0.20	0.19	0.19	0.2	0.20	0.19	0.19
Fe2O3	11.53	11.33	11.22	11.12	11.53	11.33	11.22	11.12	11.53	11.33	11.22	11.12
Al2O3	2.61	2.56	2.54	2.52	6.00	5.89	5.84	5.79	10.00	9.82	9.73	9.65
ZrO2	2.04	2.00	1.99	1.97	2.04	2.00	1.99	1.97	2.04	2.00	1.99	1.97
Others	8.55	9.40	9.82	10.25	8.55	9.40	9.82	10.25	8.55	9.40	9.82	10.25
Total	100.00	100.00	100.00	100.00	100.00	100.00	100.00	100.00	100.00	100.00	100.00	100.00
Others												
BaO	0.16	0.16	0.16	0.15	0.16	0.16	0.16	0.15	0.16	0.16	0.16	0.15
CeO2	0.10	0.10	0.10	0.10	0.10	0.10	0.10	0.10	0.10	0.10	0.10	0.10
Cr2O3	0.63	0.62	0.61	0.61	0.63	0.62	0.61	0.61	0.63	0.62	0.61	0.61
Cs2O	0.07	0.07	0.07	0.07	0.07	0.07	0.07	0.07	0.07	0.07	0.07	0.07
CuO	0.03	0.03	0.03	0.03	0.03	0.03	0.03	0.03	0.03	0.03	0.03	0.03
K2O	1.03	1.01	1.00	0.99	1.03	1.01	1.00	0.99	1.03	1.01	1.00	0.99
La2O3	2.05	2.01	2.00	1.98	2.05	2.01	2.00	1.98	2.05	2.01	2.00	1.98
MnO2	0.59	0.58	0.57	0.57	0.59	0.58	0.57	0.57	0.59	0.58	0.57	0.57
MoO3	0.04	0.04	0.04	0.04	0.04	0.04	0.04	0.04	0.04	0.04	0.04	0.04
Nd2O3	0.58	0.57	0.56	0.56	0.58	0.57	0.56	0.56	0.58	0.57	0.56	0.56
NiO	0.46	0.45	0.45	0.44	0.46	0.45	0.45	0.44	0.46	0.45	0.45	0.44
P2O5	2.65	2.60	2.58	2.56	2.65	2.60	2.58	2.56	2.65	2.60	2.58	2.56
RuO2	0.05	0.05	0.05	0.05	0.05	0.05	0.05	0.05	0.05	0.05	0.05	0.05
SO3	0.00	1.00	1.50	2.00	0.00	1.00	1.50	2.00	0.00	1.00	1.50	2.00
SrO	0.05	0.05	0.05	0.05	0.05	0.05	0.05	0.05	0.05	0.05	0.05	0.05
TiO2	0.06	0.06	0.06	0.06	0.06	0.06	0.06	0.06	0.06	0.06	0.06	0.06
Subtotal	8.55	9.40	9.82	10.25	8.55	9.40	9.82	10.25	8.55	9.40	9.82	10.25
Viscosity (Pa.s)	5.25	4.67	4.42	4.16	5.63	5.01	4.72	4.46	6.11	5.43	5.11	4.82
Melting Temp (C)	1150	1150	1150	1150	1150	1150	1150	1150	1150	1150	1150	1150

Appendix B5 Nominal Composition (wt%) of CVS3 Glasses

Glass ID	CVS3-1	CVS3-37	CVS3-38	CVS3-39	CV3-40
WL (%)	50.0	50.0	50.0	50.0	50.0
SiO2	53.33	52.14	51.07	49.99	48.92
B2O3	0.05	0.05	0.05	0.05	0.05
Na2O	12.34	12.06	11.81	11.56	11.32
Li2O	2.86	2.79	2.74	2.68	2.62
CaO	1.26	1.23	1.21	1.18	1.16
MgO	0.05	0.05	0.05	0.04	0.04
Fe2O3	6.80	6.65	6.51	6.37	6.24
Al2O3	4.87	4.76	4.66	4.56	4.47
ZrO2	4.38	4.28	4.19	4.10	4.02
Others	14.08	15.99	17.72	19.46	21.19
Total	100.00	100.00	100.00	100.00	100.00
Others					
Bi2O3	1.37	1.34	1.31	1.29	1.26
CdO	0.06	0.05	0.05	0.05	0.05
CeO2	1.69	1.65	1.62	1.58	1.55
Cr2O3	0.53	0.52	0.51	0.50	0.49
F	0.34	0.33	0.33	0.32	0.31
K2O	0.13	0.13	0.13	0.12	0.12
La2O3	0.26	0.26	0.25	0.25	0.24
MnO2	1.12	1.10	1.07	1.05	1.03
MoO3	0.05	0.04	0.04	0.04	0.04
Nd2O3	6.02	5.89	5.77	5.64	5.52
NiO	1.40	1.37	1.34	1.32	1.29
P2O5	0.79	3.00	5.00	7.00	9.00
SO3	0.20	0.20	0.20	0.19	0.19
WO3	0.11	0.11	0.10	0.10	0.10
Subtotal	14.08	16.00	17.73	19.46	21.19
Viscosity (Pa.s)	4.00	3.72	3.46	3.24	3.03
Melting Temp (C)	1350	1350	1350	1350	1350

Appendix B6 Nominal Composition (wt%) of HTB651 Glasses

Series	Baseline	Phosphate			Chromium		Titanium					
Glass ID	HTB651-1	HTB651-2	HTB651-3	HTB651-4	HTB651-5	HTB651-6	HTB651-7	HTB651-8	HTB651-	HTB651-10	HTB651-11	HTB651-12
WL (%)	60.0	60.0	60.0	60.0	60.0	60.0	60.0	60.0	60.0	60.0	60.0	60.0
SiO2	42.27	41.52	40.65	39.78	42.15	42.06	41.85	41.00	40.16	38.80	38.90	38.80
B2O3	0.00	0.00	0.00	0.00	0.00	0.00	0.00	0.00	0.00	0.00	0.00	0.00
Na2O	17.70	17.39	17.02	16.66	17.65	17.62	17.52	17.17	16.82	16.30	16.30	16.30
Li2O	0.00	0.00	0.00	0.00	0.00	0.00	0.00	0.00	0.00	0.00	0.00	0.00
CaO	1.44	1.42	1.39	1.36	1.44	1.43	1.43	1.40	1.37	1.30	1.30	1.30
MgO	0.00	0.00	0.00	0.00	0.00	0.00	0.00	0.00	0.00	0.00	0.00	0.00
Fe2O3	7.70	7.56	7.40	7.24	7.67	7.66	7.62	7.47	7.31	7.10	7.10	7.10
Al2O3	9.10	8.94	8.75	8.56	9.07	9.05	9.00	8.82	8.64	8.40	12.00	8.40
ZrO2	4.95	4.87	4.76	4.66	4.94	4.93	4.90	4.81	4.71	4.50	4.50	8.00
Others	16.85	18.30	20.03	21.74	17.08	17.25	17.68	19.34	21.00	23.60	20.60	20.60
Total	100.00	100.00	100.00	100.00	100.00	100.00	100.00	100.00	100.00	100.00	100.70	100.50
Others												
Bi2O3	1.36	1.34	1.31	1.28	1.36	1.36	1.35	1.32	1.30	1.30	1.30	1.30
CeO2	1.91	1.88	1.84	1.80	1.90	1.90	1.89	1.85	1.81	1.70	1.70	1.70
Cr2O3	0.32	0.31	0.30	0.30	0.60	0.80	0.31	0.31	0.30	0.30	0.30	0.30
F	0.39	0.38	0.37	0.37	0.39	0.39	0.38	0.38	0.37	0.40	0.40	0.40
La2O3	0.30	0.29	0.29	0.28	0.30	0.30	0.30	0.29	0.28	0.30	0.30	0.30
MnO2	1.04	1.02	1.00	0.98	1.04	1.03	1.03	1.01	0.99	0.90	0.90	0.90
Nd2O3	6.11	6.00	5.88	5.75	6.09	6.08	6.05	5.93	5.81	5.70	5.70	5.70
NiO	1.59	1.56	1.53	1.49	1.58	1.58	1.57	1.54	1.51	1.50	1.50	1.50
P2O5	3.30	5.00	7.00	9.00	3.29	3.28	3.27	3.20	3.13	3.00	3.00	3.00
SO3	0.24	0.23	0.23	0.22	0.24	0.24	0.24	0.23	0.23	0.20	0.20	0.20
SrO	0.29	0.29	0.28	0.27	0.29	0.29	0.29	0.28	0.28	0.30	0.30	0.30
TiO2	0.00	0.00	0.00	0.00	0.00	0.00	1.00	3.00	5.00	8.00	5.00	5.00
Subtotal	16.85	18.30	20.03	21.74	17.08	17.25	17.68	19.34	21.00	23.60	20.60	20.60
Viscosity (Pa.s)	3.62	3.42	3.20	2.99	3.59	3.56	3.51	3.28	3.08	2.77	4.16	3.22
Melting Temp (C)	1350	1350	1350	1350	1350	1350	1350	1350	1350	1350	1350	1350

Appendix B7 Nominal Composition (wt%) of CC103 Glasses

Glass ID	CC103-1	CC103-2	CC103-3	CC103-4	CC103-5
WL (%)	18.3	30.0	45.0	50.0	55.0
SiO2	52.15	46.75	61.23	59.16	57.09
B2O3	9.07	17.07	11.96	11.40	10.82
Na2O	14.74	6.25	11.17	11.17	11.17
Li2O	2.27	6.69	6.84	6.84	6.84
CaO	0.32	0.19	0.12	0.15	0.19
MgO	0.03	0.02	0.08	0.10	0.12
Fe2O3	3.40	1.40	0.47	0.61	0.76
Al2O3	11.34	16.21	4.77	6.20	7.63
ZrO2	3.40	0.02	0.03	0.04	0.05
Others	3.29	5.41	3.33	4.33	5.33
Total	100.00	100.00	100.00	100.00	100.00
Others					
Cl	0.07	0.12	0.18	0.21	0.23
Cr2O3	2.52	4.14	6.21	6.91	7.60
F	0.02	0.03	0.04	0.05	0.05
K2O	0.05	0.08	0.11	0.13	0.14
La2O3	0.01	0.02	0.03	0.04	0.04
MnO2	0.25	0.41	0.62	0.69	0.75
MoO3	0.07	0.11	0.16	0.18	0.20
Nd2O3	0.04	0.06	0.09	0.10	0.11
NiO	0.05	0.09	0.14	0.15	0.17
P2O5	0.07	0.11	0.16	0.18	0.20
SO3	0.03	0.06	0.09	0.10	0.10
ZnO	0.11	0.19	0.28	0.31	0.34
Subtotal	3.22	5.29	7.93	8.81	9.69
Viscosity (Pa.s)	6.48	7.41	1.68	2.00	6.00
Melting Temp. (C)	1300	1150	1450	1400	1400

Appendix C

Schedules of Canister Centerline Cooling Treatments

Appendix C Canister Centerline Cooling Schedules of Low and High Temperature Glasses

Low Temperature Glass			High Temperature Glass		
Time (hr)	Temp. (C)	Rate (C/min)	Time (hr)	Temp. (C)	Rate (C/min)
0	1150		0	1350	
1	1072	-1.30	1	1183	-2.78
2	949	-2.05	2	1022	-2.68
3	863	-1.43	3	912	-1.83
4	800	-1.05	4	836	-1.27
8	656	-2.40	8	672	-2.73
12	576	-0.33	12	587	-0.35
16	488	-0.37	16	501	-0.36
20	407	-0.34	20	419	-0.34
24	340	-0.28	24	350	-0.29
28	286	-0.23	28	294	-0.23
32	242	-0.18	32	248	-0.19
36	206	-0.15	36	211	-0.15
40	176	-0.13	40	181	-0.13

Appendix D

Measured Melt Viscosities of HLW Glasses

Appendix D1 Melt Viscosity of PFP2 Glasses in a Tempearture Range between 980 C and 1350 C

PFP2-1		PFP2-2		PFP2-3		PFP2-4	
T (C)	Vis (Pa.s)	T (C)	Vis (Pa.s)	T (C)	Vis (Pa.s)	T (C)	Vis (Pa.s)
1148	12.79	1149	13.83	1248	5.90	1246	7.97
1098	20.67	1099	22.59	1197	9.19	1196	10.56
1048	34.97	1049	39.14	1148	14.69	1147	17.01
1099	20.50	1100	22.45	1199	9.11	1196	10.58
1149	12.82	1149	13.78	1250	5.90	1246	7.60
1199	9.60	1199	10.12	1299	4.21	1295	5.18
1249	5.95	1249	6.32	1247	5.83	1346	3.07
1148	11.04	1149	14.59	1099	20.19	1246	3.22
998	47.24	1000	69.02	1048	43.51	1096	12.63
		1149	17.34			996	68.24
		1049	42.75				
		1099	24.28				
		1149	17.43				
		1199	10.96				
		1249	7.63				
		1149	14.95				
		999	75.01				

Appendix D2 Melt Viscosity of CVS3 Glasses in a Tempearture Range between 1140 C and 1450 C

CVS3-1		CVS3-37		CVS3-38		CVS3-39		CVS3-40	
T (C)	Vis (Pa.s)	T (C)	Vis (Pa.s)	T (C)	Vis (Pa.s)	T (C)	Vis (Pa.s)	T (C)	Vis (Pa.s)
1294	8.87	1344	6.31	1344	7.04	1344	7.92	1344	8.72
1244	14.14	1295	9.85	1295	10.90	1294	12.44	1295	14.07
1194	23.20	1244	15.58	1244	17.36	1244	20.09	1245	23.05
1245	14.36	1294	10.06	1294	11.13	1294	12.64	1295	14.17
1294	9.09	1345	6.62	1345	7.31	1344	8.09	1345	8.92
1344	5.94	1396	4.42	1396	4.86	1396	5.46	1396	5.98
1395	4.02	1446	3.08	1446	3.34	1446	4.00	1447	4.02
1295	9.11	1346	6.66	1346	7.33	1345	8.03	1346	8.99
1145	40.68	1194	27.48	1194	30.55	1194	35.43	1194	42.02
1095	76.08	1144	48.67	1144	54.86	1144	66.21		

Appendix D3 Melt Viscosity of HTB651 Glasses in a Tempearture Range between 1140C and 1450C

HTB651-1		HTB651-2		HTB651-3		HTB651-4		HTB651-5		HTB651-6	
T (C)	Vis (Pa.s)	T (C)	Vis (Pa.s)	T (C)	Vis (Pa.s)	T (C)	Vis (Pa.s)	T (C)	Vis (Pa.s)	T (C)	Vis (Pa.s)
1345	6.33	1393	4.07	1394	4.62	1394	4.79	1344	6.11	1394	3.74
1295	10.44	1344	6.45	1344	7.11	1345	7.52	1294	10.06	1344	5.84
1245	17.80	1294	10.41	1294	11.81	1295	12.55	1244	17.01	1294	9.52
1295	10.61	1344	6.50	1344	7.17	1345	7.62	1294	10.27	1344	5.94
1345	6.50	1394	4.08	1394	4.58	1395	4.82	1344	6.31	1394	3.77
1395	4.13	1444	2.76	1445	3.12	1446	3.27	1395	4.03	1445	2.51
1445	2.79	1394	4.07	1395	4.57	1396	4.78	1445	2.67	1395	3.76
1345	6.51	1244	18.04	1244	20.44	1245	21.88	1345	6.39	1244	16.34
1195	33.07	1194	32.85	1194	37.89	1195	45.69	1194	32.50	1194	30.21
1144	67.98	1144	66.35	1144	83.25	1145	250.83	1144	65.78	1144	61.98

HTB651-7		HTB651-8		HTB651-9		HTB651-10		HTB651-11		HTB651-12	
T (C)	Vis (Pa.s)	T (C)	Vis (Pa.s)	T (C)	Vis (Pa.s)	T (C)	Vis (Pa.s)	T (C)	Vis (Pa.s)	T (C)	Vis (Pa.s)
1344	5.56	1292	7.56	1294	6.37	1246	7.19	1295	8.63	1246	14.09
1295	8.96	1243	12.67	1244	10.50	1196	12.02	1246	15.06	1197	28.66
1245	15.08	1192	22.00	1194	18.10	1146	21.55	1195	29.42	1147	103.16
1295	9.11	1243	12.77	1244	10.65	1195	12.23	1245	15.58	1196	37.13
1345	5.65	1293	7.61	1295	6.44	1246	7.43	1295	9.00	1246	18.30
1395	3.65	1343	4.78	1345	4.08	1296	4.55	1345	5.63	1297	8.49
1446	2.40	1394	3.12	1395	2.70	1346	2.93	1396	3.69	1347	4.34
1345	5.68	1294	7.47	1295	6.40	1246	7.41	1296	8.94	1247	12.37
1195	28.01	1143	42.31	1144	34.51	1095	44.28	1145	55.21		
1144	54.29	1093	90.01	1094	72.97	1044	103.16	1094	124.26		

Appendix D4 Melt Viscosity of CC103 Glasses in a Tempearture Range between 780C and 1420C

CC103-2		CC103-3	
T (C)	Vis (Pa.s)	T (C)	Vis (Pa.s)
786	4159.11	1091	173.78 - 107.15
831	1577.61	1142	107.15 - 102.33
889	533.33	1192	91.20 - 69.18
937	271.64	1243	52.00
1002	109.90	1295	26.49
1058	60.67	1296	29.51
1102	35.65	1348	13.37
1103	34.59	1348	14.13
1152	18.24	1378	9.10
		1408	6.76
		1420	6.24

Appendix E

7-Day PCT Data of HLW Glasses

Appendix E1 Chemical Durability Testing Results of CCW Glasses (7-day PCT)

Element	B	(g/m^2)	Cr	(g/m^2)	Li	(g/m^2)	Na	(g/m^2)	P	(g/m^2)	S	(g/m^2)	Si	(g/m^2)	pH	
Glass ID	(1)	(2)	(1)	(2)	(1)	(2)	(1)	(2)	(1)	(2)	(1)	(2)	(1)	(2)	(1)	(2)
CCW-1-1	0.02	---	0.00	---	0.04	---	0.08	---	0.00	---	1.14	---	0.00	---	---	---
CCW1-2	0.02	---	0.21	---	0.06	---	0.21	---	0.21	---	1.92	---	0.00	---	---	---
CCW1-3	0.06	0.06	1.86	1.88	0.55	0.56	1.16	1.19	0.82	0.89	16.78	17.05	0.00	0.00	---	---
CCW1-4(1)	0.78	0.79	13.65	13.86	4.23	4.29	10.37	10.55	0.00	0.00	113.52	115.44	0.05	0.05	---	---
CCW1-4(2)	0.80	0.93	13.51	15.20	4.38	4.76	11.17	12.63	0.22	0.22	123.43	137.45	0.04	0.04	8.60	8.49
CCW1-4(3)	0.51	0.56	14.09	15.41	4.53	4.92	9.89	11.98	0.18	0.18	123.06	135.41	0.02	0.02	8.40	8.41
CCW1-4(4)	0.81	0.73	14.61	14.40	2.98	4.43	12.17	11.63	0.81	0.19	120.47	128.04	0.04	0.04	7.95	8.36
CCW1-5	1.26	1.29	24.38	24.80	6.00	6.14	15.64	16.02	0.74	0.71	143.50	146.18	0.07	0.07	---	---
CCW2-1	0.00	0.00	0.01	0.01	0.01	0.00	0.01	0.01	0.00	0.00	0.05	0.04	0.00	0.00	6.82	6.51
CCW2-2	0.49	0.57	6.55	9.24	4.74	6.45	8.39	12.19	0.22	0.00	89.63	126.81	0.03	0.04	8.31	8.39
CCW2-3	0.64	0.53	16.55	15.32	3.08	2.77	9.39	8.23	0.36	0.37	114.83	101.21	0.02	0.02	8.31	8.28
CCW2-4	0.25	0.24	12.62	12.70	0.98	0.93	3.80	3.76	0.63	0.66	50.46	49.59	0.00	0.00	7.80	7.78
CCW3-1	0.38	0.44	6.51	7.72	2.63	2.82	8.46	9.49	0.28	0.24	91.06	100.63	0.02	0.03	8.02	8.08
CCW3-2	0.42	0.46	8.81	24.92	3.27	3.52	8.78	9.75	0.21	0.18	99.32	108.60	0.02	0.02	8.24	8.24
CCW3-3	0.46	0.52	14.27	16.94	5.03	5.67	10.52	11.85	0.20	0.23	125.35	143.30	0.01	0.02	8.50	8.51
CCW3-4	0.53	0.57	23.01	24.36	6.66	6.86	12.27	12.94	0.23	0.22	155.17	160.03	0.01	0.01	8.56	8.58
CCW4-1	0.46	0.51	13.62	14.30	4.89	5.01	9.87	10.25	1.04	1.07	118.56	122.98	0.01	0.01	8.48	8.52
CCW4-2	---	0.45	---	12.11	---	2.21	---	10.11	---	0.00	---	92.43	---	0.02	7.81	7.81
CCW4-3	---	---	---	---	---	---	---	---	---	---	---	---	---	---	8.51	9.01

Appendix E2 Chemical Durability Testing Results of CC103 Glasses (7-day PCT)

Element	B (g/m^2)	Cr (g/m^2)	Li (g/m^2)	Na (g/m^2)	Si (g/m^2)	pH
Glass ID						
CC103-2	0.91	0.02	0.84	0.21	0.37	9.63
CC103-3	0.34	0.02	0.50	0.15	0.31	9.99
CC103-4	4.41	0.22	2.10	0.69	0.51	11.65
CC103-5	11.99	0.37	3.61	0.42	0.84	11.90

Appendix E3 Chemical Durability Testing Results of PFP2 Glasses (7-day PCT)

Element	B	(g/m^2)	Li	(g/m^2)	Na	(g/m^2)	P	(g/m^2)	Si	(g/m^2)	pH	
Glass ID	(1)	(2)	(1)	(2)	(1)	(2)	(1)	(2)	(1)	(2)	(1)	(2)
PFP2-1	0.27	0.29	0.34	0.36	0.05	0.05	0.00	0.00	0.20	0.21	9.91	9.99
PFP2-2	0.24	0.24	0.33	0.34	0.02	0.02	0.23	0.30	0.19	0.19	9.66	9.78
PFP2-3	0.22	0.22	0.31	0.31	0.02	0.02	0.23	0.24	0.17	0.18	9.57	9.62
PFP2-5	0.22	0.22	0.32	0.34	0.02	0.02	0.25	0.27	0.17	0.17	9.33	9.49
PFP2-1(CCC)	0.66	0.71	0.62	0.66	0.18	0.19	0.00	0.00	0.22	0.23	9.81	9.82
PFP2-2(CCC)	1.13	1.19	0.90	0.96	0.09	0.30	0.61	0.46	0.21	0.23	9.72	9.70
PFP2-3(CCC)	0.66	0.70	0.62	0.64	0.09	0.09	0.38	0.38	0.22	0.22	9.49	9.46
PFP2-5(CCC)	1.96	2.08	0.98	1.04	0.09	0.09	0.30	0.33	0.18	0.19	9.18	9.14

Appendix E4 Chemical Durability Testing Results of CVS3 Glasses (7-day PCT)

Element	B	(g/m^2)	Li	(g/m^2)	Na	(g/m^2)	P	(g/m^2)	Si	(g/m^2)	pH	
Glass ID	(1)	(2)	(1)	(2)	(1)	(2)	(1)	(2)	(1)	(2)	(1)	(2)
CVS3-37	0.64	0.45	0.19	0.19	0.37	0.37	0.18	0.18	0.15	0.15	10.49	10.55
CVS3-38	0.34	0.54	0.29	0.30	0.32	0.33	0.10	0.10	0.14	0.15	10.87	11.03
CVS3-39	0.21	0.24	0.23	0.24	0.27	0.28	0.07	0.07	0.14	0.14	10.72	10.81
CVS3-40	0.25	0.25	0.20	0.21	0.24	0.23	0.07	0.07	0.13	0.13	10.50	10.59
CVS3-37(CCC)	0.39	0.36	0.33	0.33	0.33	0.33	0.20	0.20	0.14	0.14	10.92	10.99
CVS3-38(CCC)	0.23	0.27	0.69	0.68	0.34	0.33	0.58	0.58	0.16	0.16	10.87	10.93
CVS3-39(CCC)	0.31	0.31	1.05	1.06	0.38	0.37	0.76	0.76	0.17	0.17	10.85	10.93
CVS3-40(CCC)	0.32	0.39	0.96	0.94	0.32	0.32	0.54	0.53	0.16	0.16	10.69	10.75

Appendix E4 Chemical Durability Testing Results of CVS3 Glasses (7-day PCT)

Element	B	(g/m^2)	Li	(g/m^2)	Na	(g/m^2)	P	(g/m^2)	Si	(g/m^2)	pH	
Glass ID	(1)	(2)	(1)	(2)	(1)	(2)	(1)	(2)	(1)	(2)	(1)	(2)
CVS3-37	0.64	0.45	0.19	0.19	0.37	0.37	0.18	0.18	0.15	0.15	10.49	10.55
CVS3-38	0.34	0.54	0.29	0.30	0.32	0.33	0.10	0.10	0.14	0.15	10.87	11.03
CVS3-39	0.21	0.24	0.23	0.24	0.27	0.28	0.07	0.07	0.14	0.14	10.72	10.81
CVS3-40	0.25	0.25	0.20	0.21	0.24	0.23	0.07	0.07	0.13	0.13	10.50	10.59
CVS3-37(CCC)	0.39	0.36	0.33	0.33	0.33	0.33	0.20	0.20	0.14	0.14	10.92	10.99
CVS3-38(CCC)	0.23	0.27	0.69	0.68	0.34	0.33	0.58	0.58	0.16	0.16	10.87	10.93
CVS3-39(CCC)	0.31	0.31	1.05	1.06	0.38	0.37	0.76	0.76	0.17	0.17	10.85	10.93
CVS3-40(CCC)	0.32	0.39	0.96	0.94	0.32	0.32	0.54	0.53	0.16	0.16	10.69	10.75

Appendix F

Normalized Releases of Selected HLW Glasses in Rinse Water at Room Temperature

Appendix F Nomalized Releases of Selected HLW Glasses in Rinse Water at Room Temperature

Element	B	(g/m^2)	Li	(g/m^2)	Na	(g/m^2)	P	(g/m^2)	Si	(g/m^2)
Glass ID	(1)	(2)	(1)	(2)	(1)	(2)	(1)	(2)	(1)	(2)
PFP2-1(CCC)	0.006	0.005	0.009	0.007	0.003	0.002	0.000	0.000	0.001	0.001
PFP2-2(CCC)	0.008	0.004	0.023	0.011	0.003	0.002	0.043	0.024	0.001	0.001
PFP2-3(CCC)	0.011	0.006	0.031	0.017	0.007	0.004	0.048	0.025	0.002	0.001
PFP2-5(CCC)	0.006	0.004	0.020	0.013	0.003	0.002	0.025	0.016	0.001	0.001
CVS3-37(CCC)	0.019	0.013	0.019	0.006	0.009	0.003	0.000	0.000	0.000	0.000
CVS3-38(CCC)	0.000	0.004	0.027	0.011	0.008	0.002	0.021	0.010	0.000	0.000
CVS3-39(CCC)	0.022	0.012	0.051	0.028	0.013	0.004	0.032	0.019	0.000	0.000
CVS3-40(CCC)	0.014	0.013	0.037	0.027	0.010	0.005	0.021	0.015	0.000	0.000
HTB651-2	N/A	N/A	N/A	N/A	0.021	0.017	0.000	0.000	0.002	0.005
HTB651-3	N/A	N/A	N/A	N/A	0.015	0.012	0.000	0.000	0.001	0.003
HTB651-4	N/A	N/A	N/A	N/A	0.015	0.016	0.001	0.004	0.002	0.003
HTB651-5	N/A	N/A	N/A	N/A	0.023	0.009	0.000	0.000	0.002	0.002
HTB651-6	N/A	N/A	N/A	N/A	0.019	0.014	0.000	0.000	0.001	0.004
HTB651-7	N/A	N/A	N/A	N/A	0.014	0.012	0.000	0.000	0.001	0.003
HTB651-8	N/A	N/A	N/A	N/A	0.012	0.012	0.000	0.000	0.001	0.004
HTB651-9	N/A	N/A	N/A	N/A	0.015	0.014	0.000	0.000	0.001	0.004